TITLE PAGE

Report Title: LOW-ENGINE-FRICTION TECHNOLOGY FOR ADVANCED NATURAL-GAS RECIPROCATING ENGINES

Annual Technical Progress Report

Reporting Period: April 1, 2005 – May 31, 2006

for

DoE Cooperative Agreement No. DE-FC26-02NT41339

Submitted by

Victor Wong, Tian Tian, Luke Moughon, Rosalind Takata, Jeffrey Jocsak

Massachusetts Institute of Technology
Room 31-155, 77 Massachusetts Avenue
Cambridge, MA 02139

and

Rudy Stanglmaier, Ted Bestor, Kirk Evans, Kris Quillen

Sub-Contract University
Colorado State University
Fort Collins, CO 80523

June 30, 2006

Submitted to:
NETL AAD Document Control Building 921
Department of Energy
National Energy Technology Laboratory
P.O. Box 10940
Pittsburgh, PA 15236-0940

DISCLAIMER

ABSTRACT

This program aims at improving the efficiency of advanced natural-gas reciprocating engines (ANGRE) by reducing piston and piston ring assembly friction without major adverse effects on engine performance, such as increased oil consumption and wear. An iterative process of simulation, experimentation and analysis is being followed towards achieving the goal of demonstrating a complete optimized low-friction engine system. To date, a detailed set of piston and piston-ring dynamic and friction models have been developed and applied that illustrate the fundamental relationships among mechanical, surface/material and lubricant design parameters and friction losses. Demonstration of low-friction ring-pack designs in the Waukesha VGF 18GL engine confirmed total engine FEMP (friction mean effective pressure) reduction of 7-10% from the baseline configuration without significantly increasing oil consumption or blow-by flow. This represents a substantial (30-40%) reduction of the ring-pack friction alone. The measured FMEP reductions were in good agreement with the model predictions. Further improvements via piston, lubricant, and surface designs offer additional opportunities. Tests of low-friction lubricants are in progress and preliminary results are very promising.

The combined analysis of lubricant and surface design indicates that low-viscosity lubricants can be very effective in reducing friction, subject to component wear for extremely thin oils, which can be mitigated with further lubricant formulation and/or engineered surfaces. Hence a combined approach of lubricant design and appropriate wear reduction offers improved potential for minimum engine friction loss. Piston friction studies indicate that a flatter piston with a more flexible skirt, together with optimizing the waviness and film thickness on the piston skirt offer significant friction reduction. Combined with low-friction ring-pack, material and lubricant parameters, a total power cylinder friction reduction of 30-50% is expected, translating to an engine efficiency increase of two percentage points from its current baseline towards the goal of 50% ARES engine efficiency.

The design strategies developed in this study have promising potential for application in all modern reciprocating engines as they represent simple, low-cost methods to extract significant fuel savings. The current program has possible spinoffs and applications in other industries as well, including transportation, CHP, and diesel power generation. The progress made in this program has wide engine efficiency implications, and potential deployment of low-friction engine components or lubricants in the near term is possible as current investigations continue.

TABLE OF CONTENTS

LIST OF FIGURES

LIST OF TABLES

LOW-ENGINE-FRICTION TECHNOLOGY FOR ADVANCED NATURAL-GAS RECIPROCATING ENGINES

Annual Technical Progress Report
Reporting Period: April 1, 2005 – May 31, 2006
Massachusetts Institute of Technology
DoE Cooperative Agreement No. DE-FC26-02NT41339

EXECUTIVE SUMMARY

This program aims to improve the efficiency of advanced natural-gas reciprocating engines (ANGRE) by reducing piston and piston ring assembly friction without major adverse effects on engine performance, such as increased oil consumption and wear. The approach is to apply or adapt existing computer models to evaluate the friction reduction potential of power-cylinder component design, surface treatment, and lubrication concepts. The promising low-friction candidate design concepts are validated experimentally on a full-size large-bore natural-gas engine at Colorado State University (CSU). Waukesha Engine Dresser, Inc. provides the engine, parts, and engineering support for the program.

The program has five major tasks, as shown in the Milestones chart, summarized as follows. Task 1 and 2 have been completed and reported earlier and are thus not included in the Milestone Chart nor included in this report. Task (1): Assess opportunities for friction reduction by performing preliminary analyses and evaluating existing empirical data; Task (2): Modify or adapt existing engine friction and lubrication models to ANGRE engines and to develop friction reduction concepts and recommendations; Task (3): Assess friction reduction opportunities, develop and recommend friction-reducing designs. Task (4): Test and demonstrate recommended concepts in a full-scale ARES Waukesha engine; (5) Analyze test results and iterate on initial recommendations. Task (5) is conducted concurrently with Task 3 and 4. Cumulatively, Tasks (1)-(3) have been completed. In Task (4), demonstration of low-friction ring-packs is complete, and testing of low-friction lubricants is in progress (preliminary results are very promising); however, validation of low-friction pistons and surface treatments will await completion of the lubricant experiments. The major remaining activities in the next reporting period focus on Task 4 and completing Task 5 and documentation.

Specifically, in Task (3), the detailed analysis recommended a low-friction ring-pack to consist of a top piston ring with a "skewed-barrel" profile (geometry of ring profile), a reduced-tension oil-control ring, together with a second (scraper) ring with a negative twist (torsional preload). The study also recommended that a flexible (less rigid) piston skirt with a generally flatter piston-skirt geometric profile is preferred to minimize metal-metal contact during piston-liner impact and lubrication. Honing or groove patterns on the piston/rings or liner that are oriented more perpendicular to the piston motion generally reduce friction and wear. The analysis also considered optimal depths and widths of dimples and grooves. For lubricants, the study considered the effects of changing lubricant viscosity either uniformly throughout, or preferentially at various parts, of the engine cycle. It is recommended that reducing the level of viscosity everywhere in the cycle is more effective than lowering it only

at mid-stroke but increasing it preferentially at top (or bottom) dead centers to reduce metal-metal contact friction. Friction modifiers are effective in reducing asperity contact friction but may have other practical implementation concerns. The study recommended that a combined application of lubricant and material technology be pursued to simultaneously reduce friction, wear and oil consumption.

In Task (4), demonstration of low-friction ring-pack designs in the Waukesha VGF 18GL engine confirmed total engine FEMP (friction mean effective pressure) reduction of 7-10% from the baseline configuration without significantly increasing oil consumption or blow-by flow. This represents a substantial (30-40%) reduction of the ring-pack friction alone. The measured FMEP reductions were in good agreement with the model predictions. Further improvements via piston, lubricant, and surface designs offer additional opportunities. Tests of low-friction lubricants are in progress near the end of this reporting period. Preliminary results are very promising and will be discussed in detail in the next report.

Task (5) provides careful review of the results and, through team discussions, determines the proper combination and schedule of additional analysis and experimentation. It appears that testing of material/surface design should be implemented synergistically in conjunction with further lubricant experiments. Piston design validation should follow any additional combined low-friction oil and material experiments. Results indicate that piston and lubricants offer as much friction reduction benefit as the ring-pack. Expanded studies in these areas beyond the current program would therefore be appropriate and are recommended.

During this reporting period, April 2005 through May 2006, the project team participated in the following conferences: The ASME-ICED 2005 Fall and 2005/2006 Spring Conferences, in which specific ARES/ARICE tracks were held. In addition, an Industry-University Workshop on Low-Engine Friction was held at MIT in December 2005, in which all major manufacturers of ARES engines participated with strongly supporting feedback to continue the informal technical consortium. Five (5) technical papers have been peer-reviewed and published: at ASME-ICED 2005 STC (1 paper), ASME-ICED 2005 FTC (2 papers), SAE 2006 Congress (1 paper), and ASME-ICED 2006 STC (1 paper). Three (3) additional papers have either been submitted or prepared and will be presented in the next reporting period. MIT, CSU, Waukesha and our lubricant partner continue to hold periodic conference calls to maintain communication on technical progress as well as gain guidance from industry experts. We aim at further enhancing our interactions with industry in the ARES/ARICE community, including universities and national laboratories in the future.

The design strategies developed in this study have promising potential for application in all modern reciprocating engines as they represent simple, low-cost methods to extract significant fuel savings and to reduce harmful environmental effects, without compromising engine performance. The current program has possible spinoffs and applications in other industries as well, including transportation, CHP, and diesel power generation. Discussions with various government agencies and University-Industry workshops will be continued to ensure that the full potential for friction reduction in these areas will be fully explored and areas for further investigation identified. The progress made in this ARES program has wide implications beyond one focused industry. Potential deployment of low-friction engine components or lubricants in the near term is quite possible if future continued funding permits.

LOW-ENGINE-FRICTION TECHNOLOGY FOR ADVANCED NATURAL-GAS RECIPROCATING ENGINES
Annual Technical Progress Report
(June 1, 2004 – June 30, 2005)
DoE Cooperative Agreement No. DE-FC26-02NT41339

I. INTRODUCTION

A. Objectives

The objectives of this program remain as the reduction of parasitic losses of advanced natural gas reciprocating engines (ANGRE) through lowering friction in the power cylinder (piston and ring-pack). Computer models are being evolved and applied to assess the opportunities of piston and piston ring-pack design, surface finish, and lubrication strategies aimed at friction minimization. We have been investigating fundamental design parameters and performance relationships to reduce friction without causing adverse effects such as increased wear and oil consumption. The concepts developed from the analyses are being validated experimentally via concurrent experiments. The program objectives are being accomplished through systematic analysis of experimental data sets, using recommendations of promising low-friction piston/ring-pack/lubricant options, and actual testing and demonstration in an ANGRE engine.

B. Scope of Work

A combined analytical and experimental program is undertaken. The scope of work includes evaluating the performance and designs of current large-bore natural gas engine and power cylinder components, and modifying or adapting existing analytical tools for ANGRE applications. Computer modeling and analysis will be used to understand and to optimize friction reduction concepts. Concept validation will be conducted experimentally on a Waukesha VGF engine; concurrent computer parametric studies on design parameters will be performed and validated by engine tests. Testing will be done at Colorado State University.

C. Tasks to Be Performed

This reporting period focused primarily on lubricant and surface analysis (ring-pack design results presented earlier) results and low-friction ring-pack demonstration data. The program has several major tasks, as shown in the following Milestones chart, two of which have been completed and presented in the previous reporting period. These tasks related to the assessment of friction reduction opportunities, and to the design and recommendation of friction-reducing ring-pack designs. Low-friction ring-pack experiments have been completed and low-friction lubricants tests are being conducted. Remaining tasks include: (1) Complete testing of low-friction lubricants; (2) Recommend surface and material designs for power cylinder components to be tested; (3) Analyze combined lubricant and surface finish effects in the power cylinder; (4) Analyze test results and iterate on further lubricant designs to reduce potential side effects of wear (5) Review final engine experimental results and prepare documentation, (6) Recommend further research, development, or deployment.

D. Major Accomplishments

In this reporting period, the major accomplishments include the following:

- Demonstration of low-friction ring-pack designs confirmed total engine FEMP (friction mean effective pressure) reduction of 7-10% from the baseline configuration without significantly increasing oil consumption or blow-by flow. This represents a substantial (30-40%) reduction of the ring-pack friction alone. The measured FMEP reductions were in good agreement with the model predictions. Further improvements via piston, lubricant, and surface designs offer additional opportunities.
- Testing of low-friction lubricants is in progress at the latter part of this reporting period. Preliminary results indicate promising results.
- The combined analysis of lubricant and surface design indicates that low-viscosity lubricants can be very effective in reducing friction, subject to component wear considerations for extremely thin oils. Engineered surfaces can reduce wear. Hence a combined approach of lubricant design and appropriate wear reduction offers improved potential for minimum engine friction losses.

E. Current Status

Of the three main approaches to reduce power cylinder friction via piston/ring designs, lubricant properties, and surface characteristics, we have completed the testing of ring-pack design. Testing of low-friction lubricants is in progress and we expect promising results. Analyses of all three approaches have been performed and strategies proposed. The remaining challenges are as follows: (A) Results have shown that there is a synergistic benefit of using low-friction lubricant concurrently with implementing low-friction low-wear material/surface designs. Accordingly, although concepts for low-friction surface textures have been proposed, the actual testing of low friction and wear materials could take longer than originally anticipated. (B) Studies strongly indicate that piston friction is comparable to ring-pack friction and deserves as detailed a study and testing as low-friction ring-packs. Extended studies of piston friction reduction beyond the current period may be appropriate. A cooperative partnership has begun with a large lubricant manufacturer to design and provide lubricants for future testing. Potential deployment of low-friction engine components or lubricant in the near term may be possible, if future continued funding permits.

F. Report Outline

This report presents three main sections: (A) Extended ring-pack friction analyses conducted in this current period, focusing primarily on lubricant and surface design strategies; (B) Further piston analyses carried out last year, considering additional design parameters such as piston ovality and geometric designs. For completeness, however, the cumulative results of the piston study are presented in this report. The third section (C) presents the cumulative ring-pack demonstration experiments performed using the Waukesha engine, not including the current lubricant tests that have just been started. We expect to include the lubricant results in the next report. Overall summary and continuing planned are discussed.

PROJECT MILESTONE PLAN DoE Form 4600.3

(Low Engine Friction Technology for Advanced Natural Gas Reciprocating Engines)

Milestone Plan Period: October 1, 2004 – September 30, 2006

#	MAJOR TASKS
3	Design & Performance Analysis
3.1	(a) Piston analyses for improved piston friction reduction
3.2	(b) Perform parametric and system analyses to include effects of material, surface characteristics such as roughness, wear trends, and lubricant
3.3	(c) Recommend low-friction design options for ring/piston, material, and lubricant systems.
4	**Demonstrate Optimal Design Concepts**
4.1	Establish Baseline Tests (Done)
4.2	Validate effects of individual component design parameter changes to include piston, material, &
4.3	Demonstrate complete low-friction engine system with aggregate improvements
5	**Analyze Test Results of Additional System Parameters (Piston, Material, & Lube); Iterate**
6	**Manage Reporting & Education**
6.1	Prepare periodic reviews and reports
6.1.1	- Monthly team telephone conferences
6.1.2	- Deliver annual reports
6.1.3	- Deliver final report

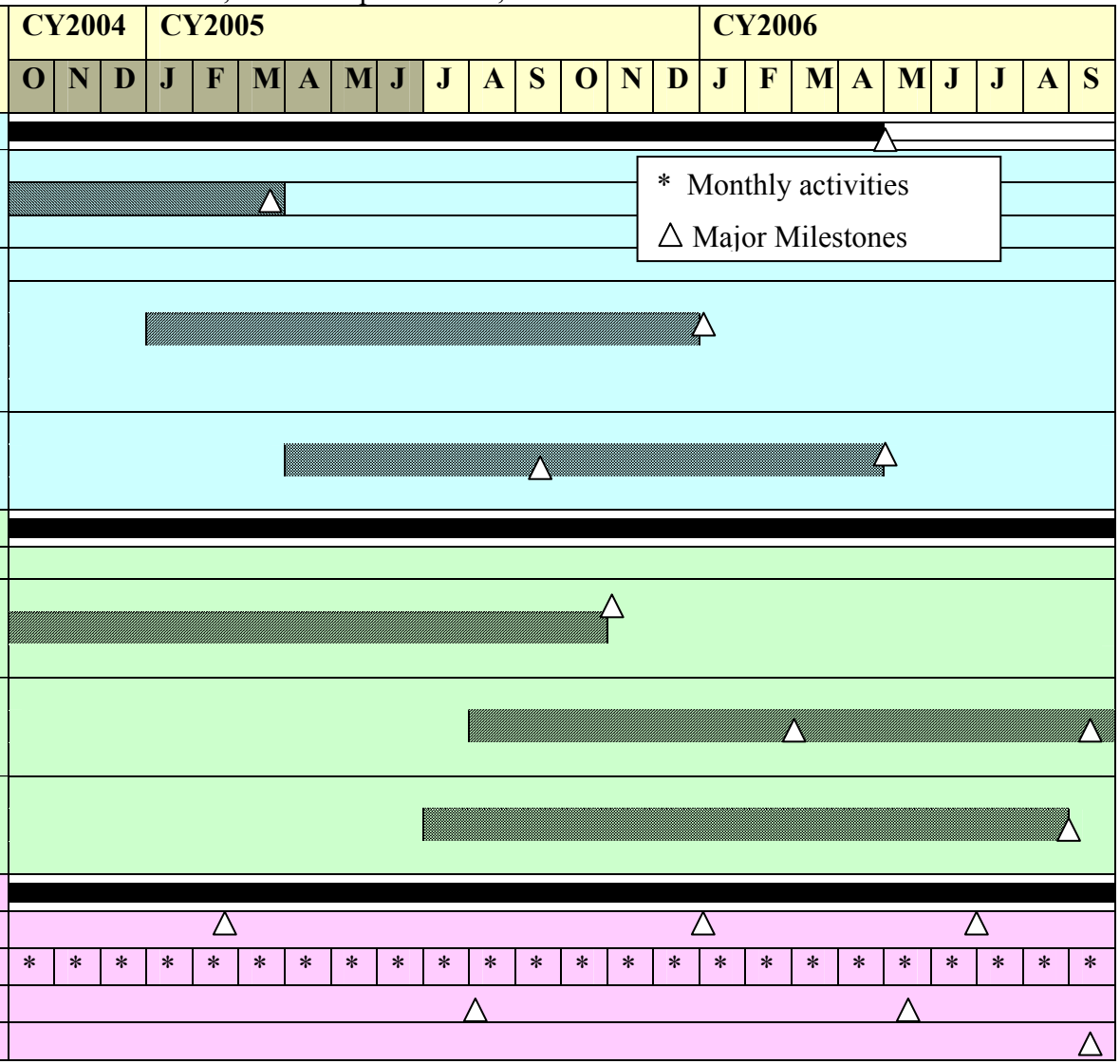

II. RESULTS AND DISCUSSION

(A) DESIGN AND PERFORMANCE ANALYSIS OF RING-PACK FRICTION

1. Extended Modeling and Analysis of Lubricant and Surface Effects

1.1. Methodology

In the last reporting period, computer models have been applied to extensively study mechanical design aspects of piston rings on engine friction, viz. ring profile of the top ring, ring-twist of the second ring, and oil control ring tension. During this period, computer models have been further developed to address lubricant and surface characteristics on ring-pack friction. Previous results from using the models resulted in recommendations for piston-ring geometry, to reduce ring friction. At this stage, the models have been used for parametric studies on lubricant and surface parameters for the rings, as well as for piston design parameters. Analytical studies have been carried out in conjunction with working a lubricant supplier to furnish lubricant for experimental verification of the lubricant analytical studies. However, most of the results on lubricant studies have been reported in the previous annual report. Hence, this report devotes more emphasis to surface analysis.

1.2. Overview of lubricant properties and requirements

Modern engine lubricant must perform many different functions, and fulfill many requirements. To this end, the typical lubricant contains a number of components and additives, designed to control viscosity, reduce boundary friction and wear, control lubricant degradation, and perform numerous other functions. While the lubricant viscosity is the focus of this study, other requirements should be taken into consideration in the design of an engine lubricant.

One of the main lubricant requirements is stability. The oil must maintain a stable state at all temperatures and conditions, so that it does not either react to create corrosive elements or form deposits that can reduce engine performance. The lubricant must also be able to mitigate the effects of any compounds that are formed in the engine or enter via intake air. Detergents and dispersants allow the oil to keep such components in suspension – preventing them from being deposited on surfaces or creating wear - and to inhibit reactions that lead to undesirable products such as acidic compounds [1].

In addition to these functions, the lubricant often also contains compounds that reduce wear and control viscosity. Anti-wear additives can be used to reduce wear due to metal-to-metal contact, while other additives are used to control attack on piston, cylinder and ring surfaces by acidic combustion products. The viscosity must also be controlled so that it maintains an acceptable value at both cold-start and running temperatures. Viscosity Index (VI) improvers can be used to reduce the variation of viscosity with temperature, so that the oil can be thin enough at start-up to lubricate the engine but not too thin at high temperatures to allow excessive boundary contact at running conditions [1]. One side effect of these VI improvers is to make the oil viscosity depend not only

upon temperature but upon the shear rate in the oil. Not all lubricants contain VI improvers (those that do not are termed "straight" weight oils), but for those that do this viscosity variation must be taken into account.

1.3. Overview of liner surface structure

While they may appear smooth to the naked eye, the surfaces of both the rings and the cylinder walls are rough on the scale of interest – the thickness of the oil film separating the two. The texture of these surfaces can greatly affect both the amount of contact that occurs among asperities and the flow of oil between them. Understanding the effect of surface texturing on the interaction between the surfaces, and between the lubricant and the surfaces, is essential in understanding the lubrication of components currently in use and designing new surfaces to reduce friction.

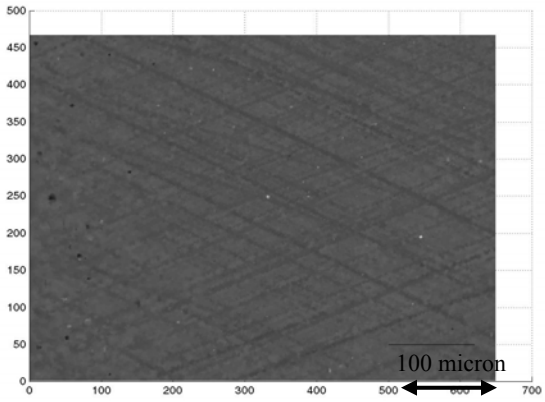

a) typical honed surface (slide-honed, WLI measurement)

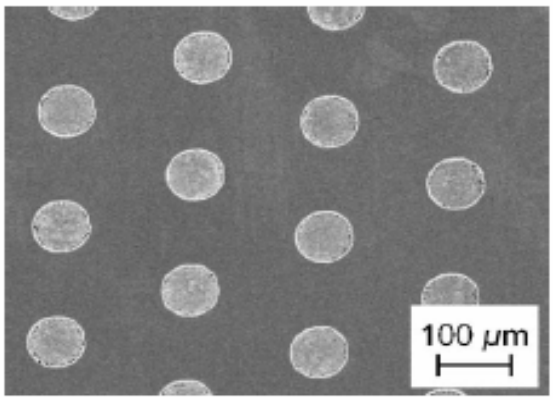

b) Example of a "dimpled" surface.[39]

Figure 1-1: Typical examples of honed and laser-textured surfaces

Two examples of surface finishes are shown in Figure 1-1. Figure 1-1a shows an example of a surface commonly found on cylinder liners today – a plateau finish clearly showing the cross-hatch marks that result from the honing process. Figure 1-1b shows a less common texture, the surface has a dimpled pattern created by laser machining. While very uncommon at present, such designed surfaces are the subject of numerous studies and may be a key part of decreasing sliding friction and wear between the rings and liner.

1.3.1. Current production cylinder liner finishes

Today, most cylinder liner surfaces have a honed finish whose properties are stochastically controlled. That is, statistical parameters such as the surface roughness and skewness (see Figure 3-3a) are determined by the honing process, but the placement of specific features in specific locations is not possible. A typical honed surface, of which an example profile is shown in Figure 1-2 and a surface view in Figure 1-1a, has a negative skewness and a cross-hatch pattern of grooves, both created by the honing procedure.

Figure 1-2: Typical plateau honed profile

A typical honing tool is shown in Figure 1-3. The tool consists of a head with honing sticks or stones that are covered with abrasive particles, and are held outward radially by springs. The head is spun and at the same time moved axially in and out of the cylinder. The honing sticks are pressed outward into the bore and polish the surface. The process generally proceeds from a coarse grit to a fine one, so that deep grooves and large ridges are made during the initial rough honing passes. Then, the ridges are worn down to a relatively smooth finish by the subsequent fine passes, while the deep valleys remain. Such a process generally results in a plateau finish – a surface with negative skewness - in which the surface is relatively flat with many deep valleys. Such negatively skewed surfaces are thought to reduce friction by effectively breaking in the liner before actual engine use, and thus reducing actual breaking–in time, as well as by reducing asperity contact between ring and liner in a mixed lubrication regime [2,3,4].

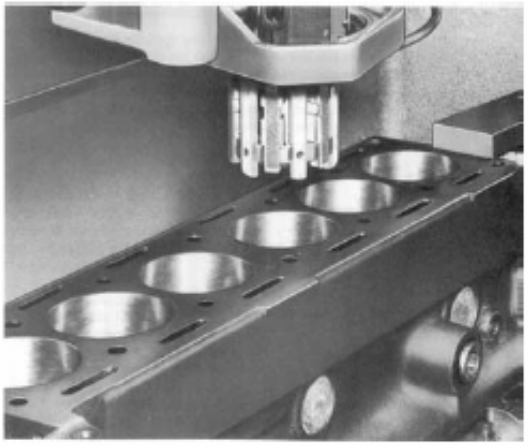

Figure 1-3: Typical cylinder bore honing tool [5]

In addition to creating a plateau surface, the combination of the rotating and axial feeding movements of the honing machine creates angled grooves on the surface, as shown in Figure 1-4. The relation between the rotation and feeding rates determines the angle of the cross-hatch grooves. The size and angle of these grooves has an influence on friction as well as oil consumption and wear. Several studies have predicted an increase in oil film thickness and decrease in friction for more transverse (relative to the cylinder axis) textures [2-6], although concerns about oil consumption and scuffing wear prevent

very shallow-angle cross-hatch grooves from being implemented in production cylinder liners.

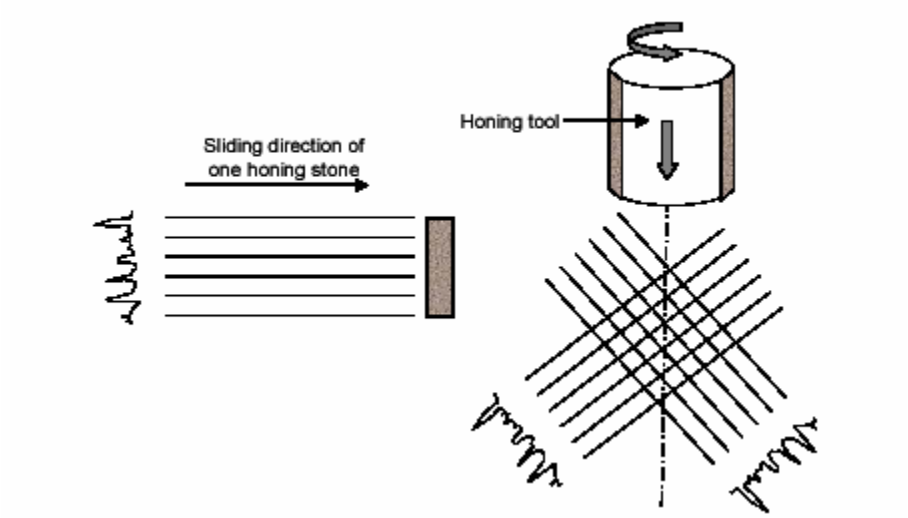

Figure 1-4: Schematic of honing process [4]

1.3.2. Advanced finishes and textures

Deterministically controlled textures, in which individual features, such as the dimples shown in Figure 1-1b, are added to a surface, are already in use in some industries and show promise for friction and wear reduction in engine applications. For example, very small "micro-texturing" has been added to the "landing" sections of magnetic storage media for several years, to prevent stiction when recording heads contact the surface [7]. Although the mechanism for friction reduction here is different than that encountered in the case of the piston ring/liner interface, the success of this technique has encouraged other investigations into the possibility of engineering the surface structure.

Numerous studies, both analytical and experimental, have considered the effect of advanced textured surfaces on friction, wear, and other parameters in sliding applications. Research on face-seals, where loads and speeds are approximately constant during service, has shown great potential for increasing load capacity and lifetime with the addition of micro-texturing. Some experimental prototypes have been successfully field-tested in pumps, where they showed increased load capacity and greatly decreased wear over standard seals [8]. Studies of reciprocating sliding conditions have also indicated that friction may be reduced, although there is a lack of agreement over the mechanism for this effect. Still, both analytical and experimental results have shown potential for friction reduction, and laser-textured cylinder liners that promise low wear and oil consumption have been made commercially available by Gehring GmbH [9] in Germany.

Several methods are available for creating micro-textured surfaces, including chemical etching, machining, abrasive-jet machining, and laser texturing. Each method has advantages and disadvantages, and some may be more appropriate for use in a given application than others. Etching, for example, is versatile in the shapes it can produce, but the process is time-consuming and the profiles of the features are determined by the

chemical erosion process and cannot be controlled (i.e., round-profiled dimples cannot be produced). Regular and abrasive-jet machining also have some limitations on profile shape, and may not be appropriate for cylinder liner texturing if machining heads are too large to access the inner liner surface. Laser texturing technology is currently believed to be a very promising technique based on its flexibility and speed [8]. A possible drawback is that the laser technique may create "burrs" of melted and re-deposited material around the edges of features so that surfaces may require a subsequent polishing step, however this problem may be solved with more optimized techniques in the future. An example of a laser-machining station is shown in Figure 1-5.

Figure 1-5: Typical laser texturing machinery (from Control Micro Systems, Inc.)

.

1.4. Scope of current-year work

The purpose of the current-year work was to investigate methods by which ring/liner friction can be reduced in the Waukesha VGF 18GL engine via lubricant and surface design. We focused on lubricant viscosity and surface finish of the cylinder liner. For both studies, existing ring-pack friction and lubrication models were used, with minor modifications as were required to complete the study.

In the area of lubricant properties, viscosity and its dependence on temperature and shear rate were considered. The role of lubricant viscosity in controlling the balance between hydrodynamic and boundary friction was studied, as was the effect of variation of viscosity during the engine cycle. Effects of viscosity on both friction and wear were analyzed. Also, some consideration was given to boundary friction coefficient and its role in ring/liner friction.

In the area of surface texturing, a parametric study was performed to evaluate the effects of both grooved and dimpled textures on the cylinder liner. Simplified surfaces were used to calculate flow and stress factors for the cases considered, which were then used in the ring-pack model to predict ring/liner friction. While the model used did not allow a detailed analysis of the effects of these textures on asperity contact and oil flow, this type of parametric study can give an indication of which textures are effective and how changing the different parameters affects friction and wear.

The possibility of optimizing the lubricant and surface together was also investigated. With this combined approach, a greater friction reduction is possible than in the individual cases, and it is also possible to reduce negative side-effects such as increased wear and oil consumption.

2. Model Formulation: Ring-Pack Lubrication and Friction

2.1. Ring-pack modeling

The ring-pack simulation used in this study was developed by Dr. Tian Tian [10] at MIT. In addition to modeling friction and lubrication between the ring and liner, the package contains an advanced ring dynamics module, allowing it to analyze details of ring movement such as flutter and collapse, and calculate parameters such as the ring dynamic twists and gas blow-by flows. In the study of surface finish a modified version of this model, developed by Jeffrey Jocsak [4] also at MIT, was used. This modified package includes sub-models that can account for a greater variety of surface textures than the original program, in both contact and fluid flow analysis. It is used concurrently with a numerical simulation created by Yong Li of MIT, which is used for the calculation of the flow and stress factors which are used in the analysis of rough surface fluid flow. A general diagram of the ring/liner system analyzed in these models is shown in Figure 2-1.

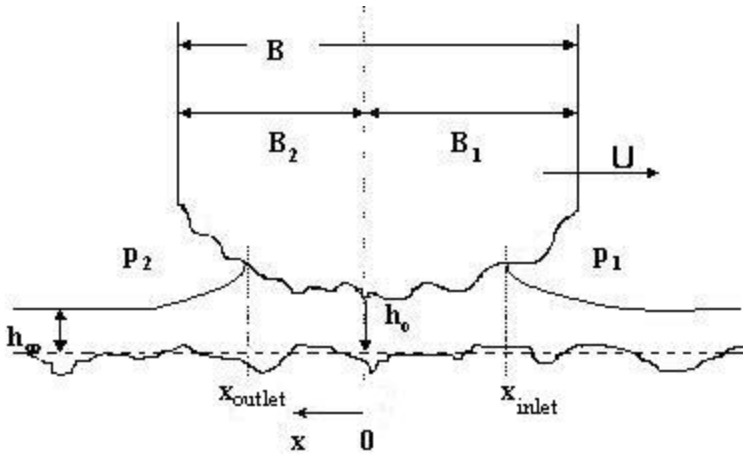

Figure 2-1: Schematic of ring/liner system. Surface roughness and ring curvature are exaggerated.

Calculation of ring/liner friction requires simultaneous solution of several relationships: a balance of radial forces on the ring must be satisfied, along with mass and momentum conservation for the lubricant flowing under the ring and a contact relationship for asperity contact. These relationships are interrelated by the oil film thickness and oil wetting locations on the ring. The hydrodynamic pressure, P_{hyd}, is strongly dependent on film thickness and wetting location, while the amount of asperity contact that occurs also depends on the film thickness. As the ratio between these two

pressures changes, the radial force balance changes also. A solution is found at an oil film thickness and wetting condition at which the ring load is supported by asperity, oil and gas pressures, and all boundary conditions are satisfied.

2.2. Modes of ring/liner lubrication

The ring can experience three modes of lubrication - hydrodynamic, mixed, and boundary - illustrated in Figure 2-2. In pure hydrodynamic lubrication, there is no contact between the ring and liner, and the ring load is entirely support by hydrodynamic pressure in the oil film. In this regime, the ring/liner friction results entirely from shear stress within the oil. In pure boundary lubrication, the entire ring load is support by solid-solid contact between the ring and liner, with no hydrodynamic contribution. In this case, ring/liner friction consists entirely of rubbing friction losses. When the ring load is partially supported by the oil pressure, and partially by asperity contact, mixed lubrication occurs. In this situation, friction losses stem from both oil shear and metal-metal rubbing.

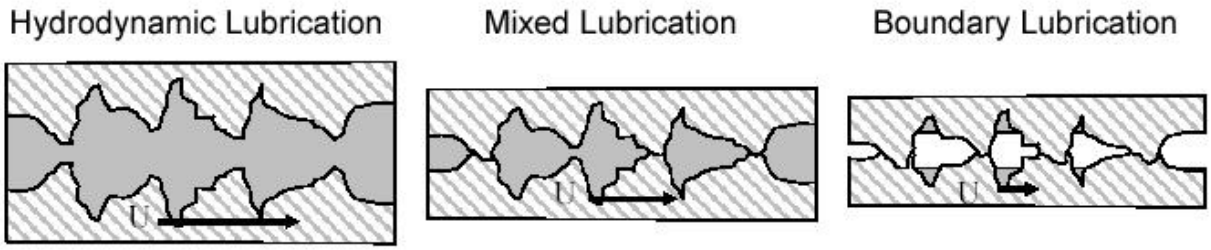

Figure 2-2: Modes of ring/liner lubrication

In the current model, the two surfaces are described stochastically, so it is not possible to ascertain whether any given asperity (local roughness peak) is contacting any other asperity. Instead a statistical limit is used, which determines the oil film thickness at which it is assumed negligible asperity contact occurs. This statistical limit is based on the combined roughness of the two surfaces, σ (where roughness is defined as the standard deviation of the surface height, measured from the mean):

$$\sigma = \sqrt{\sigma_{liner}^2 + \sigma_{ring}^2} \tag{2.1}$$

where σ is the combined surface roughness, σ_{liner} is the liner roughness, and σ_{ring} is the ring roughness. The amount of contact occurring is assumed to be negligible when the nominal separation between ring and liner and is greater than some factor, Ω, times this combined roughness. The model used in this study uses a value of $\Omega = 4$, where at the surface separation of $h = \Omega * \sigma = 4\sigma$, statistically, the probability of contact is less than 2%. Then, it is assumed in the analysis that:

$$\begin{aligned} \frac{h}{\sigma} &\le \Omega = 4 \quad && contact\ \ occurs \\ \frac{h}{\sigma} &> \Omega = 4 \quad && no \quad asperity\, contact \end{aligned} \tag{2.2}$$

where h is the mean oil film thickness.

2.3. Radial force balance

The ring load, including ring tension and gas pressure behind the ring, must be supported by some combination of asperity contact pressure, hydrodynamic pressure in the lubricant film, and gas pressures acting on the ring face. This balance is represented by the equation:

$$\sum F_r = 0$$
$$= \int_{x_1}^{x_2} P_{hyd}\,dx + \int_{-b_1}^{b_2} P_c\,dx + P_1(B_1 + x_1) + P_2(B_2 - x_2) - P_b(B_1 + B_2) - T_r(B_1 + B_2) \tag{2.3}$$

where P_{hyd} is the hydrodynamic pressure in the oil film, P_c is the asperity contact pressure between the ring and liner, P_1 is the gas pressure on the upper (combustion chamber) side of the ring, P_2 is the gas pressure on the lower (crank case) side of the ring, P_b is the gas pressure behind the ring, B_1 and B_2 are the upper and lower widths of the ring, x_1 and x_2 are the upper and lower wetting locations (x_1 is negative), and T_r is the ring tension, as shown in Figure 2-3. The ring inertia is not included in the radial force balance because it is much smaller than the other terms [10].

This relationship must be solved iteratively with asperity contact and hydrodynamic models, in order to determine oil film thickness, wetting locations, and pressure distribution in the lubricant.

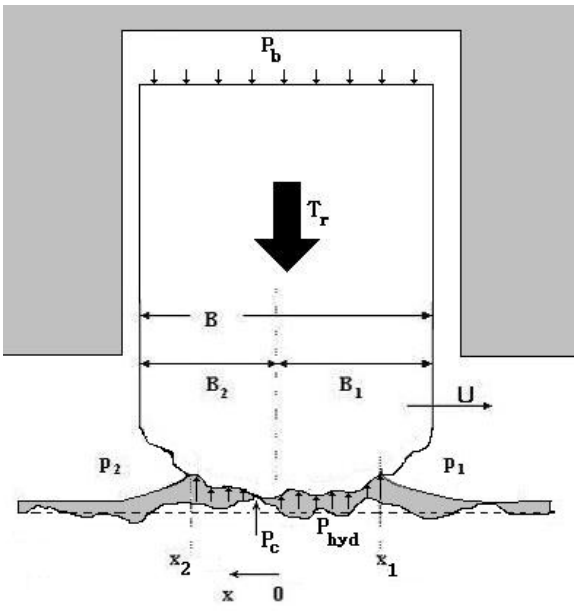

Figure 2-3: Schematic of ring/liner system

2.4. Asperity contact model

When solid to solid contact occurs between the ring and liner, an analysis that is based on the Greenwood and Tripp [1] asperity contact model, using a correlation developed by Hu [11], is used. Greenwood and Tripp's model describes the relationship of the elastic pressure of two contacting asperities with the distance between them:

$$P_c = \begin{cases} K' E' A\left(\Omega - \dfrac{h}{\sigma}\right)^z & \dfrac{h}{\sigma} \le \Omega \\ 0 & \dfrac{h}{\sigma} > \Omega \end{cases} \tag{2.4}$$

where P_c is the asperity contact pressure, K' is a constant related to the asperity geometry and distribution, E' is a constant related to the properties of the contact materials, A is a constant that can be used to calibrate predictions with measured data, σ is the combined roughness of the two surfaces, h is the nominal distance between the surfaces, Ω is the ratio of h/σ beyond which contact pressure is assumed to be negligible, and z is a constant. The coefficient K' is given by:

$$K' = \frac{8\sqrt{2}}{15}\pi(N\beta'\sigma)\sqrt{\frac{\sigma}{\beta'}} \tag{2.5}$$

where N is the number of asperities per unit contact area, and β' is the asperity radius of curvature. The coefficient E' is given by:

$$E' = \frac{2}{\left(\dfrac{1-\nu_1^2}{E_1}\right) + \left(\dfrac{1-\nu_2^2}{E_2}\right)} \tag{2.6}$$

where E_1 and E_2 are the Young's moduli for the two contacting surfaces, and ν_1 and ν_2 are their corresponding Poisson's ratios.

The relationship given in Eqn. 2.4 must be integrated over the apparent contact area to obtain a total contact force for the ring and liner. This can be done numerically, if deterministic surfaces are provided, or a stochastic model can be used. The analytical method used in this study uses a stochastic model, based on the Pearson system of frequency curves, which can describe surface characteristics based on RMS roughness, skewness, and kurtosis [1] (for definitions of Sk and Ku see Section 3.2). When reasonable assumptions are made for the values of asperity density and radius of curvature, this model can be used for predicting asperity contact pressure between ring and liner.

This asperity contact model assumes that deformation of the asperities is entirely elastic, and that plastic deformation does not occur. Although it is unrealistic to assume that this is the case in an engine, especially during the break-in period, it has been shown

by Greenwood & Tripp that the asperity contact pressure calculated for pure elastic deformation is very similar to that calculated with plastic deformation taken into account. Certain assumptions about asperity shapes and distribution are also made in this model, which are described in greater detail in 11]. Also, it should be noted that surface coatings such as oxide films or chemical layers created by friction modifiers have not been considered.

2.5. Lubricant flow and stress conditions – averaged Reynolds analysis

When hydrodynamic or mixed lubrication occurs, an averaged flow-factor Reynolds analysis is used to model the lubricant pressure and flows, and the interaction between the lubricant and surface asperities. Hydrodynamic support of the ring load depends on a "wedge" effect in which relative motion between sliding surfaces and changing flow area combine to increase pressure in the lubricant. The fluid pressure is then able to support an external load. Because of this effect, a positive pressure increase will occur in the oil in the converging section of the ring/liner interface, and pressure will decrease in the diverging section, as shown in Figure 2-4. The figure also shows cavitation in the oil film, which may or may not occur, depending on engine parameters and running conditions. Cavitation and oil detachment conditions are discussed further below. If the net pressure in the lubricant is positive the ring load can, at least partially, be supported by this hydrodynamically generated oil pressure.

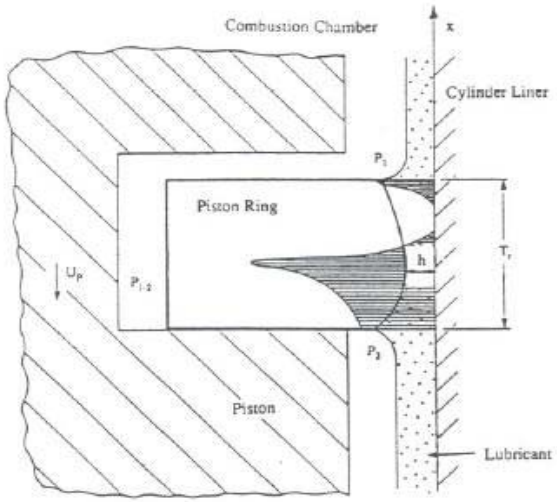

Figure 2-4: Schematic showing pressure distribution in the oil between ring and liner [14]

Analysis of the lubricant pressure and flow between ring and liner is based on Reynolds' equation, which is applicable for thin film flows where viscous phenomena dominate fluid inertia. The Reynolds relationship is derived from conservation of momentum for the fluid (Navier-Stokes relations) and conservation of fluid mass (Continuity), and (for a one-dimensional system) is given by:

$$\frac{\partial}{\partial x}\left(\frac{h^3}{\mu}\frac{\partial p}{\partial x}\right) = -6U\frac{\partial h}{\partial x} + 12\frac{\partial h}{\partial t} \tag{2.7}$$

when both sliding surfaces are smooth, and h is the nominal separation between the surfaces, μ is the fluid viscosity, p is the pressure within the fluid, and U is the relative sliding speed.

In reality, the sliding surfaces are never perfectly smooth. When the oil film thickness is much larger than the roughness of both surfaces, this roughness has very little effect and can be neglected. However, when the oil film thickness and surface roughnesses are of the same order of magnitude, the effects of the surface texturing must be considered.

Both deterministic and stochastic methods are available for describing roughness effects. Deterministic techniques include more detail about actual surface features, and can account more accurately for fluid flows and asperity contact between the ring and liner. However, such techniques are complex and time-consuming to apply, and may not be necessary when a simpler understanding of trends and general effects of different surface parameters is desired. This study uses a stochastic approach, based on the averaged flow factor method of Patir and Cheng [15].

The averaged flow factor technique uses several factors to account for the differences between flow between two smooth surfaces, and flow between rough surfaces. The Reynolds equation for smooth-walled flow is still used, together with three factors which account for the averaged effects of surface roughness:

$$\frac{\partial}{\partial x}\left(\phi_p \frac{h^3}{\mu}\frac{\partial p}{\partial x}\right) = -6U\frac{\partial}{\partial x}(h\cdot\phi_g + R_q\cdot\phi_s) + 12\frac{\partial h}{\partial t} \tag{2.8}$$

where ϕ_p is the pressure flow factor, ϕ_g is the geometric flow factor, ϕ_s is the shear flow factor, and R_q is the combined RMS roughness of the surfaces. Each factor is determined for a given surface, and accounts for the effect of the surface texturing on a given aspect of the fluid flow. The pressure flow factor represents the effect of the roughness on pressure-driven flow, while the shear flow factor represents the effects of surface roughness on shear-driven flow.

The geometric flow factor simply accounts for the fact that, as rough surfaces get closer together, they contact. The film thickness, h, used in the Reynolds equation is the nominal film thickness, taken as the mean distance between rough surfaces. However, the thickness required for shear flow calculation is the *mean* film thickness, which is equal to h in full hydrodynamic lubrication, but diverges from it when asperity contact occurs. When contact occurs, it is assumed that the overlapping asperities are simply sheared off, essentially changing the distribution of surface heights. Then, the location of the surface mean changes. The geometric flow factor takes this into account. When two surfaces are not contacting there is no change in surface mean heights and $\phi_g = 1$, nominal and mean surface separations are the same. When contact occurs, the mean film thickness becomes larger than the nominal, and $\phi_g > 1$.

Several methods for calculating flow factors are available. The technique used for factor calculation in this study is described in more detail in Section 2.7, below.

2.6. Boundary conditions

In addition to the flow factors, several boundary conditions are required to solve the Reynolds relationship given above. Continuity of pressures is required, so that the oil pressure at the top oil attachment point is equal to the gas pressure above the ring (P_1) and the oil pressure at the lower oil attachment point is equal to the gas pressure below the ring (P_2):

$$\begin{aligned} P(x_1) &= P_1 \\ P(x_2) &= P_2 \end{aligned} \tag{2.11}$$

Also, at the inlet, conservation of mass must be satisfied, so that the amount of oil flow under the ring at the inlet must be equal to the supply that was present on the liner prior to the arrival of the ring:

$$Q(x_{inlet}) = Uh_{\infty} \tag{2.12}$$

where $Q(x_{inlet})$ is the volumetric oil flow rate (per unit width) at the oil attachment point, and h_{∞} is the oil film thickness before attachment occurs. This condition is not valid when the ring inlet is fully-flooded - when there is more oil available than can be accommodated under the ring, and the excess is deposited on the leading ring face, as shown in Figure 2.5. In this case, the oil flow at the ring inlet is assumed to be equal to the amount flowing under the height of the ring surface at inlet:

$$Q(x_{inlet}) = U \cdot h(x_{inlet}) \tag{2.13}$$

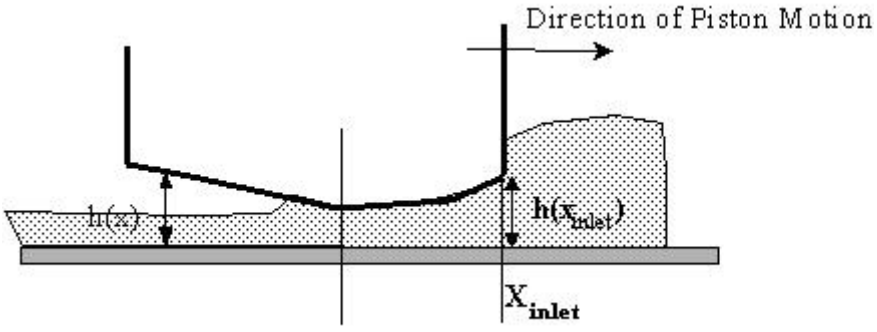

Figure 2-5: Illustration of fully-flooded inlet condition

An outlet condition must also be specified. A commonly used outlet condition is the Reynolds boundary condition:

$$\left.\frac{dp}{dx}\right|_{x=x_{outlet}} = 0 \tag{2.14}$$

which states that the pressure gradient in the oil must disappear at the ring outlet. This boundary condition can apply near the mid-stroke region of the cycle, where high relative speeds maintain hydrodynamic support of the ring, and at low enough gas pressures so that cavitation is not prevented. Near the end-strokes the Reynolds outlet condition is not applicable because, along with mass conservation, it requires oil to accumulate under the ring faster than it is being supplied at the inlet. In this region, then, a film-non separation boundary condition [16] is used, in which it is assumed that all of the oil exiting the ring/liner interface at the outlet stays attached to the ring, where it accumulates:

$$q_{x,outlet} = a \tag{2.15}$$

where $q_{x,outlet}$ is the flow rate of oil at the oil detachment point, and a is the accumulation rate of oil on the ring, defined as:

$$a \equiv h(x_{outlet}) \cdot \frac{dx_{outlet}}{dt} \tag{2.16}$$

2.7. Determination of flow and stress factors

The flow and stress factors that are used in the averaged Reynolds equation, and to determine shear stress are calculated deterministically, using the outputs from a numerical program developed by Yong Li at MIT. This model determines fluid flows and stresses between a smooth surface and the rough surface of interest, represented by a numerical matrix of surface height values. This matrix may be measured from an actual surface, (for example, using white-light interferometry) or generated analytically, as was done in this study. Comparing the deterministically calculated "actual" flows and stresses from this program to those calculated assuming smooth conditions and nominal surface separations provides the flow and stress factors.

Figure 2-6 outlines the program schematically. Conservation of mass and momentum are applied for the fluid, for each element in a grid. In the figure, q_x and q_y are the flows through a single control volume element in the x and y directions, respectively, and Δx and Δy are the distances between mesh points, which must be supplied as input. The cyclic boundary condition requires flows leaving the bottom of the flow region to re-enter at the top, thus conserving mass in the system. In the case of a piston ring, which can experience tangential oil flows, this is a more realistic boundary condition than the non-flow boundary condition applied by Patir and Cheng.

Pressure flow and stress factors are obtained by applying a pressure gradient across the system and calculating the resulting flow rate and shear stress. Shear factors are obtained by applying a relative motion to one surface, and calculating the resulting flows and stresses. All of these calculations must be made at a number of different mean film thicknesses, as the factors are functions of oil film thickness (or, more precisely, of the ratio of oil film thickness to surface roughness, h/σ.)

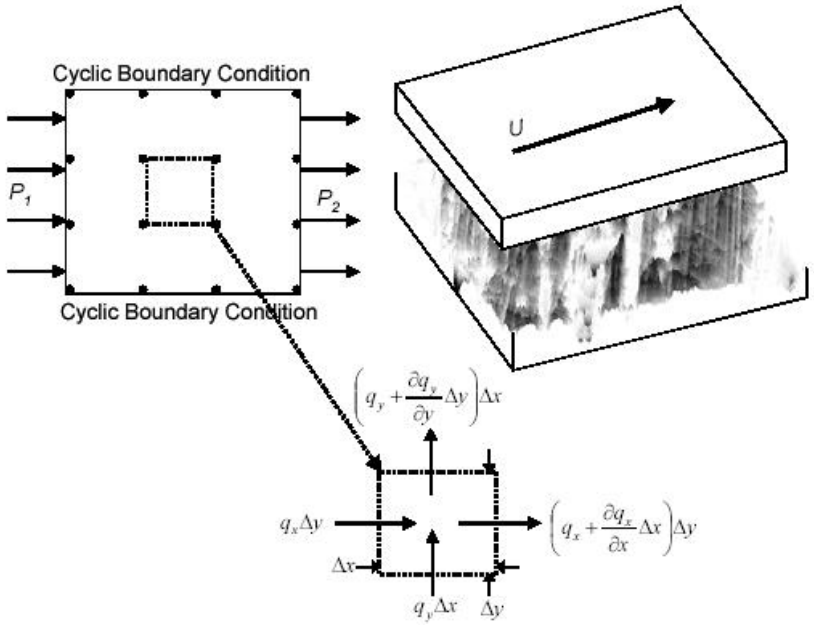

Figure 2-6: Schematic for Li's deterministic fluid flow and stress program

Once the flows and stresses are calculated numerically, the pressure and shear flow and stress factors are calculated by comparing these values to those calculated for smooth surfaces under the same flow conditions, and with the same nominal film thicknesses. The geometric flow and stress factors can be calculated from geometry only, and are defined by:

$$\phi_g = \frac{1}{h}\cdot\frac{1}{m(n-1)}\sum_{i=1}^{n-1}\sum_{j=1}^{m} H_s \tag{2.17}$$

$$\phi_{fg} = \frac{1}{h}\cdot\frac{1}{m(n-1)}\sum_{i=1}^{n-1}\sum_{j=1}^{m} \frac{1}{H_s} \tag{2.18}$$

where ϕ_g is the geometric flow factor, ϕ_{fg} is the geometric stress factor, m and n are the number of nodes in the x and y directions, h is the nominal surface separation, and H_s is the actual surface separation (when contact occurs $H_s = 0$). When there is no contact between the surfaces, both geometric factors are unity, the nominal and mean film thicknesses are equal. When contact occurs, the geometric stress factor, ϕ_{fg}, becomes unbounded and cannot be calculated. In these cases, H_s is set to a minimum height at which a limiting shear stress is assumed to occur. A detailed explanation for this substitution is given in [4].

The other flow and stress factors require input from the Li's numerical simulation for their calculation. With these values, calculation of flow factors proceeds from the

definitions of the factors - each is defined as the ratio of actual flow to that which is predicted by a smooth-wall model:

$$\phi_p = \frac{q_p}{\left(\frac{h^3}{12\mu}\frac{\Delta P}{\Delta x}\right)} \tag{2.19}$$

where ϕ_p is the pressure flow factor, q_p is the deterministically calculated flow between the two surfaces due to a pressure gradient, h is the nominal surface separation, μ is the fluid viscosity and $\Delta P/\Delta x$ is the applied pressure gradient;

$$\phi_s = \frac{q_s}{\left(\frac{U \cdot R_q}{2}\right)} \tag{2.20}$$

where ϕ_s is the shear flow factor, q_s is the flow between the two surfaces due to a relative velocity, U is the relative velocity between the surfaces, and R_q is the combined surface roughness (R_q is present in the denominator because it also appears in the averaged Reynolds equation modifying ϕ_s, see. Eqn. 2.8);

$$\phi_{fp} = \frac{\tau_p}{\left(\frac{h}{2}\frac{\Delta P}{\Delta x}\right)} \tag{2.21}$$

where ϕ_{fp} is the pressure stress factor and τ_p is the shear stress in the fluid due to an applied pressure gradient and;

$$\phi_{fs} = \frac{\tau_s}{\left(\frac{\mu U}{h}\right)} \tag{2.22}$$

where ϕ_{fs} is the shear stress factor, and τ_s is the shear stress in the fluid due to a relative motion between the surfaces.

Each of the flow and stress factors are calculated for a number of film thicknesses. Once these values are obtained, a curve-fitted equation is derived for each, which is then used for flow factor calculation in the ring-pack simulation program.

A number of assumptions are made in the numerical calculation program, and some inherent limitations dictate the manner of program use and the situations to which it can be applied. The size of the rough surface "patch" analyzed must be chosen with care, in order to be both small compared to the actual expected sliding area of ring and liner, and large compared to the surface texturing of interest. This is because the method makes the assumption that the effects of surface texturing can be well-represented by the averaged effect of the combined features, without taking into account the effects of each feature alone. Then, the patch must contain a large enough sample of the pattern of interest to

adequately represent all of the features and evaluate averaged effects. Also, since calculations are made based on sliding between nominally parallel surfaces, the patch must be small compared to the wetted area between ring and liner so that the curvature of the ring does not cause calculation inaccuracies. These requirements necessarily limit the size of surface features and patterns that can be studied using the averaged flow factor method, which must be small compared to the ring/liner wetted area.

Several assumptions are also made in the numerical calculations of fluid flows and stresses. Asperity level cavitation is not taken into account, so that negative pressures do develop in diverging areas. In reality, cavitation is likely to occur when dissolved air leaves solution in the oil, at approximately ambient pressure. While the no-cavitation assumption was also made by Patir and Cheng [15], further investigation of micro-scale cavitation effects is required. Also, realistic deformation of surfaces, upon contact, is not considered. Instead it is assumed that contacting surfaces shear off cleanly, and the removed portions are then no longer part of the calculation. Because the simulation is numeric, and thus based on discrete data points, a method of interpolation is also required. A linear interpolation method is imposed between surface height data points, and a viscous wedge flow solution applied. Further information about this model and its limitations are given in [4].

2.8. Calculating ring/liner friction

The above equations must be solved simultaneously to find the film thickness and wetting locations of the lubricant. Once this has been done (an adjustable step-size iterative algorithm is used), the results can be used to calculate the ring/liner friction (as well as many other parameters). The total ring/liner friction force is the sum of friction due to asperity contact and that due to shear in the lubricant.

The contact friction is assumed to be proportional to the asperity contact pressure, where the proportionality constant used is the boundary friction coefficient, f_b:

$$F_{f,asp} = \int f_b P_{asp} dA \tag{2.23}$$

The hydrodynamic component of friction results from shear stress within the oil, and is derived from Newton's relationship:

$$\tau(x) = \mu \left. \frac{\partial u}{\partial y} \right|_{y=0} \tag{2.24}$$

where μ is the oil viscosity, u is the fluid velocity in the x direction, and the y direction is across the fluid film. Substituting in for u:

$$F_{f,hyd} = \int_{wettedarea} \left(\frac{\mu U}{h} \left(\phi_{fg} + \phi_{fs} \right) - \phi_{fp} \frac{h}{2} \frac{dp}{dx} \right) dA \tag{2.25}$$

The total ring/liner friction force is then given by:

$$F_f = F_{f,asp} + F_{f,hyd} \tag{2.26}$$

This friction force is useful for assessing where, during the engine cycle, friction is generated, and what parameters contribute to friction. For reporting actual friction losses in an engine, however, another measurement is used. The work lost to friction, rather than the friction force, is the important parameter to consider when assessing a low-friction design. This is because this work determines the amount of extra fuel that will be required to overcome friction - the more fuel necessary, the lower the engine efficiency. Friction work is reported as the FMEP, friction mean effective pressure, which is the friction work normalized by engine displacement, and is given by:

$$FMEP = \frac{\int_{cycle} F_f dx}{V_d} \tag{2.27}$$

where V_d is the displaced volume of the cylinder (or of the entire engine, if the friction work evaluated is also for the entire engine).

2.9. Model applicability and limitations

Although it takes into account many of the complexities of the power cylinder system, the ring model used is nevertheless an approximation of reality, and is based on several assumptions that limit its applicability. Some of these are inherent in the averaged Reynolds method itself, while others stem from limitations in the current understanding of related phenomena.

Because it uses an averaged flow factor method, rather than a deterministic fluid analysis, the model used is limited in the surfaces to which it is applicable, as well as in the phenomena it can describe. It is inaccurate at very small film thicknesses (h/σ close to 1 or less) because, when it is continually interrupted by asperity peaks and flow blockages, the fluid flow is more strongly influenced by the actual, deterministic surface features than average effects. Also, textures to be analyzed cannot have features that are too large or "non-smooth." In the former case, the features and pattern under study must be small compared to the ring width, or the assumption that the cumulative effect of the texture features can be well-represented by average factors will be violated. (Details of patch size selection criteria are given in [4].) In the latter case, some textures may violate basic assumptions in development of the Reynolds equation, so that the Reynolds analysis itself may not be applicable for these surfaces.

One of the simplifications made in the development of the Reynolds equation is that, because the oil film is thin, there is no pressure gradient across the film thickness. However, for surface features that are very deep, have non-smooth edges, or otherwise cause too much disruption to a laminar flow, this will not apply. Figure 2-7 illustrates a case in which vortices appear in a deep feature, violating the stated assumption. In other cases sharp edges may cause turbulence, features may be too close together, or other

phenomena may disrupt the assumed flow pattern [17]. When textures of this nature are to be analyzed, a more detailed analytical method should be employed.

Also, in the calculation of the flow and stress factors, it is assumed that the gap between the two surfaces is completely filled with oil. In an actual engine it is likely that the ring/liner clearance will not be entirely filled, especially when surface texturing is present. For example, lubricant may not entirely fill a honing groove, or may be pushed to one side of the groove by pressure from the gases and ring movement, leaving a non-lubricated region. The averaged flow factor analysis does not account for this type of situation.

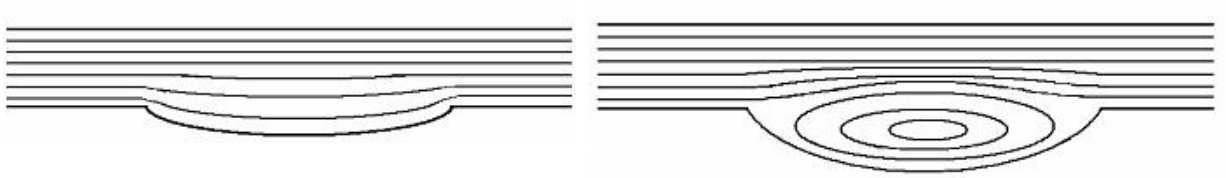

Figure 2-7: The averaged flow factor method is not applicable when surface features are too disruptive

Another limitation of the averaged method lies in its lack of ability to account for non-averaged phenomena. The averaged flow-factor analysis cannot describe many details of the flow and contact between ring and liner that may be of great importance in the actual ring/liner system. For example, flow of lubricant along honing grooves may play a major role in lubricant transport and friction, but this phenomenon cannot be modeled with the averaged method. Again, when phenomena of this nature is of interest, a more detailed, deterministic method is required.

In addition to some inherent limitations in the ring lubrication model itself, a limited understanding of related phenomena has lead to some simplifications. Oil transport is a very complicated phenomenon, and all of the mechanisms that affect it are currently not understood. Thus, the oil transport model used in the ring-pack analysis is necessarily simplified. In all of the analyses discussed, it is assumed that ample lubricant is available to the oil control ring, as well as to the second ring on down-strokes. Transport of oil into the "dry region" of the liner is not well-understood and the results shown should be considered to be preliminary. Also, all results shown are calculated on the pin side of the piston, and effects of piston rotation and secondary motion are not considered. Although it is possible to consider piston secondary motion with the current ring-pack model, the added complication of including this effect may have impeded clear understanding of the parameters under study, and so it was not included.

3. Analysis of Effects of Surface Characteristics on Ring-pack Friction

Modification of the surface textures of the ring or cylinder liner may reduce ring/liner friction. Such modification may also increase friction, however, or cause other adverse effects, so care must be taken to match the texturing to the system and conditions under study. Several mechanisms are proposed for the effect of surface finish on friction, including the removal of wear particles from the sliding interface by negative textures, use of negative textures as "lubricant reservoirs" to supply otherwise poorly-lubricated areas, and increase in hydrodynamic support due to "micro-hydrodynamic" action of surface features. In addition, several types of surface modification are considered. These can be separated into the two broad categories of stochastic modifications, including the control of statistical surface parameters such as the roughness and skewness, and deterministic modifications, which consist of placing specific features, such as dimples, at specific locations on the surface.

This study focuses on adding deterministic textures to the cylinder liner, and the effects of such texturing on the hydrodynamic support of the ring load. An averaged Reynolds analysis, using deterministically calculated flow factors, was used to perform a parametric study on both grooved and dimpled textures. The main friction-reducing effect of such textures is to increase flow resistance, thereby increasing oil film thickness. When film thickness is increased, asperity contact is reduced and hydrodynamic friction also decreases, because of the corresponding decrease in oil shear rate. While limitations of the model must be taken into account, results of this study indicate that both grooved and dimpled surface features can cause a reduction in ring/liner friction, where the optimum texture is determined by engine parameters and running conditions.

3.1. Background and review of current surface texture research

Surface texturing has been recognized as a method for enhancing the tribological properties of surfaces for many years. Adding a controlled texture to faces in relative motion can have many positive effects, such as reduction of friction and wear and increase in load capacity. Early studies recognized the potential of microasperities to provide hydrodynamic lift during film lubrication [18-20], while later research indicated that small-scale texturing could also trap wear particles [21] in boundary and dry lubrication. A further use of microtextured surfaces may be found in the use of partial texturing – a textured region can take the place of macro-geometry such as steps or inclined planes meant to provide hydrodynamic lift [22]. All of these effects may decrease friction and wear between two sliding surfaces, but some experimental results also show a negative effect from surface texturing. In some cases texturing is not optimized for a given case, in others there is no optimal case – any kind of texturing may be worse than a smooth surface. Research and analysis presented to date demonstrates both the potential to improve tribological properties via surface texturing, and the need to understand materials, lubricants, and running conditions before a surface texture is applied.

Micro-topography consists of micron-scale surface features, either negative (cut into the "flat" surface) or positive (protruding). Early textures were limited to grooves and troughs, while new techniques have allowed complex patterns of different shapes,

including circular, triangular, and other geometric shapes, to be used. Asperity shape, geometry, depth, area ratio (the ratio of asperity to flat area) and orientation can all impact the effectiveness of a given texture.

Several methods are now available for creating this surface micro-topography. Mechanical techniques such as viborolling and abrasive machining can be used to create grooves, while other methods including reactive ion etching (RIE), other forms of etching, and lithography can produce a variety of shapes in both metals and ceramics. In recent years laser surface texturing (LST) has emerged as a versatile and high-speed texturing method that can provide well controlled surface characteristics for a variety of materials. This method has been used in the magnetic storage industry for several years, and is currently the focus of several studies [8].

Recent and past studies have explored the effects of these various methods and of different microasperity parameters on friction, wear, and other issues. A limited number of analytical models have been proposed, mostly considering hydrodynamic effects of microtexturing, while the majority of studies have been experimental. The outcome of research to date indicates that optimal surface texturing parameters depend on the running conditions studied and on the dominant mode of lubrication considered. Surface texturing can provide a benefit in several ways: decreasing friction during well-lubricated sliding by providing hydrodynamic lift, acting as reservoirs for lubricant, and removing wear particles from the sliding interface. Each of these modes is discussed in further detail below.

3.1.1. Boundary and non-lubricated sliding

When lubrication is poor (or non-existent) or hydrodynamic lubrication is made difficult for other reasons, the main effect of micro-texturing is likely to be its ability to remove wear particles from the sliding interface. In general, it is expected that this particle-removal action will reduce friction and wear, as in many engineering situations most friction is due to plowing. Suh, et. al [21,23] performed much of the pioneering research in this field, demonstrating that the addition of grooves to a surface caused wear particles to be removed from the interface, and measuring reduced sliding friction for many cases.

Other research, however, has shown that friction can increase when grooves and other textures are added to sliding surfaces. In cases where plowing is not the main friction mechanism, removing particles from between sliding surfaces can cause an increase in friction due to adhesion, because the surfaces can come into closer contact when wear particles are not present to keep them apart. In other cases, a beneficial chemical reaction may generally occur between sliding surfaces and wear particles, and when the particles are removed the reaction no longer occurs. Petersson and Jacobson [24] conducted an experimental study in which adding dimples greatly increased the sliding friction of silicon coated with diamond-like carbon (DLC), because a beneficial tribo-film did not form in the textured case. In other tests, adding texturing can increase friction but the mechanism is not clear. While many studies have shown that texturing removes wear particles from a sliding interface, a good understanding of the chemical

interaction of the two sliding materials is required to predict what effects on friction will be.

In poorly lubricated cases, surface dimples may also decrease friction by acting as "lubricant reservoirs" that help to maintain an adequate lubricant supply. Blatter, et. al [25] demonstrated that the presence of small grooves (on a sapphire disk, sliding against steel) could cause a delay in the loss of lubrication in a case where a small amount of oil was introduced at the beginning of a sliding test, which was then allowed to run until failure (a sudden increase in friction coefficient). For some grooved cases, the number of cycles for which lubricated sliding was maintained was an order of magnitude greater than that for smooth surfaces. Lubricant reservoirs may be particularly useful where lubricant availability is intermittent. In these cases, dimples may act as "lubricant capacitors," storing oil when it is readily available and re-supplying it to the sliding interface when it is scarce.

3.1.2. Hydrodynamic effects

Like large scale converging surfaces, micro-scale asperities can create an asymmetric oil pressure distribution that results in hydrodynamic lift. In cases of mixed lubrication, this added lift can alter the balance between hydrodynamic and boundary lubrication, reducing the amount of asperity contact that takes place, and thus reducing both friction and wear. Also, even when contact does not occur, an increase in oil film thickness reduces shear within the oil, reducing hydrodynamic friction. Several studies, both analytical and experimental, have considered the effects of surface patterns in hydrodynamically lubricated cases.

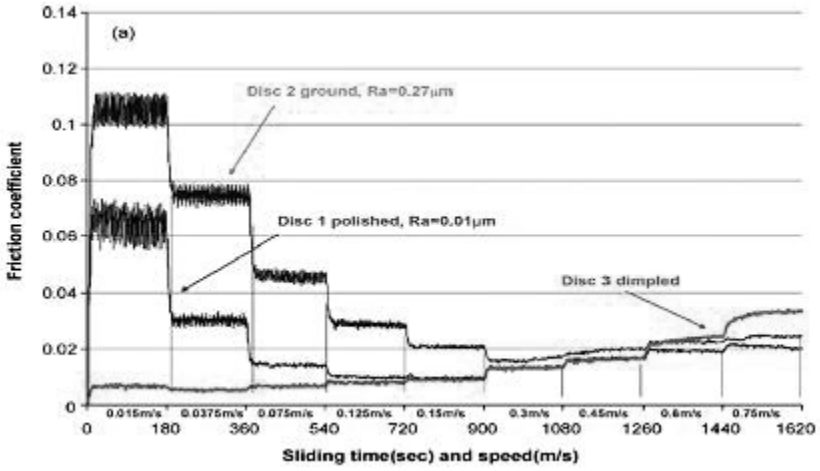

Figure 3-1: Adding dimples delayed the onset of asperity contact in this test, from Kovalchenko, et. al [26]

Because they can assist in creating hydrodynamic pressure in the fluid film, textured surfaces have an effect on the lubrication regime of sliding surfaces. Kovalchenko et.al. looked closely at the lubrication regime effect in a series of experiments using a pin-on-disk test rig with unidirectional sliding, with a textured disk [26]. This study produced Stribeck-like curves for various lubricants and load conditions,

and different dimpled area densities (the depth:diameter ratio for the dimples was maintained at an "ideal" value in all cases). In general, dimpling expanded the range of parameters under which hydrodynamic lubrication took place, extending the non-contact regime to low speeds and viscosities. An example of Kovalchenko's results is shown in Figure .

Sadeghi, et al. has also demonstrated that texturing can reduce asperity contact, analytically showing that adding dimples in the end-stroke region of a reciprocating slider can reduce overall friction by reducing contact in this area [27]. A deterministic model of mixed lubrication was used in this study, which showed that friction reduction for a reciprocating cycle is possible when round dimples are added to one surface. (The metric for "friction" used here was the cycle average friction coefficient. This over-represents the importance of end-stroke friction compared to friction power loss, which represents the actual energy required to overcome friction.) An example of Sadeghi's predictions are shown in Figure 3-2, which shows an almost complete removal of asperity contact in the textured region.

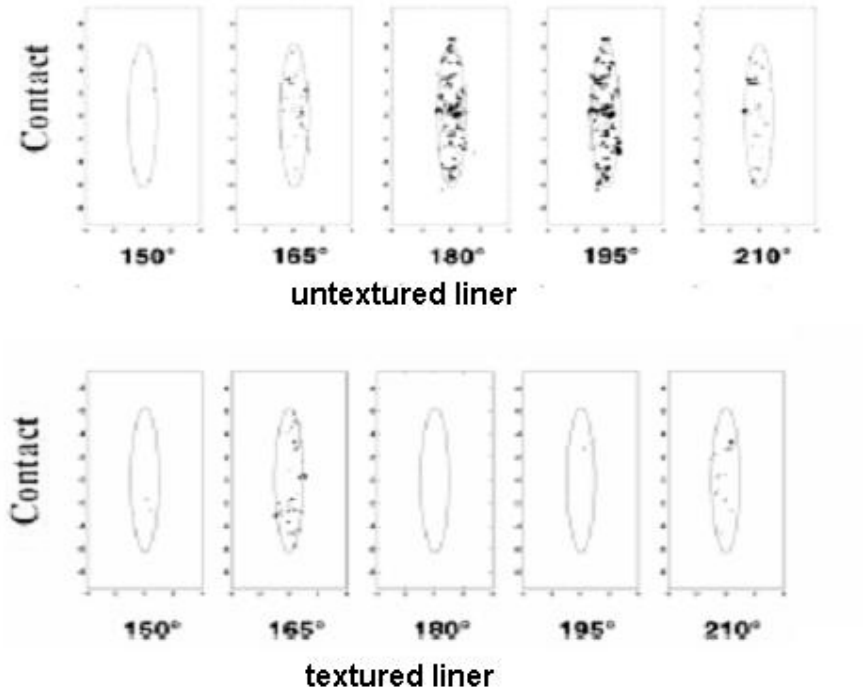

Figure 3-2: Modeling shows a reduction in asperity contact when liner texturing is added [27]

Studies have also shown that friction can be reduced when surface dimples are added even when no contact occurs. Etsion, et. al. have completed several analytical and experimental studies considering the effects of round dimples on sliding friction and load support. Early studies, based on a CFD model in which contact was not considered, predicted increased load support in face seals with the addition of dimples, where the ratio of depth:diameter was the main factor in optimizing the texturing. A depth:diameter ratio of approximately 0.1 was predicted to be optimal for almost all cases [28]. (As in

the case of Sadeghi, the measurement of friction used in Etsion's study is mean cycle friction coefficient.) In-place testing in working pumps showed increased life and reduced wear as predicted [8]. Subsequent analysis of "piston-ring like" cases showed that optimized dimpling could also decrease friction in reciprocating sliding, again, due purely to hydrodynamic friction reduction as asperity contact was not considered. Reciprocating-slider testing showed reduced friction, as well as a dependence on oil supply, suggesting that the dimples were effective only in a well-lubricated regime, and may actually be harmful in poorly-lubricated situations [29,30].

Many other studies, both analytical and experimental, have studied the effects of surface texturing. Stephens and Siripuram [31] as well as Hsu [32] considered the effects of different dimple shapes. Stephens and Siripuram considered circular, square, diamond, hexagonal and triangular cross-sections, and concluded that friction reduction was generally independent of shape. Hsu, however, concluded that dimple shape could have some effect, and that, in particular, shapes with an orientation more perpendicular to the sliding direction could delay the onset of asperity contact. (Results also indicated, however, that round dimples had almost no effect, in disagreement with several others). Other researchers have also predicted that texture orientation has an effect on friction and oil film thickness. Michail and Barber [33] predicted increased oil film thickness for textures more perpendicular to the sliding direction, while Jocsak [4] also predicted increased film thickness and reduced friction for lower honing groove cross-hatch angles (grooves more perpendicular to the sliding direction).

Many experimental and analytical studies have predicted friction reduction with the addition of appropriate texturing to sliding surfaces. As can be seen from this brief literature review, however, there is no general agreement on what types of textures should be added, what texture parameters are the controlling factors in friction reduction, and even what the effects of various texture parameters are. Much work still remains in this field before a good understanding of the effects of surface texturing is achieved.

3.2. Describing surface textures and finishes

Several different systems have been created for stochastically describing surface textures, while in deterministic studies patterns must generally be represented by actual measured or simulated data sets. Both stochastic parameters and deterministic descriptions are used in this analysis of surface texture effects, with deterministic surfaces used to calculate flow and stress factors and stochastic parameters used to define asperity contact mechanics. The deterministic surfaces are generated using a method described in Section 3.4.1, while the system of stochastic parameters used is described below.

Several methods and standards exist for measuring and characterizing surface finish. Techniques such as white-light interferometry (WLI) can give three-dimensional measurements of surface textures, while profilometers and similar instruments provide two-dimensional measurements of surface height along a linear path. Both types of measurement can be used directly when a deterministic description of a given surface is desired. However, in many cases the use of a deterministic measurement in an analysis or as a description of a given surface is too complicated or time-consuming, and

stochastic parameters are used. These parameters statistically describe the variation in height of a surface, and can provide a general understanding of surface characteristics.

There are several different standards which are used to define stochastic parameters for surface measurement, most of which describe only variations in the surface height, and not spatial variations along the length and width. In this study, three parameters are used to describe surface height distribution: the roughness, skewness, and kurtosis. These three parameters are all derived from a statistical analysis of the distribution of surface heights, where the roughness, σ, is defined as the standard deviation of the surface heights, the skewness, Sk, is the third standardized moment about the mean, and the kurtosis, Ku, is the fourth:

$$\sigma = \sqrt{\frac{1}{N}\sum_{i=1}^{N}(x_i - \bar{x})^2} \tag{3.1}$$

$$Sk = \frac{\frac{1}{N}\sum_{i=1}^{N}(x_i - \bar{x})^3}{\sigma^3} \tag{3.2}$$

$$Ku = \frac{\frac{1}{N}\sum_{i=1}^{N}(x_i - \bar{x})^4}{\sigma^4} \tag{3.3}$$

where N is the number of data points included in the distribution, x_i is the surface height at a given point, and $\bar{x}$ is the mean surface height. These parameters can also be defined using the probability distribution function of the surface height distribution, if this function is known.

The surface roughness, σ, is simply the standard deviation of surface heights, and is an approximate representation of the height of the surface asperities above the mean. Skewness can be thought of as the asymmetry of the distribution. A negatively skewed surface has a plateau surface and many low valleys, while a positively skewed one has wide, flat valleys along with high peaks, as illustrated in Figure 3-3a. Kurtosis is often described as the "peakedness" of the distribution, and represents the number of surface height measurements that are very far from the mean. A surface with high kurtosis has a very wide distribution ("thick tails") of surface heights, with many high peaks and low valleys, while a low kurtosis surface is relatively flat, with most of the surface heights close to the mean, as shown in Figure 3-3b. For a Gaussian surface, skewness = 0, and the kurtosis = 3. The effect of these parameters on friction was not considered in this study, as the focus was on larger scale patterns, but they have been considered extensively by others [4,34].

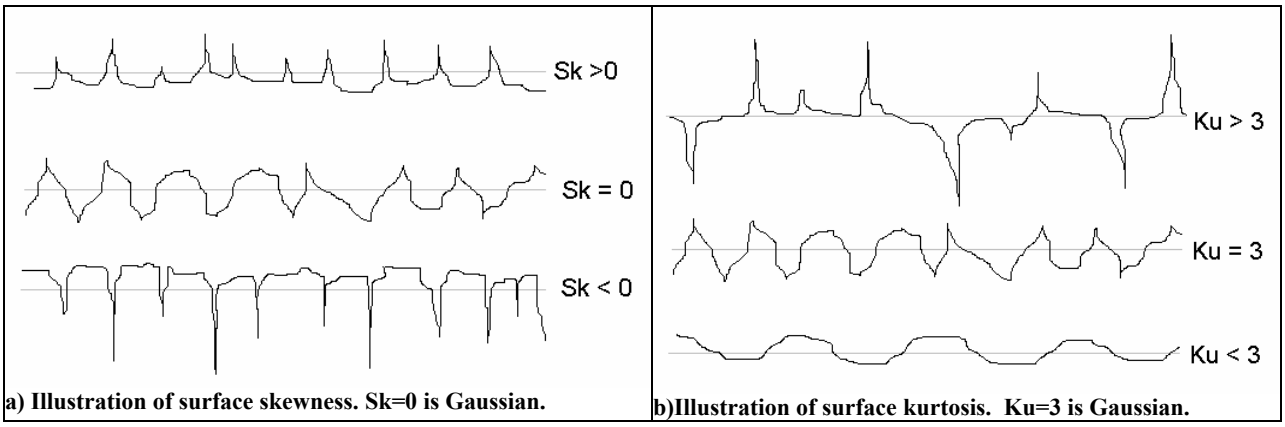

a) Illustration of surface skewness. Sk=0 is Gaussian.

b)Illustration of surface kurtosis. Ku=3 is Gaussian.

Figure 3-3: Illustrations of surface skewness and kurtosis

These parameters can be used, along with the Pearson system of frequency curves, to represent a rough surface in the calculation of contact pressure. The Pearson system is a curve-fitting method that derives the probability distribution function of a surface from its roughness, skewness and kurtosis. This distribution is then used to determine the amount of contact expected to occur, statistically, at a given separation between surfaces, and to then determine the contact force.

3.3. Averaged flow-factor Reynolds analysis

An averaged flow-factor Reynolds analysis was used in this study to evaluate the effects of grooved and dimpled surfaces. This method, and its limitations, are described in detail in Section 2. Because this method was used, the surface features studied were limited to a relatively small size, compared to many that have been studied in the literature. Also, the method does not allow the detailed analysis of flows and stresses that would be possible using a deterministic method. Still, the averaged method can provide information about the effects of various surface finishes, and reveal the trends in film thickness and ring/liner friction whose discovery was the object of this parametric study.

The averaged flow factor method can also shed some light on the physical effects of rough surfaces, in the interpretation of the flow and stress factors themselves. While a physical explanation of the factors' meanings is not agreed upon, understanding the various interpretations can give some intuition into the effects of rough surfaces. Also, looking at the relative importance of each factor in affecting fluid flow and stresses can aid in understanding the relative importance of the various physical parameters in the ring/liner system.

3.3.1. Physical interpretation of factors

The flow and stress factors represent the difference between the sliding of two smooth surfaces and the sliding of rough, textured surfaces. The physical effect of surface roughness on fluid flow is complex and depends on the nature of the actual surfaces under study. However, it is possible to give a general physical interpretation of what the factors represent, to partly describe what occurs in the lubricant between rough surfaces.

Figure 3-4 illustrates one possible interpretation. For two smooth surfaces, there is a clear definition of the distance between them, which is also the thickness of the oil film if it is entirely filling the gap. For rough surfaces, the definition of gap height becomes complicated – its actual value depends on the surface features – and so an average value is used. Generally, this average value is taken as the difference between the mean surface heights of the rough surfaces, h_{mean} as shown in Figure 3-4b. In determining flow and stress factors, a comparison is made of smooth surface conditions vs. rough surface conditions at the same film thickness, where for the rough surface h_{mean} is used, and for the smooth surfaces h is used.

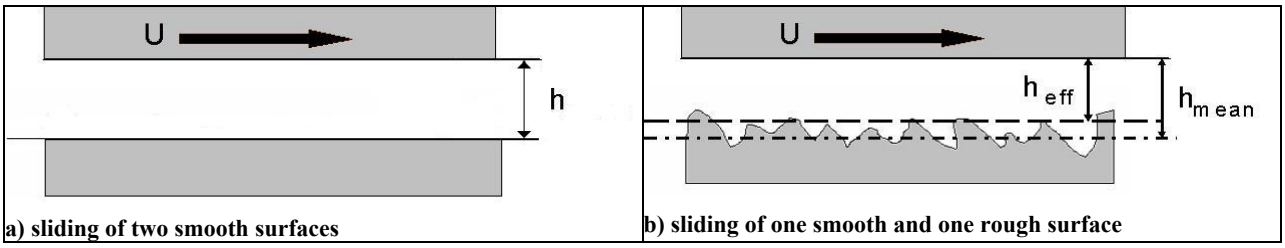

Figure 3-4: Flow and stress factors can be interpreted in relation to an effective film thickness

The effect of the roughness, however, is to make the effective region in which flow occurs even smaller than h_{mean}. If fluid remains trapped and stagnant in the roughness valleys, an effective flow thickness will be smaller than h_{mean}, and be closer to h_{eff}, in Figure 3-4b. In this interpretation, the roughness impedes flow simply by making the effective flow area smaller. For a pressure-driven case, the roughness will impede flow and increase pressure in the fluid for any rough surface. For shear-driven flow, fluid transport will be impeded if the stationary surface has a higher roughness, while it will be increased (due to transport of the stagnant fluid trapped in the valleys) if the moving surface is rougher.

The reduced effective film thickness also has an effect on shear stress. For a thinner oil film the shear rate within the fluid is higher, so shear stress is also higher. These effects can be observed in Section 3.3.2 below, which shows the effects of the different flow and stress factors on oil film thickness and ring/liner friction.

A second interpretation of the flow factors is based on their locations in the equation for oil flow rate:

$$Q = -\phi_p \frac{h^3}{12\mu}\frac{dP}{dx} + \frac{U}{2}\left(h\phi_g + R_q\phi_s\right) \tag{3.4}$$

In this equation, the pressure flow factor appears with the viscosity, μ, while the shear flow factor is coupled with the film thickness. Then, the effect of the pressure flow factor can be considered to modify the viscosity, and an "equivalent viscosity" can be defined:

$$\mu_{eq} \equiv \frac{\mu}{\phi_p} \tag{3.5}$$

An increase in ϕ_p can be thought of as a decrease in equivalent viscosity, and vice versa. Then, a low pressure flow factor indicates increased flow resistance, (high equivalent viscosity) as expected. Similarly, an equivalent film thickness:

$$h_{eq} \equiv h \cdot \phi_g + R_q \phi_s \tag{3.6}$$

is defined, with the shear and geometric flow factors. A decreased shear flow factor reduces the equivalent film thickness, decreasing shear-driven flow. The shear flow factor is related to the relative velocities of the sliding surfaces, so that when the rougher surface is stationary the shear flow factor will be negative, thus causing a decrease in equivalent film thickness.

3.3.2. Relative contributions of flow and stress factors

Each of the flow and stress factors has some effect on predictions of flow and stress within the lubricant. The pressure flow factor, however, has by far the dominant effect on flow, stress, and overall friction losses for the ring and liner. This suggests that the main effect of adding roughness to a sliding surface is on pressure-driven flow, and specifically in increasing the resistance to pressure-driven flow, and thus increasing hydrodynamic pressure within the fluid. Thus, the main effect of adding roughness appears to be increasing load support, or, for a given load, increasing film thickness. This has the simultaneous friction-reducing effects of reducing asperity contact, if there was any to begin with, and decreasing shear rate, and thus shear stress, in the fluid.

Figure 3-5 and Figure 3-6 show the effects of changing each of the flow and stress factors. A "smooth" case, in which flow factors were kept at their smooth surface values, is compared to cases in which a single factor is changed to its value for a surface with horizontal grooves, a surface with very different flow and stress factors than the smooth case. Then, each curve shows the effect of changing a single factor. As the figures show, changing the pressure flow factor has the dominant effect, with a smaller contribution from the shear stress factor. The shear flow and pressure stress factors have negligible effects, and cannot be distinguished from the "smooth" baseline in the figures.

Figure 3-6, which shows the total friction force between the ring and liner, also illustrates that the effects of the different factors are approximately additive. The change in pressure flow factor causes a large decrease in friction force, while changing shear stress factor causes a small increase. When all factors are changed to their rough surface values, the resulting friction force is the summation of those resulting the individual factor changes.

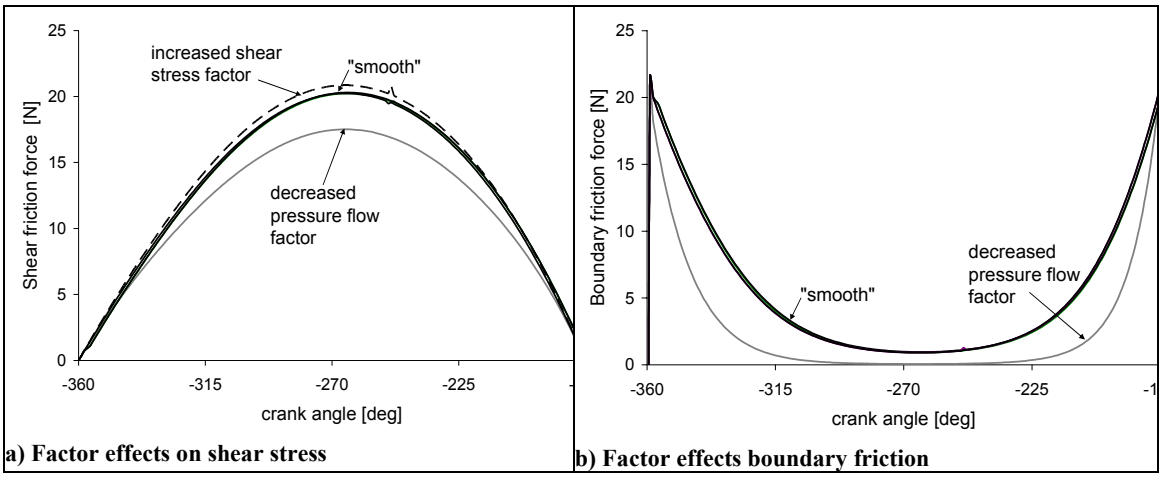

Figure 3-5: Flow and stress factor effects on hydrodynamic and boundary friction

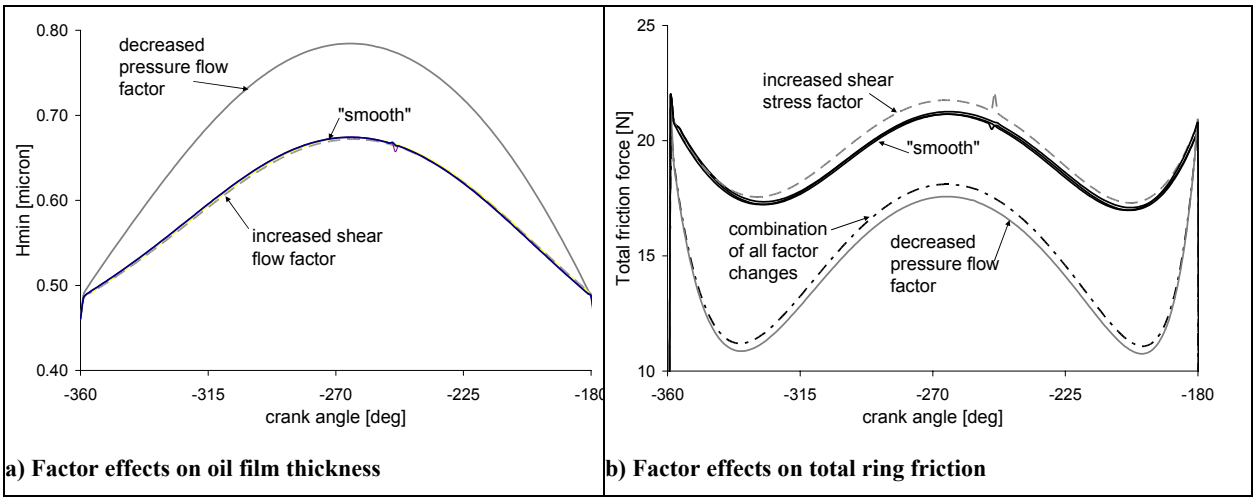

Figure 3-6: Flow and stress factor effects on oil film thickness and total ring/liner friction

3.4. Parametric study: grooves and round dimples

The averaged Reynolds equation method, summarized above and in Section 2, was used to study the effects of dimpled and grooved surface features on ring/liner friction. Surfaces with dimpled and grooved surface textures were first generated using a MATLAB program written for this purpose. Several programs written to facilitate the calculation and curve-fitting of flow factor relationships were used to obtain flow and stress factors. These factors were then used in the MIT ring-pack simulation program to predict ring/liner friction for different cylinder liner surface textures. Although not able to predict complexities of lubricant flow and surface contact that require a deterministic approach, this study was able to demonstrate trends in frictional losses with changing surface parameters.

This study did not consider the effects of stochastic surface properties such as roughness and skewness. Rather, the effects of patterns of discrete features, specifically dimples and grooves, were studied. Parameters considered include: for the dimples,

diameter, depth, area ratio, and arrangement (hexagonal or rectangular); and for the grooves, width, depth, area ratio, angle, and arrangement (cross-hatch or parallel grooves). Area ratio is the percentage of the surface occupied by the surface features. The range of parameter values studied is given in Table 3-1.

As for the lubricant study, this study of surface texturing focused on the oil control ring, and all friction results presented below are for the oil control ring/liner interface only. This is because, as noted previously, the oil control ring contributes the majority of ring-pack friction, and most of the remaining losses stem from the top ring in the "dry region" where hydrodynamic effects are not expected to make any impact on friction (since there is little to no oil present). Thus, all predicted FMEP trends are for the oil control ring only, although they can be expected to also be representative of trends for the entire ring-pack, as surface texturing of the type studied should have little effect on the other major sources of ring-pack friction.

Table 3-1: Range of surface texture parameters studied

Parameter	**Range**
Dimples:	
Diameter	5-25 μ
Depth	3-8 μ
Area Ratio	10-22%
Arrangement	hexagonal or rectangular pattern
Grooves:	
Width	11-30 μ
Depth	3-8 μ
Area Ratio	15-35%
Angle	0-90^{o}
Arrangement	parallel or cross-hatch pattern

3.4.1. Method of surface construction

The textured surfaces used in this parametric study were simplified so that the effects of the surface features under consideration could be considered alone, rather than being coupled with the effects of a realistic surface roughness. Instead of using a rough texture, then, the "flat" part of the surface was assumed to be smooth, with either grooves or round dimples the only features present. Two examples of these surfaces are shown in Figure 3-7. In both Figure 3-7a and Figure 3-7b the vertical scale is exaggerated, so that the feature depth seems very large and the profile very sharp. In fact, the grooves and dimples studied were quite shallow.

The surfaces were generated using a two-stage process. In the first stage, the desired feature parameters were used as inputs to generate a matrix that indicated where the given features were to be placed on the surface. Then, this matrix was convolved with a second matrix that was built based on the desired feature profile. In all of the cases presented below, the features were given a Gaussian profile, because of its ease of

construction and smooth shape. Because of the modular structure of the surface-generating program, however, it is easy to accommodate different profiles as well as different patterns and shapes.

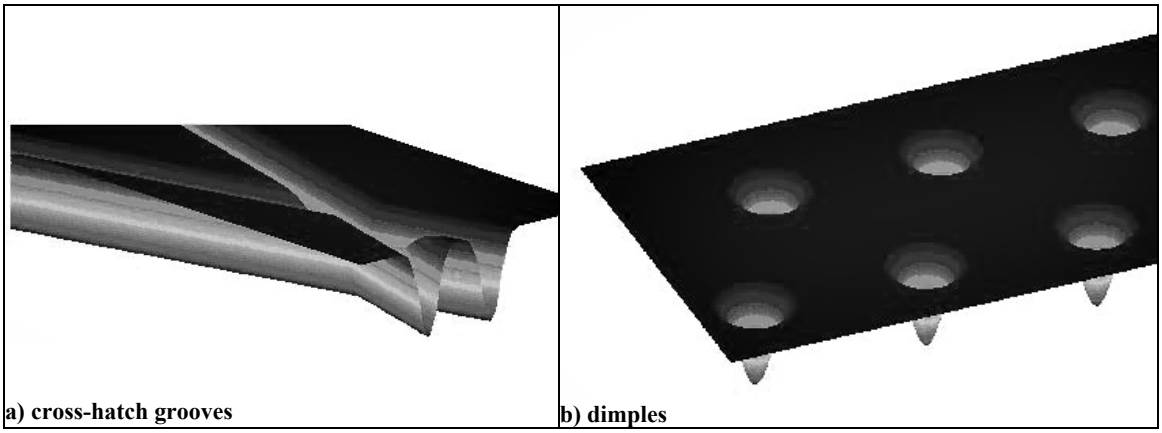

Figure 3-7: Examples of generated surfaces

It should be noted that the definition of groove angle was based on a cross-hatch groove pattern, as shown in Figure 3-8. The stated groove angle, in all results presented below, is twice the angle between the groove and a line perpendicular to the flow direction. This standard was adopted because optimization of a cross-hatch pattern, which is commonly found on honed cylinder liners, was thought to be the most likely application of the groove analysis. The same definition of angle was used for both cross-hatch and parallel groove patterns.

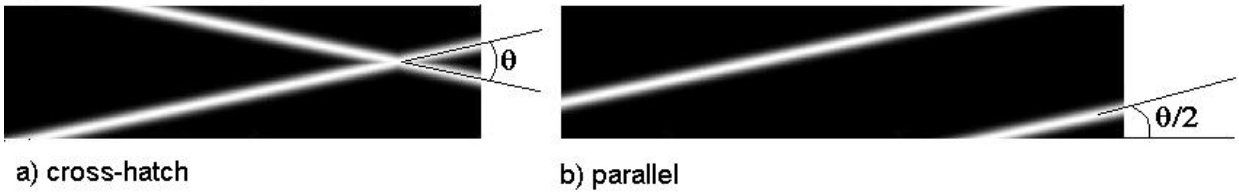

Figure 3-8: Definition of groove angle for cross-hatch and parallel patterns

3.4.2. Grooves: effect of linear surface features on sliding friction

Surfaces with various grooved patterns were studied, to find the effects of the groove parameters on ring/liner friction. Groove angle had the largest effect. Within the range studied, very small angles (grooves more perpendicular to flow direction) caused a reduction in friction, while grooves more parallel to the flow caused a friction increase. Depth also had a large effect, with deeper textures generally showing reduced friction. In some cases, an ideal depth at which friction was minimized was found. Friction also decreased with increasing area ratio, and with groove width to a point, after which increasing width had no effect.

Both flow factor and FMEP results are presented below. Pressure flow factor, which has the largest effect on ring/liner friction, is shown, as are friction results. It should be noted that, for very deep textures in particular, the surfaces studied may be on the edge of the range of applicability for the averaged-flow-factor model. Also, this model is known to have inaccuracies at very small film thicknesses.

3.4.2.1. Flow factor results

Only pressure flow factor results are presented below, because this factor has the main effect on ring/liner friction, as demonstrated in Section 3.3.2. In general, a lower pressure flow factor indicates a decrease in ring/liner friction, because of the implied increase in hydrodynamic pressure generation.

Groove pattern had almost no effect on flow factor or ring/liner friction calculations. Figure 3-9 shows an example comparison of pressure flow factor calculations for cross-hatch and parallel ("single") groove patterns. In general, very little difference was found between cross-hatch and parallel groove results, as is indicated in the figure. Because of this, only parallel-groove results are presented in the remainder of this report.

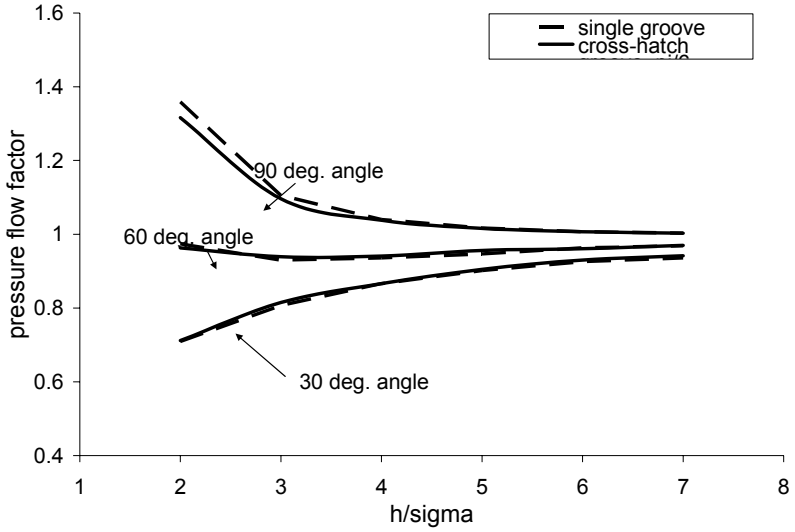

Figure 3-9: Flow factor results for parallel and cross-hatch groove patterns are very similar

Figure 3-10 shows the effects of groove angle on pressure flow factor. As Figure 3-10a shows, pressure flow factor decreases with decreasing groove angle – as the grooves become more perpendicular to the flow direction. For large angles, $\theta > 60^{o}$, pressure flow factor increases beyond 1, the smooth surface value, and increases for larger angles. This means that for large groove angles, the presence of the grooves causes fluid to flow more easily, reducing load support and, as is shown in Section 3.4.2.2, also increasing friction.

For more perpendicular grooves, the diverging/converging nature of the texturing creates a "micro-hydrodynamic" pressure peak in the fluid, where oil that enters the groove is pushed against the opposite wall, which creates flow resistance and a pressure increase. This flow impedance causes a reduction in flow and thus pressure flow factor. For grooves with larger groove angles, which run more parallel to the flow direction (the largest angle considered is 90°, in which the grooves run at 45° to the flow direction) oil that enters the groove is partially pressed against the opposite wall, but is also able to flow along the groove relatively easily. For high groove angles, then, the effect of the addition of the grooves is to increase the effective flow area for the fluid, by adding the area within the grooves. This increases fluid flow, thus increasing the pressure flow factor.

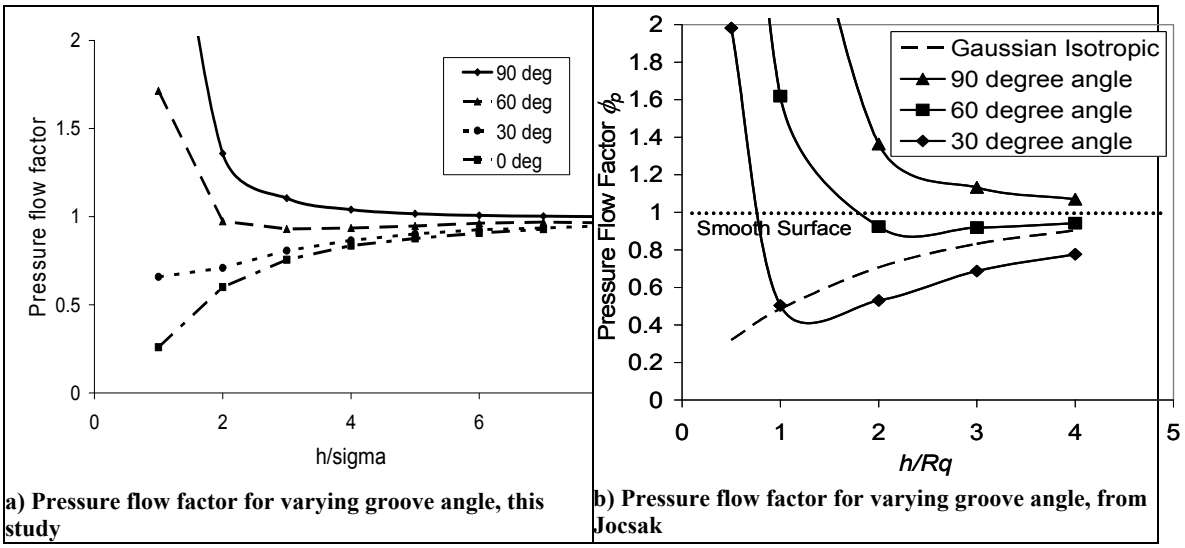

a) Pressure flow factor for varying groove angle, this study

b) Pressure flow factor for varying groove angle, from Jocsak

Figure 3-10: Groove angle effects, with comparison to previous calculations by Jocsak [4]

Figure 3-10b shows results from Jocsak [4], looking at the same groove angles as were considered in the present study. The same flow factor calculation methods were used in both studies, however Jocsak's results consider more realistic surfaces, with realistic roughness and groove profiles. Because the surface roughness is included, Jocsak's pressure flow factors are lower than those obtained in the current study. Also, groove spacing, rather than area ratio, is kept constant in Jocsak's study. Despite these discrepancies, the two sets of results show a good match in trends.

Figure 3-11 shows the effects of varying groove depth on pressure flow factor. As Figure 3-11a shows, there is no change in the pressure flow factor with groove depth, when ϕ_p is presented as a function of h/σ (σ is the RMS surface roughness). This is because the effects of groove depth on pressure flow factor are the same as the effects of groove depth on surface roughness, so that the flow factor as a function of h/σ does not change. This suggests that there is a fundamental relationship between ϕ_p and groove depth, that mirrors the relationship between depth and the standard deviation of the surface heights, σ.

When studying a specific case in which the approximate value of the oil film thickness is known, it is useful to consider changes in ϕ_p at film thicknesses close to the

expected values. Figure 3-11b shows the pressure flow factor as a function of h alone, for different groove depths. As the figure shows, at a given film thickness, ϕ_p decreases with groove depth. The depth of the grooves influences the micro-hydrodynamic effect, just as, in the macro-hydrodynamic case, the size of a step in surface height influences the amount of hydrodynamic pressure generated. (In the case of a macro-sized step bearing, the pressure generation is expected to be related to film thickness, depth, groove width and the distance between grooves [35]). For the surfaces studied, the flow impedance increases with groove depth, suggesting that hydrodynamic action and thus oil pressure also increases with depth.

It should be noted that Figure 3-11 shows flow factor results for grooves at an angle of 30^o, so that the effect of increasing depth is to decrease ϕ_p. For larger groove angles, ($\theta > 60^o$) the effect of increasing depth is actually to increase the pressure flow factor, because in this case the effect of the grooves is to reduce flow impedance and thus increase ϕ_p. The effect of increasing groove depth is to amplify the effect of the grooves, whether that be to block flow, for low groove angles, or increase it, for high groove angles. Because the purpose of this study was to identify surface textures that may be used to reduce friction, the flow factor results shown below are for a low groove angle ($\theta = 30^o$).

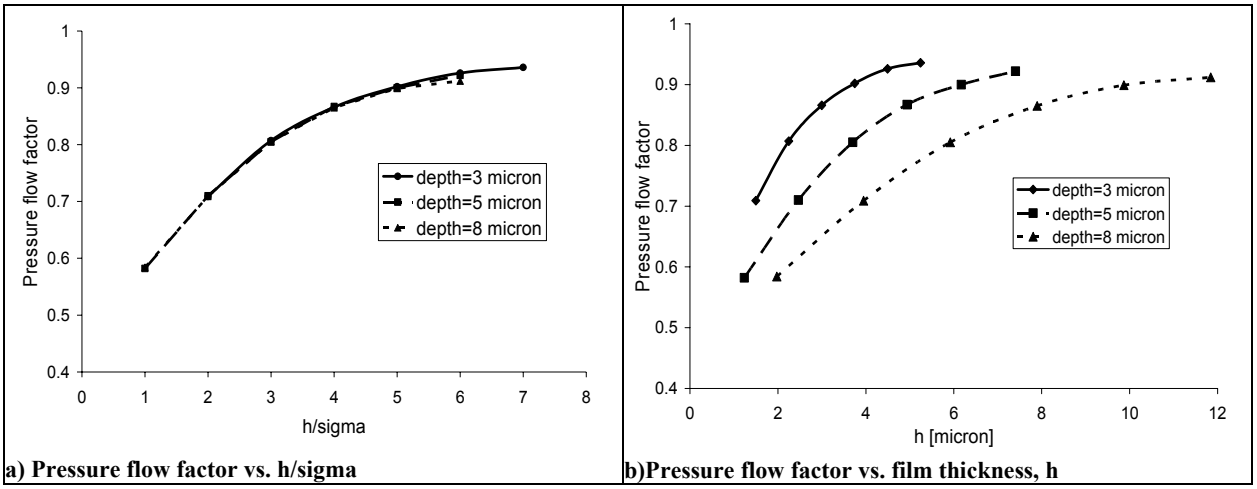

a) Pressure flow factor vs. h/sigma **b)Pressure flow factor vs. film thickness, h**

Figure 3-11: Effect of groove depth on pressure flow factor, 30^o angle, width=20μ, area ratio=0.24

Plotting the pressure flow factor as a function of h/σ can show fundamental effects of surface texturing on pressure-driven fluid flow, including its relationship to surface roughness. It is also useful to show the relationship of ϕ_p to film thickness itself, however, when the effects of a given surface texture in a specific case are of interest. Thus, flow factor results in both this section and section 3.4.3.1, which presents the flow factor analysis for dimpled surfaces, are plotted vs. both h/σ and h, in order to illustrate both general and specific effects.

Figure 3-12 shows the effects of area ratio on the pressure flow factor. On the physical surface, the effect of increasing area ratio is to decrease the distance between grooves, so that the effect of increasing area ratio can be also interpreted as the effect of a

reduced groove spacing. The decrease in ϕ_p with increasing are ratio may then be due to the effect of groove spacing on hydrodynamic action within the grooves. When grooves are very far apart, they can be considered to be independent in their effects on the lubricant flow and pressure. When they are closer together, there may be a cross-influence between grooves, where the presence of each groove affects the flow within the others. For the textures studied, the spacing between the grooves is relatively small (on the order of a few groove widths) so that some cross-influence is expected. More closely spaced grooves (higher area ratio) will have more influence on each other, and may work together to increase flow resistance.

The effect of area ratio may also be due to the simple fact that, when more of the surface is occupied by converging and diverging regions, there is a larger hydrodynamic effect. More "microhydrodynamic" bearings are present, so their net effect is greater. A combination of this and the cross-influence of more closely spaced grooves is likely the main contributor to the effect of area ratio on ϕ_p.

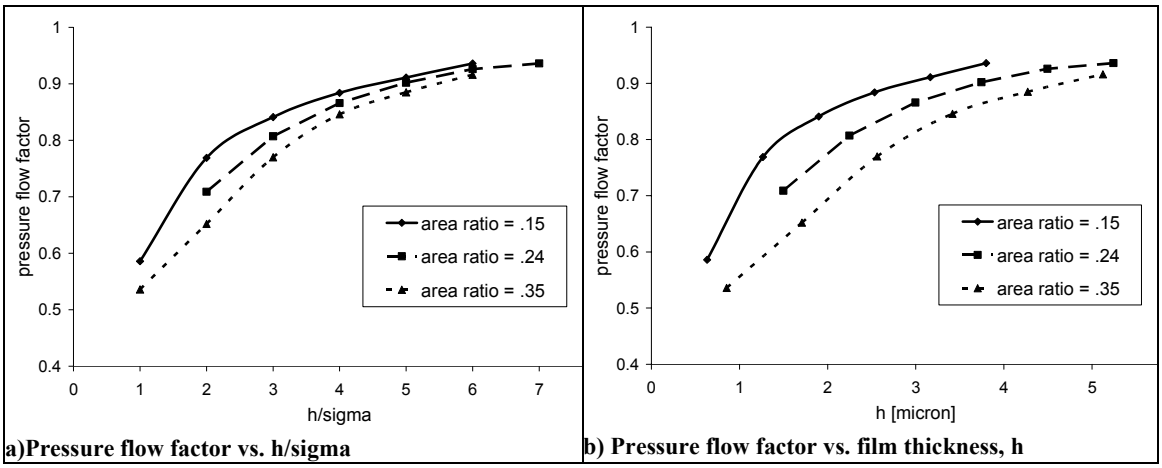

a)Pressure flow factor vs. h/sigma **b) Pressure flow factor vs. film thickness, h**

Figure 3-12: Effect of groove Area ratio on pressure flow factor, 30° angle, width=20μ, depth=3μ

Figure 3-13 presents the changes in pressure flow factor with changing groove width. As the figure shows, the groove width has almost no effect on the pressure flow factor except at very small film thicknesses. This may indicate that the width has only a small effect on micro-hydrodynamic action within the groove – the pressure build-up due to the converging geometry of the groove exit is not strongly influenced by the width. There is no clear explanation for the change in trend at small film thickness, where groove width suddenly becomes important. It should be noted, however, that flow factor analysis becomes inaccurate at very small h/σ values, where the film thickness is close to the surface roughness, because the roughness asperities and flow blockages make the flow situation too far removed from a smooth, Reynolds case. Then, these thin-film effects may not be realistic, and should be studied further with a deterministic analysis.

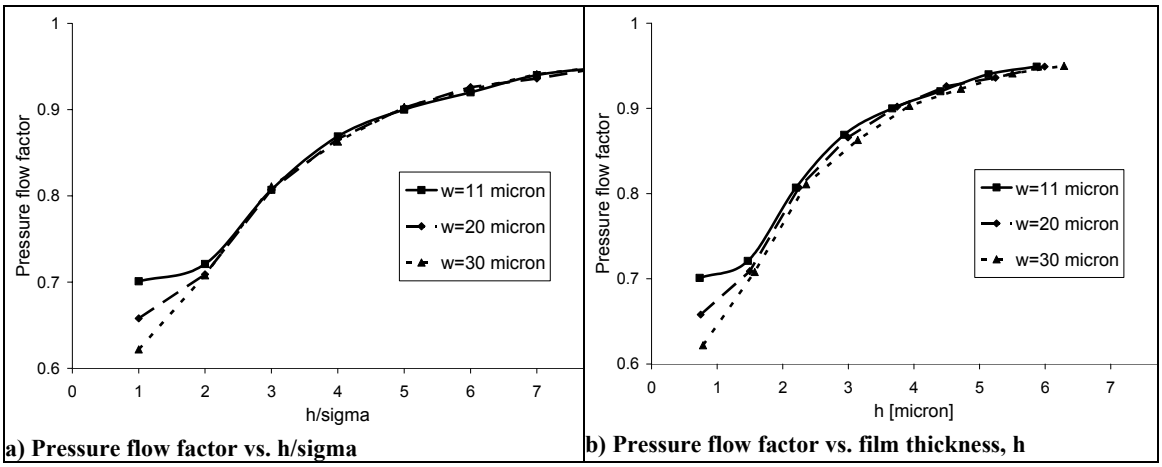

a) Pressure flow factor vs. h/sigma **b) Pressure flow factor vs. film thickness, h**

Figure 3-13: Effect of groove width on pressure flow factor, 30° angle, Area ratio = 0.24, depth=3μ

3.4.2.2. Ring/liner friction results

Friction results were consistent with expectation given the flow factor results presented above. Friction tends to decrease with increasing depth and decreasing groove angle, and also shows some reduction with increasing area ratio and width. The change in FMEP between best and worse cases is relatively large, up to ~30% between the highest and lowest friction examples (not including large groove angles, which cause friction to increase). While this result cannot be used to predict actual friction reductions in realistic situations, it indicates that liner surface texturing may have a major effect on ring/liner friction, and is worth studying further.

Ring/liner friction depends on the surface texture in two ways: oil film thickness, which influences both hydrodynamic friction and asperity contact, depends on the influence of the texturing on the oil flow (represented by flow and stress factors in this study); and asperity contact friction depends on the surface roughness and other features of the surface texture. For this parametric study, as described in Section 3.4.1, the surfaces are smooth except for the added grooved or dimpled patterns. This allows the hydrodynamic effects of the patterns to be studied more easily, but makes the asperity contact mechanics very unrealistic.

To account for this issue, the ring-pack friction program was modified slightly so that the surface properties related to contact mechanics were separated from those related to oil flows. Then, for each friction case studied the contact mechanics were to be kept the same, even as flow parameters were allowed to vary. For the sake of simplicity, the surface used to calculate contact pressures was kept constant as a Gaussian surface with a roughness of $\sigma = 0.21\mu$. This roughness is typical of the "truncated" roughness of a cylinder liner, where the surface is negatively skewed and the effects of the deep valleys are ignored. The presence of the surface features should have little to no effect on the contact mechanics, since the features are negative – that is, they are formed by the removal of material, rather than the addition – and so no extra asperities are added when the texturing is added. Changing area ratio of the texturing will affect the amount of surface area available for contact, but this should have only a small effect as the contact

force should be proportional to the material properties (hardness) and the load, and not to the apparent area of contact [23].

While contact surface features were kept constant, the surface properties controlling oil flows and stresses were varied. These surface properties were defined by the curve-fitted flow factor equations, which are functions of h/σ and derived from the values calculated deterministically using Li's program, and the surface roughness, σ, which together determine the value of a given flow or stress factor at a given film thickness, h. The value input as σ effectively defines the depth of the texture under study, since the flow and stress factor equations contain no information relating to the surface roughness itself, but only to its effects relative to h/σ. Then, friction results are presented as FMEP (friction mean effective pressure) vs. σ, as this roughness was used as the input in this study. As the value of σ approximately corresponds with the depth of the surface features, the trends of FMEP with σ shown should be considered to correspond to the same trend of FMEP with respect to depth. A value of $\sigma = 0.7\ \mu$ is roughly equivalent to a groove depth of 3μ, indicating that the feature depths studied were relatively shallow. This is in agreement with the literature, which predicts maximum friction reductions for shallow features [28].

Figure 3-14 shows the change in ring/liner FMEP with groove angle as well as depth. As expected from the flow factor results, FMEP decreases with groove angle. Friction also decreases with groove depth for low groove angles, while increasing with depth for a large angle (the $\theta = 90^o$ case, not shown in the figure, demonstrated even higher friction than $\theta = 60^o$), as expected – the effects of the texture increases as depth is increased. As shown in Figure 3-15, these reductions in total FMEP are the result of decreases in both the hydrodynamic and boundary contributions to friction, as the presence of the texturing causes the oil film thickness to increase.

For the $\theta = 0^o$ grooves, the surface texturing is able to almost entirely eliminate boundary contact, as well as cause a large decrease in hydrodynamic friction. At the maximum groove depth studied FMEP is continuing to decrease, indicating that the maximum effect of these grooves may occur at a greater depth. For the $\theta = 30^o$ grooves however, a minimum FMEP is found at a roughness of $\sigma \sim 0.55\ \mu$, or a depth of slightly more than 2μ. It is expected that the hydrodynamic effect of the grooves will not increase indefinitely with depth – as the grooves become too deep, fluid at the bottom will become stagnant and no longer contribute to the hydrodynamic system. At this point, the averaged flow-factor method also becomes inadequate to describe the fluid flow, and more detailed model must be used. For grooves that are not entirely perpendicular to the flow ($\theta > 0^o$), there may also be a trade-off between the hydrodynamic effect and the increased flow area. As groove depth increases hydrodynamic effects will increase (to a point), but the extra area available for fluid transport also grows. The minimum FMEP point predicted for the $\theta = 30^o$ groove case may also reflect this trade-off.

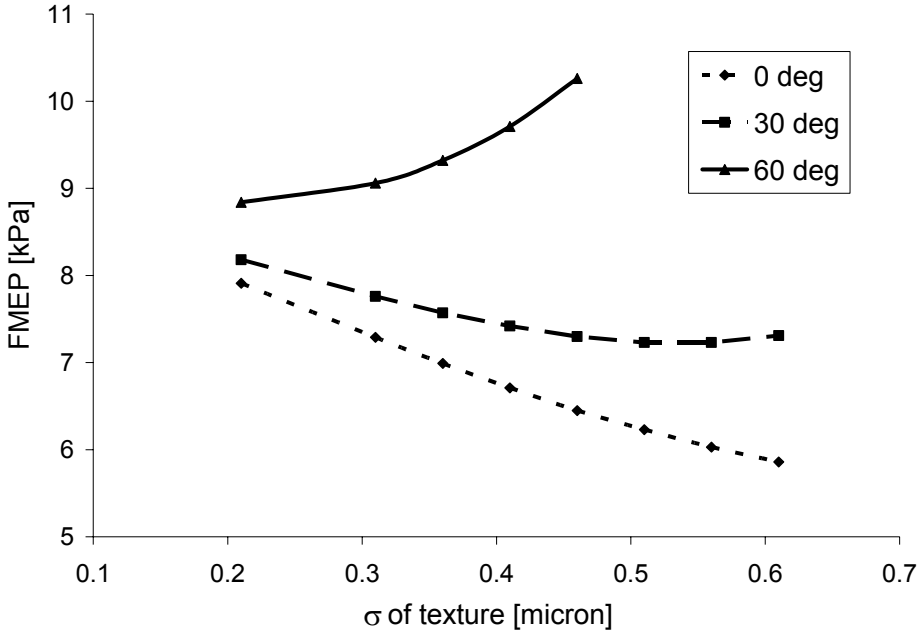

Figure 3-14: Effect of groove angle on ring/liner friction, width = 20μ, area ratio = 0.24

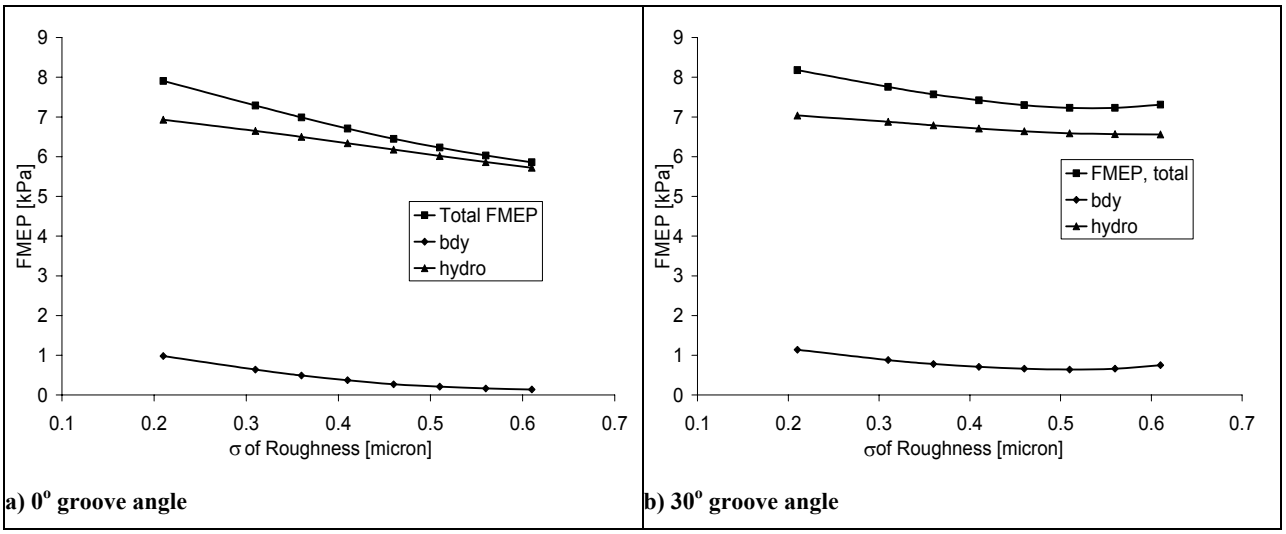

a) 0° groove angle **b) 30° groove angle**

Figure 3-15: Hydrodynamic and boundary contributions to frictional losses, 0° and 30° groove angles

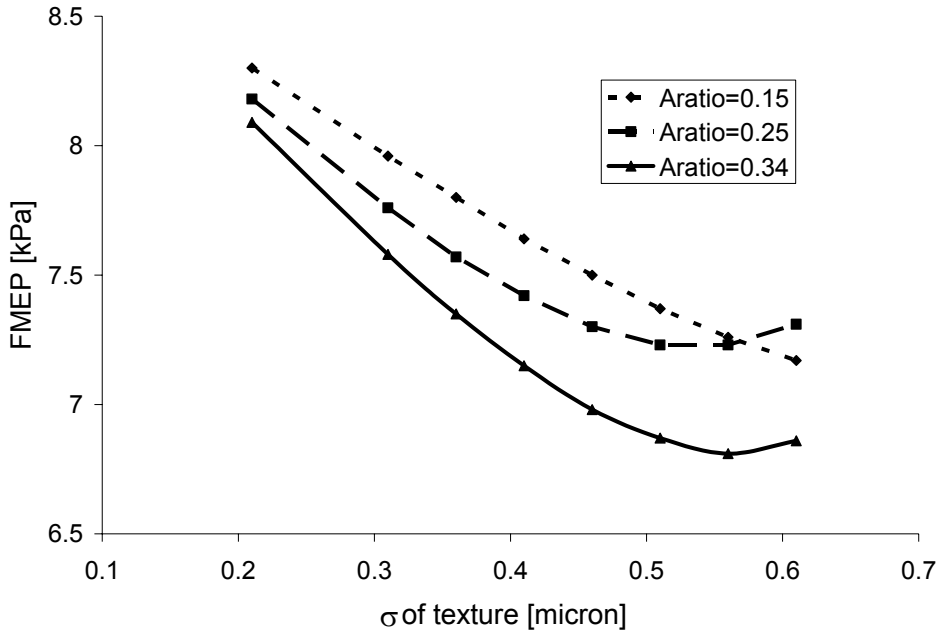

Figure 3-16: Effect of groove area ratio on ring/liner friction, angle = 30°, width = 20μ

Figure 3-16 and Figure 3-17 illustrate the effects of the area ratio and width, respectively, of the grooves on ring/liner FMEP. Again, friction decreases as depth increases, until an optimum point is reached at $\sigma \sim 0.55\ \mu$ for most of the cases. This may reflect the trade-off between hydrodynamic effect and flow area discussed above (the results shown are for $\theta = 30^{o}$). FMEP also decreases as area ratio increases, as expected from the flow factor results, and also increases with groove width but only to a point. As Figure 3-17 shows, friction decreases as the groove width increases from 11μ to 20μ, but the further increase to w=30μ has no effect.

This results from the relation of the flow factors to oil film thickness, shown in Figure 3-17. For large film thicknesses, groove width does not affect the pressure flow factor - a width effect is only shown for thin films. Because the presence of the grooves increases oil film thickness, there is a feedback effect that removes the dependence of friction on groove width as width grows. When the grooves are narrow, the hydrodynamic effect is small as is the oil film thickness, which is small enough to be in the range where groove width matters. The increase in width from 11μ to 20μ increases the hydrodynamic pressure in the oil and also the value of h, into the regime in which groove width becomes unimportant. Then, for any further increase in width the oil film thickness is in a regime where the width has no effect on the pressure flow factor, and there is thus no effect on friction.

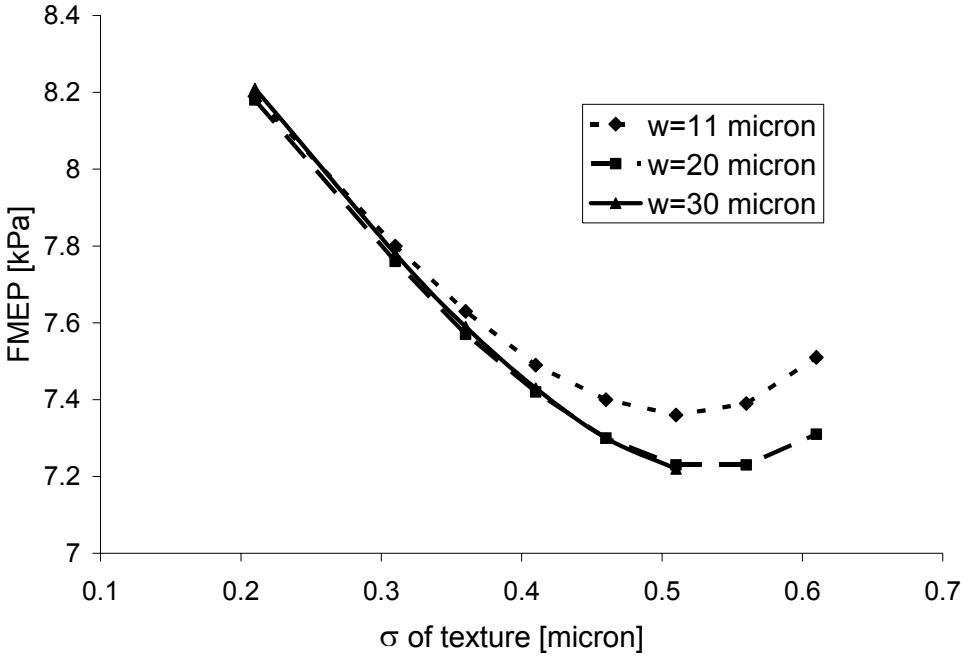

Figure 3-17: Effect of groove width on ring/liner friction, angle = 30^{o}, area ratio = 0.24

3.4.3. Round dimples: effect of discrete surface features on sliding friction

In addition to the grooved patterns, surfaces with patterns of round dimples were also studied, as such discrete surface features are also thought to hold promise for the reduction of ring/liner friction. FMEP was found to decrease as dimple area ratio and depth were increased, as was the case with the grooves, and to be minimized at an optimum dimple diameter. In general, the effects of the various dimple parameters on friction was smaller than the effects of comparable parameters for the grooved surfaces. This suggests that dimpled surfaces may allow more freedom in selecting feature parameters, and may be useful over a larger range of running conditions than grooved patterns.

Both pressure flow factor and FMEP results are presented. As for the groove analysis, it should be noted that the averaged flow factor model is limited in its applicability, and results at very small film thicknesses and for very deep textures may be pushing this limit. The results presented below are intended to illustrate the friction-reduction possibilities of dimpled surface textures, and the effects of some dimple parameters. Further analysis is required before recommendations can be made for friction-reducing surface textures in specific applications.

3.4.3.1. Flow factor results

Only pressure flow factor results are presented below, because this factor has the main effect on ring/liner friction, as demonstrated in Section 3.3.2. In general, a lower pressure flow factor indicates a decrease in ring/liner friction, because of the implied increase in hydrodynamic pressure generation.

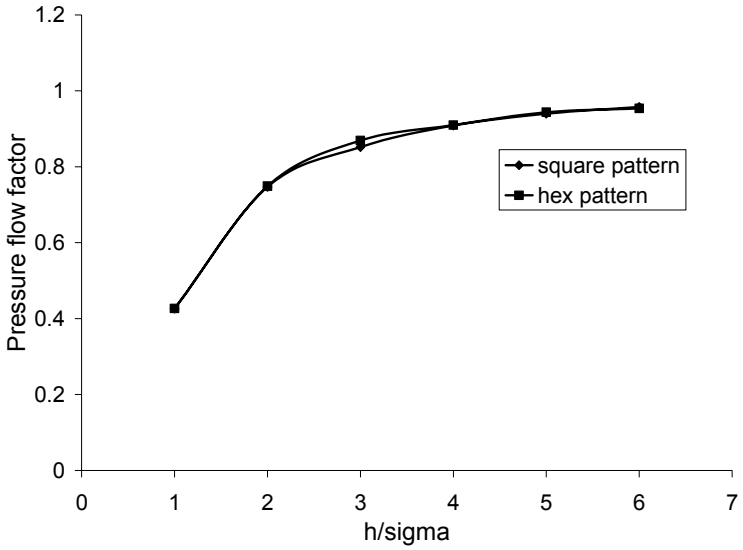

Figure 3-18: Flow factor results for square and hexagonal dimple patterns are very similar

Flow factor results for the dimpled cases showed several of the same trends that were observed for the grooved surfaces. For example, the dimple pattern had almost no effect on flow factor or ring/liner friction calculations, similar to the lack of influence of a cross-hatch vs. parallel groove arrangement on friction. Figure 3-18 shows an example comparison of pressure flow factor calculations for square and hexagonal dimple arrangements. Because the pattern appears to have no effect, all results presented below are for the hexagonal pattern only.

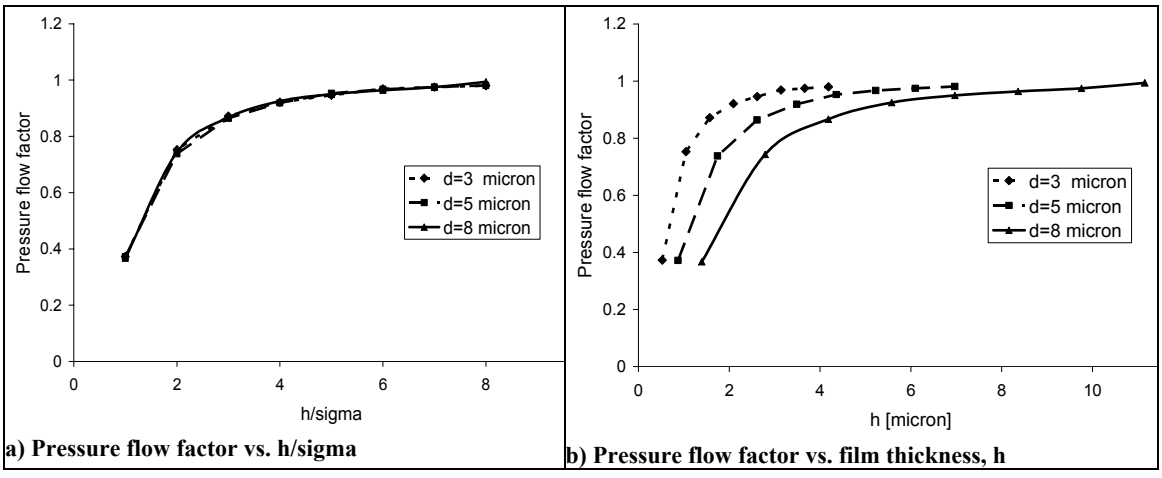

a) Pressure flow factor vs. h/sigma

b) Pressure flow factor vs. film thickness, h

Figure 3-19: Effect of dimple depth on pressure flow factor, diameter = 19μ, area ratio = 0.25

The dimpled patterns were also similar to the grooved cases in that the change in pressure flow factor with the depth of the features mirrored the changing surface roughness, so that plotting pressure flow factor as a function of h/σ shows no effect from depth changes. Figure 3-19 shows this, along with the pressure flow factor plotted vs. h only, which illustrates the effect of dimple depth at a given film thickness. Further discussion of this phenomenon is given in Section 3.4.2.1. Because it is useful to observe

both the non-dimensionalized effects of various parameters and to evaluate the pressure flow factor at an expected film thickness for a specific case, ϕ_p is shown as a function of both h/σ and h alone in the examples below.

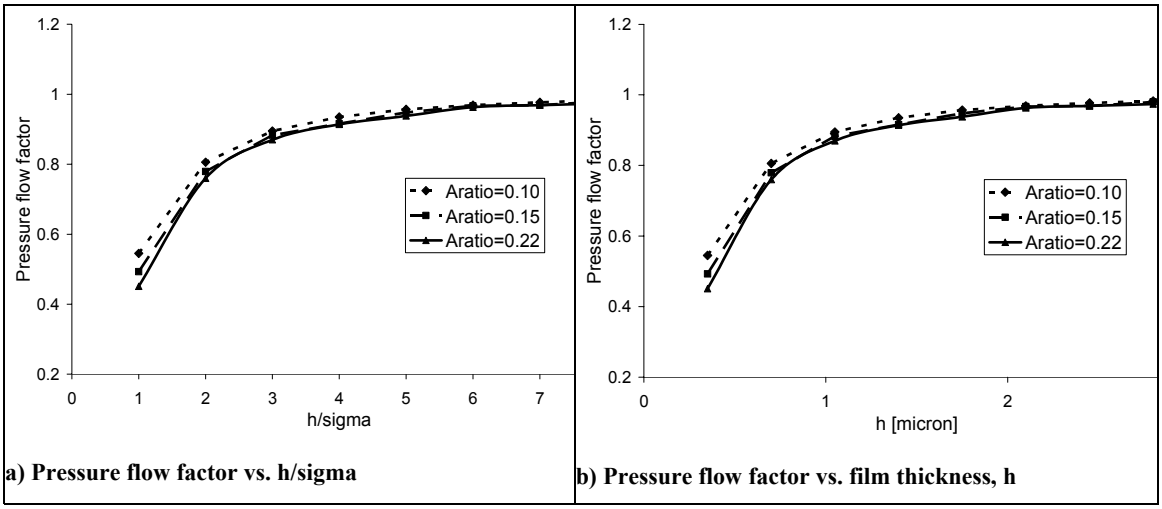

a) Pressure flow factor vs. h/sigma **b) Pressure flow factor vs. film thickness, h**

Figure 3-20: Effect of dimple area ratio on pressure flow factor, diameter = 19μ, depth = 3μ

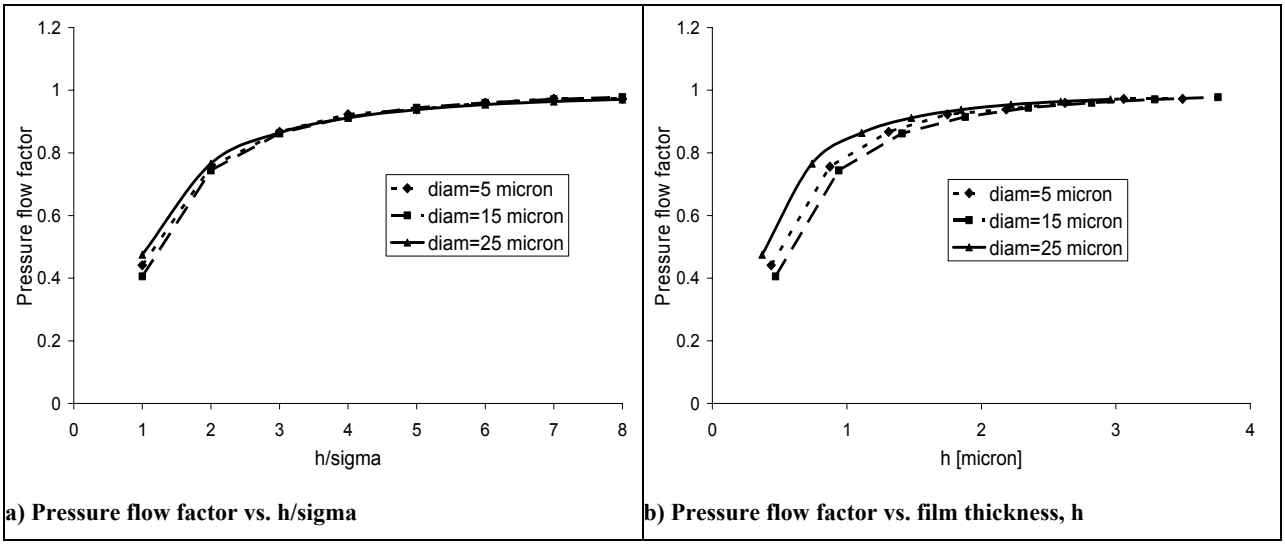

a) Pressure flow factor vs. h/sigma **b) Pressure flow factor vs. film thickness, h**

Figure 3-21: Effect of dimple diameter on pressure flow factor, depth = 3μ, area ratio = 0.25

Figure 3-20 shows the effect of dimple area ratio on the pressure flow factor. As the figure shows, pressure flow factor decreases slightly with area ratio, but the effect is weak. As for the grooves, it is expected that the effect of increasing area ratio will be to increase both the amount of interaction that occurs between dimples and the number of "micro-hydrodynamic" bearings that are present on the surface, and is expected to cause a decrease in pressure flow factor. It is unclear why this effect is so weak for the dimpled cases, although several studies have also shown this for dimpled surfaces, including Etsion et. al [28] and Ronen, et. al [36].

Figure 3-21 also shows a relatively weak effect, of the dimple diameter on pressure flow factor. In this case, there is an optimum diameter at which pressure flow factor is minimized – the mid-range diameter, d = 15μ, shows the lowest ϕ_p. The optimal dimple diameter occurs at a value where the diameter and depth combine to define a dimple shape that provides the maximum hydrodynamic pressure generation, and is also similar to an effect observed by Etsion [28] in which an optimal ratio of dimple depth:diameter was found.

3.4.3.2. Friction results

Ring/liner friction predictions for the dimpled surfaces were consistent with those expected given the flow factor results presented above. As the effects of the surface parameters on the pressure flow factor were small, changes in FMEP for different surfaces considered were also small relative to those predicted for different grooved patterns. It appears that dimpled surfaces are less sensitive to changes in feature geometry – except for dimple depth – than grooved surfaces, and may thus be easier to design for given slider geometry and running conditions. As for the friction analysis for the grooved surfaces presented above, the following results are based on an approximate analytical method and cannot be used to predict actual friction reductions in realistic situations, but they do indicate that liner surface texturing can reduce ring/liner friction, and should be studied further.

Some modifications were made to the ring-pack simulation program in order to obtain the results presented below. Details of these modifications are given in Section 3.4.2.2. In the model, the depth of the dimples was represented by the overall textured surface roughness, σ, which has therefore been used to represent dimple depth in the figures shown below. In both figures, FMEP is plotted as a function of σ, which is the RMS roughness of the surface under study. This should be understood to correspond to dimple depth, where a roughness of σ=0.5μ corresponds approximately to a depth of d=3μ.

Figure 3-22 shows the effects of both dimple depth and area ratio on ring/liner FMEP. As the figure shows, the effects of depth are much greater than those of area ratio, which has only a small influence on friction. FMEP decreases strongly with depth, and shows no sign of leveling off at large depths, as the grooved cases did. It is expected that the effect of dimples on FMEP with increasing depth will eventually disappear, as for very deep dimples the fluid in the bottom will simply be stagnant and not contribute to the hydrodynamic action of the texturing. However, this limit appears to be beyond the level of dimple depth that has been investigated here. The effect of area ratio is much smaller than that of dimple depth, so that it may not be necessary to optimize for this parameter in designing a friction-reduction surface.

Figure 3-23 shows the effects of dimple diameter on ring/liner friction. The effect of diameter is also small, with the minimum FMEP found at a mid-range value. This optimal diameter phenomenon has also been observed in the literature (see Section 3.4.2.1) and is the result of the effect of the dimple geometry on the amount of hydrodynamic pressure generation that occurs as lubricant flows through the dimple. The

effect of diameter on both the converging/diverging length and the dimple profile contribute to this effect.

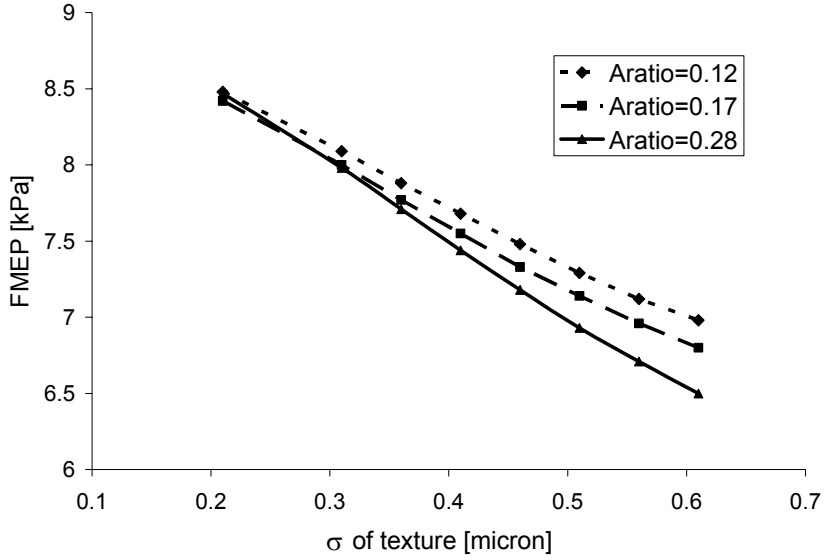

Figure 3-22: Effect of dimple area ratio on ring/liner friction, diameter = 19μ

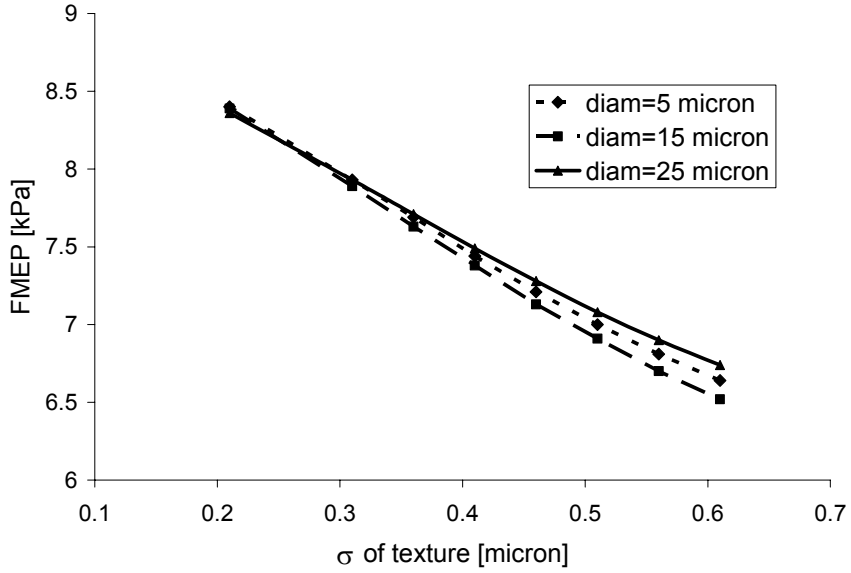

Figure 3-23: Effect of dimple diameter on ring/liner friction, area ratio = 0.25

3.5. Summary and conclusions of surface texturing parametric study

Surface features can affect sliding friction in many ways, including removing wear particles from the sliding interface and acting as fluid reservoirs to provide adequate lubrication where it is needed. This study considered the role played by surface texturing in the hydrodynamic regime, and its potential to reduce piston-ring/liner friction under this condition. An averaged flow-factor Reynolds analysis was used to evaluate the effects of patterns of either grooves or dimples on the cylinder liner. Because this averaged technique was used, a detailed study of the lubricant pressures and flows could

not be made. Still, the results of this parametric study can be used to estimate the potential of surface texturing for, and the effects of various texture parameters on, friction reduction.

In a well-lubricated regime, surface texturing affects both hydrodynamic and boundary friction between the ring and liner by influencing the hydrodynamic pressure generation within the lubricant, and thus the oil film thickness. Textures that impede lubricant flow increase oil pressure and thus increase film thickness, at a given load. This increase in h can cause a reduction in asperity contact, if any was present in the baseline case, and also reduces shear stress by reducing the shear rate in the oil. Thus, an appropriate surface texture can decrease both hydrodynamic and boundary friction between ring and liner. An inappropriate texture, however, can cause an increase in friction by allowing oil to flow more easily and thus reducing oil film thickness. It is necessary to understand the effects of different textures, and their relation to slider parameters and running conditions, in order to design surfaces for friction reduction in actual applications.

Both stochastic parameters, such as roughness and skewness, and deterministically defined features such as dimples influence the way in which a surface affects sliding lubrication and friction. This study focused on two texture categories: patterns of round dimples and patterns of grooves. For the dimpled cases, the effects of dimple diameter, depth and area ratio were studied, while for the grooved surfaces groove angle, depth, width, and area ratio effects were assessed. The results of a parametric study of both the flow factors, which give an indication of the physical effects of the surface texturing, and predicted friction losses, for Waukesha engine geometry and running conditions, were presented.

The effects of many of the surface parameters studied were similar for the dimpled and grooved surfaces. Friction was found to decrease as the depths of both dimples and grooves were increased, as well as with increasing area ratio for both pattern types. The effects of groove width and dimple diameter were both relatively small. In the case of the dimples, an optimum effect was observed in which the minimum friction was found at a mid-range diameter, because of the dependence of hydrodynamic pressure generation on the shape and size of the dimples. There may also be an optimum effect in relation to groove depth, stemming from a trade-off between hydrodynamic effects and lubricant flow area. Friction was also found to decrease strongly with groove angle, (where a groove with a lower angle is more perpendicular to the lubricant flow direction) in agreement with previous studies [4].

The analytical method used in this study is subject to several limitations and approximations, and therefore the results are not intended to be used directly in the design of friction-reducing surface textures. Rather, the trends presented here are used to illustrate the potential of appropriately designed surface textures to reduce friction both in the engine and other sliding friction applications, and to indicate the relative importance of the various texture parameters that define two common surface patterns. The study has showed that even relatively small-scale textures (compared to others that have been studied in the literature) can have a large effect on ring/liner friction, in some cases reducing FMEP by as much as 30% from a smooth surface case. Also, it may be possible

to combine the effects of lubricant viscosity and surface texturing to reduce friction even further, while mitigating unwanted side-effects such as wear and oil consumption. This possibility is discussed in Section 4.5.

4. Application of Lubricant and Surface Texture Studies to Waukesha Engine

The lubricant and surface texture studies presented in Sections 2 and 3 were applied to an analysis of the piston ring-pack in the Waukesha VGF 18GL engine. These studies were part of an on-going program whose intention is to increase the efficiency of this engine from ~42% to 50%, over a ten year period. While reducing mechanical losses is only one of several efficiency-increasing measures to be developed in this time, it is an essential part of reaching the stated goal. Application of optimized lubricant and surface features to the piston ring-pack and cylinder liner is one of many measures that will help the goal efficiency to be achieved.

4.1. The standard engine parameters

The engine under study is the Waukesha VGF 18GL, a large natural gas engine used for stationary power generation, shown in Figure 4-1. Some engine specifications and operating conditions are given in Table 4-1.

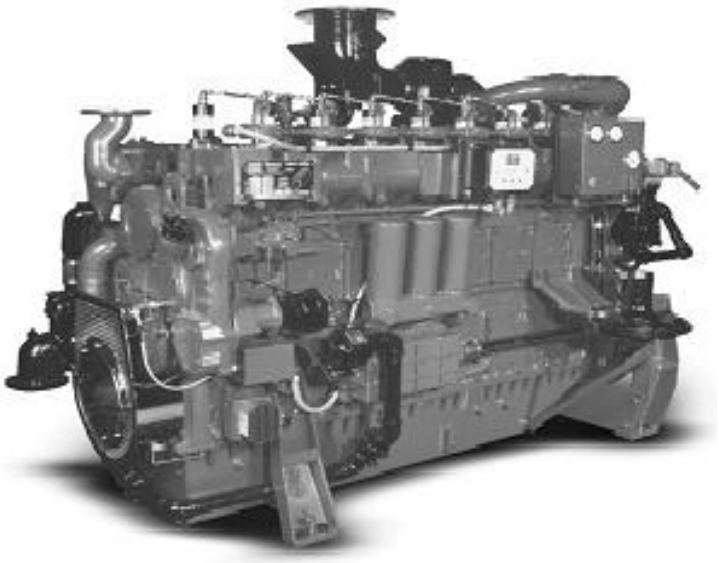

Figure 4-1: The Waukesha VGF 18GL engine

For baseline mechanical and surface roughness parameters, frictional losses in the Waukesha engine ring-pack are dominated by the oil control and top rings. The OCR is the largest contributor to friction because of its high ring tension. It is required to conform very well to the cylinder liner, while maintaining enough stiffness to resist warping and breakage, so a high tension is necessary. This results in a high ring-liner load throughout the cycle, leading to high friction.

The top ring contribution to friction is also significant, because of the large friction forces associated with boundary friction near the top dead center (TDC) of the combustion stroke. In this region, two factors combine to create high friction: first, the

oil supply to the top ring at TDC is very limited, because the oil control ring doesn't reach this high on the liner; second, combustion chamber gas pressure, following compression and combustion, is very high. The combination of high ring load and poor lubrication results in very high asperity contact pressures, and thus high friction (and also high wear). Even though piston speed is very low here, the total frictional power loss from this region is still significant. Figure 4-2 shows this high-friction "spike" for the top ring, compared to the more evenly distributed frictional losses for the OCR.

Table 4-1: Waukesha Engine baseline parameters and operating conditions

Parameter	Value	Unit
Engine type	Natural gas, SI	-
Bore x Stroke	0.152 x 0.165	m x m
Number of cylinders	6	-
Displacement	18	liter
Engine Speed	1800	rev/min
BMEP @ 1800 RPM	1380	kPa
Lubricant grade	SAE 40W	-
Top Ring Type	Skewed barrel	-
Second Ring Type	Napier	-
OCR Type	Twin land	-

Because the majority of top ring friction comes from this dry-region friction spike, however, this ring has not been considered in detail in either of the studies presented here. Top ring friction it is not expected to be strongly affected by lubricant viscosity, because most of the friction is generated in a poorly lubricated regime – if no lubricant is present, its properties cannot matter. A brief study of the effect of lubricant viscosity on oil transport into the dry region was conducted, with results presented in previous reports, but the model used to obtain these results had a relatively simple oil transport model, and more research is needed to validate the conclusions.

Also, while top ring friction may be greatly reduced by the addition of surface texturing to the cylinder liner, the mechanism by which this would occur has not been investigated here. The focus of the surface texture study was on the hydrodynamic effects of the surface features, and their ability to reduce friction in a well-lubricated regime. It may be possible to reduce top-ring friction by adding dimples near TDC to act as lubricant reservoirs, and thus increase the lubrication in this area. However, this mechanism has not been studied in the current project.

Because of these considerations, the oil control ring (OCR) was the main focus of both the lubricant and surface texturing studies. The OCR contributes most of the ring-pack friction and is strongly affected by lubricant viscosity and surface texturing. Top ring friction is significant, but stems mainly from a poorly-lubricated regime in which viscosity and surface effects are expected to be small. The trends observed for the OCR are expected to correspond to viscosity/friction trends for the entire ring-pack.

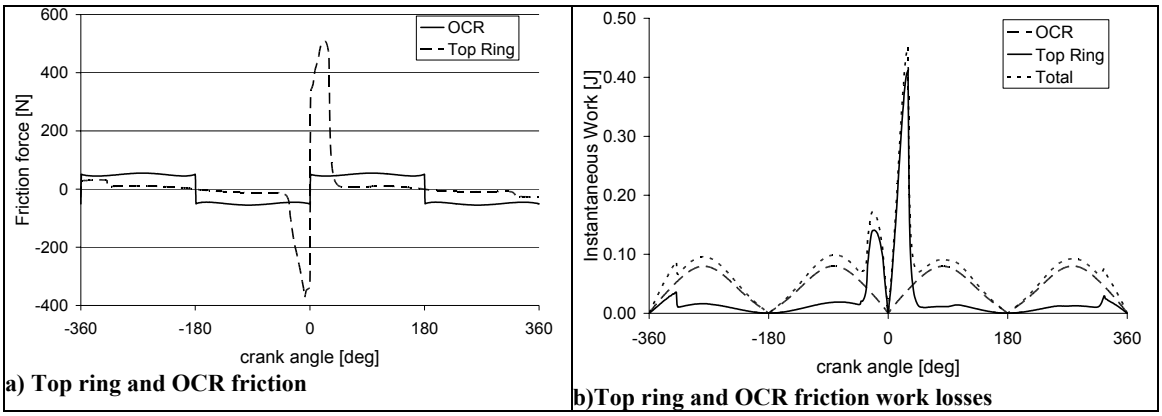

Figure 4-2: Top ring and OCR contributions to ring-pack friction losses

4.2. Lubricant viscosity and liner surface finish studies

Changes in both lubricant viscosity and surface finish can lead to reduced friction in the Waukesha engine ring-pack. Reductions in lubricant viscosity reduce hydrodynamic friction between ring and liner, and if viscosity can be maintained at a higher value near dead-centers, wear in that region can be reduced. Adding an appropriate texture to the cylinder liner may also reduce friction, both hydrodynamic and boundary, by increasing hydrodynamic pressure generation and thus oil film thickness.

In addition to the individual effects of these two parameters, an even greater friction reduction is possible when these two changes are combined. Friction reduction via lubricant viscosity reduction is possible, but not without a concurrent increase in wear. Surface texturing can also be used to reduce friction, but does so by increasing oil film thicknesses, which may cause increased oil consumption. A reduced viscosity lubricant can be combined with a textured liner surface to reduce friction while minimizing these adverse effects.

Fortunately, the side-effects of viscosity reduction and addition of surface texturing are complimentary, so that when these techniques are used concurrently the negative aspects can be minimized. Reducing lubricant viscosity causes a reduction in oil film thickness, which may lead to increased asperity contact, and thus, wear. Adding surface texturing, however, causes an increase in oil film thickness, by increasing hydrodynamic pressure generation. If lubricant and surface texturing parameters can be changed so that oil film thickness remains approximately equal to the baseline case, there should be little effect on wear and oil consumption. Friction will still be reduced, however, because of the reduced lubricant viscosity.

Application of both lubricant viscosity changes and surface texturing to the Waukesha engine power cylinder are discussed below, followed by consideration of the possibility of optimizing lubricant viscosity and surface texturing concurrently. Because the surface texturing study was a parametric exercise, no specific recommendations or friction reduction estimates can be made for the Waukesha engine, but possible benefits are estimated. Similarly, several examples are given to illustrate the effects of optimizing the lubricant and surface texturing together, but specific recommendations cannot be given. It is hoped that future analysis and testing will take a more in-depth look at the

effects of surface texturing, and that an optimized, low-friction surface pattern for the Waukesha engine will be developed.

4.3. Optimization of lubricant viscosity

Friction power losses between the piston-rings and liner stem primarily from the mid-stroke region, while wear of the rings and liner is generally concentrated at the end-strokes. Reductions in both friction and end-stroke wear may be possible if lubricant viscosity can be reduced in the mid-stroke region and increased near dead-centers. Such a strategy was applied to the Waukesha engine, described above, and predictions of friction and wear made for an optimized lubricant.

As shown in Figure 4-3, a maximum friction reduction of ~10% is predicted for the OCR, from the baseline case, when viscosity in the mid-stroke region is reduced. An additional reduction of ~1% is possible when dead-center viscosity is held high to reduce boundary friction. For the Waukesha engine, the oil control ring accounts for ~65% of the total ring-pack losses. Then, an OCR friction reduction of 11% leads to a total ring-pack friction reduction of approximately 7%. Cross and Vogel equation parameters for the minimum-friction lubricant are given in Table 4-2 (those that are not given in the table are kept equal to baseline values, for SAE40 weight oil).

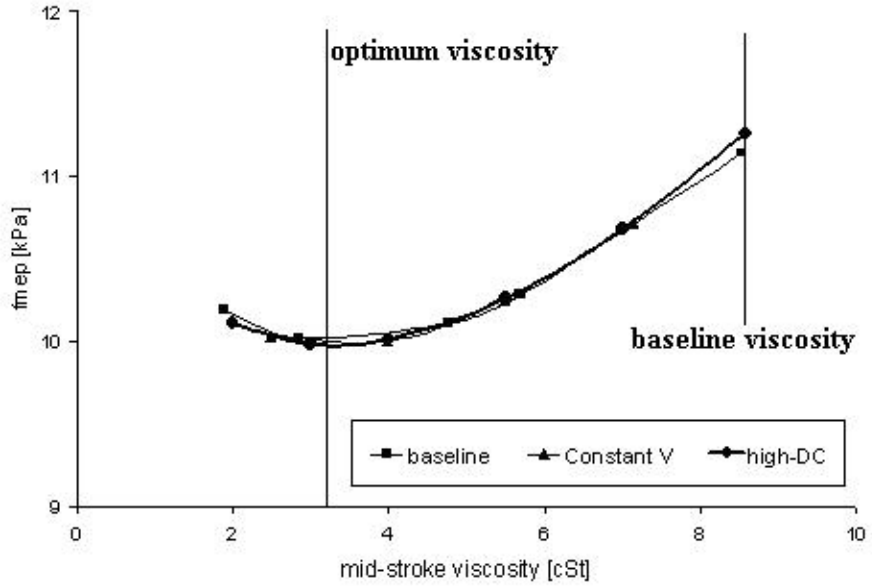

Figure 4-3: Reduction of oil control ring friction with mid-stroke viscosity. Three viscosity variation cases.

The top ring contributes most of the remainder of the ring-pack friction, but experiences most of its losses (~70%) as boundary friction in the poorly-lubricated TDC region of the stroke. Then, viscosity does not have a large direct affect on top ring friction. However, simulations show an indirect effect, where oil transport into the dry region may increase as viscosity decreases. This leads to a decrease in friction of up to 30%, leading to a ring-pack friction reduction of ~9%. However, the mechanism for this

reduction is not clear, and a simplified oil-transport model was used which does not include all recognized oil transport mechanisms. Further research is required to investigate this top ring effect.

Ring/liner wear was also briefly considered, in a simple analysis of a wear coefficient related to boundary contact force and ring/liner sliding distance. Wear was found to increase strongly with decreasing viscosity, even as friction remains low. In the interest of keeping wear low, then, it may be necessary to accept a higher-than-minimum level of ring/liner friction. Controlling viscosity variation was shown to have some potential benefit in reducing wear near the end-strokes, because of the reduction in asperity contact forces in these regions, with an integrated wear coefficient reduction of ~25% for an engine cycle.

Table 4-2: Vogel and Cross equation parameters for low-friction lubricant

Parameter	Physical meaning	Current Value	Proposed Value	Ring-pack Friction Reduction
z	viscosity "thickness"	.09	.06	7%
c_1,c2	control critical shear rate	2.3, 0.0225	4.3, 0.0225	
m	controls width of transition region	1 (more gradual transition)	5 (sharper transition)	
μ/μ_0	ratio of high shear to low shear viscosities	1	0.5	

While it may be possible to develop a lubricant with the shear-dependence properties described here, or develop a liner temperature-control system to produce the same viscosity variation with location, the costs of these systems must be balanced against the potential benefits described above. Also, it should be emphasized that the study presented here considered the effects of lubricant viscosity on the piston ring-pack only. The effects of the considered viscosity changes on the other engine components must also be considered before any change in engine lubricant is made.

4.4. Optimization of liner surface finish

Surface texturing can be used in many different ways to reduce friction between a piston-ring and the cylinder liner. In this study, the ability of small-scale surface features to act as "micro-hydrodynamic" bearings, and thus increase the hydrodynamic pressure within the lubricant, was evaluated. The action of the micro-features causes an increase in oil film thickness between the ring and liner, both decreasing asperity contact (if any is present to begin with) and decreasing oil shear rate, which reduces hydrodynamic friction.

The averaged-flow-factor Reynolds analysis method that was used in this study is limited in its ability to model details of the flows and stresses between textured surfaces,

and thus the results cannot be used to recommend a specific liner texture for the Waukesha engine, or predict actual reductions in friction resulting from a textured surface. Rather, the trends in friction with changing surface parameters may be used as a starting point for further investigation of the effects of liner texturing, and may be used to estimate the potential for friction reduction in the case of the Waukesha power cylinder.

It has been noted that the surface texture of the Waukesha engine cylinder liner is already well-optimized for low friction, with a low skewness of -2.15 (more plateau surface) and honing grooves with the relatively low honing angle of 45^o +/- 5^o [4]. Then, further friction reductions for this engine may be relatively small. Figure 4-4 shows the predicted decrease in friction with groove angle for the oil control ring, with a groove depth of ~2μ. The actual depth of the grooves in the existing Waukesha cylinder liner is not known, but known stochastic parameters including roughness and skewness indicate that this is a reasonable estimate.

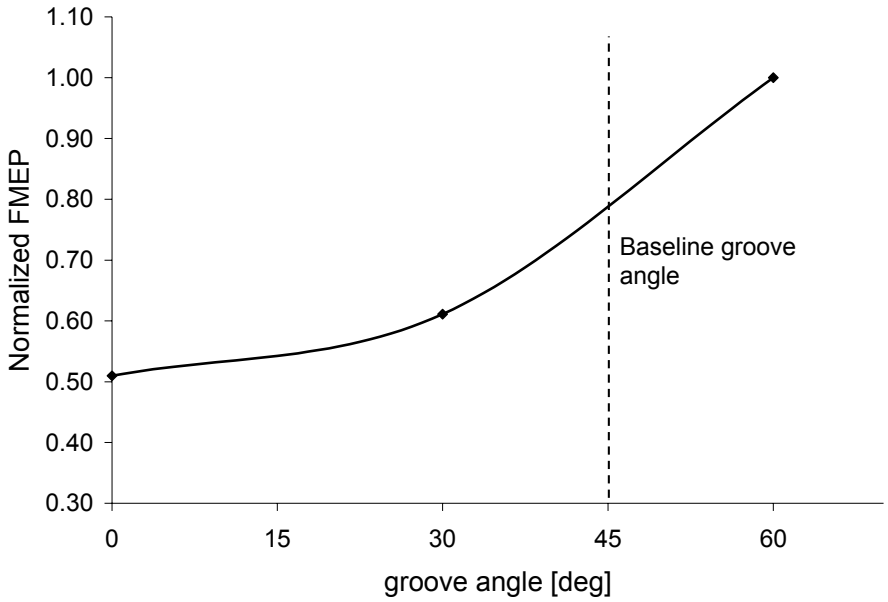

Figure 4-4: Estimate of OCR/liner friction reduction possible with reduced groove angle

Figure 4-4 indicates that, with a decrease in groove angle from 45^o to 30^o, a friction decrease of ~25% is expected. If the angle is further decreased down to a minimum value of 0^o, the total reduction in FMEP is estimated at ~37%. These estimates are for the oil control ring alone. When frictional losses for the top and second rings are added, estimated friction reductions for the ring-pack become 15%, for 30^o grooves, and 25% for 0^o grooves. Although these numbers seem very promising, the simplifications made in both the surface modeling and the modeling of the ring/liner/lubricant interaction must be considered. Rather than being actual estimates for FMEP reduction with groove angle, these numbers should be taken as estimates of the magnitude of friction reduction that could be possible.

Although the largest friction reduction is predicted for a very low groove angle, it should be noted that issues of engine wear and scuffing may be associated with honing

grooves that are very perpendicular to the cylinder axis (although there is some disagreement over whether this is the case). The reason for this is not well understood. One possibility is that honing grooves at a larger angle allow fluid to flow through them, and thus clean out wear particles that are deposited there, while more perpendicular grooves eventually fill up with particles which then cause increased wear and scuffing. Another possible explanation is that the effect of the textured surface in the high-load, low-speed conditions near TDC of combustion is much different than that in the well-lubricated mid-stroke region. In high-speed, low-load conditions, transverse textures may get "flattened" by contact pressures, while more longitudinal textures survive [40].

The existing Waukesha engine cylinder liner already has a grooved pattern due to the surface honing process. Comparing the relative effectiveness of grooved and dimpled surfaces, it is not recommended that the existing pattern be replaced by a dimpled arrangement, as this would add complications to the finishing process and most likely not incur greater friction-reduction benefits than a grooved surface. It may be useful to add a dimpled or other discrete pattern to the cylinder liner that is on a larger scale than those studied here. Many of the surface textures studied in the literature focus on much larger dimples (with diameters on the order of 100μ and larger, depths on the order of 10μ) that have been shown to reduce friction (see Section 3.1.2 for further detail). However, such large features cannot be studied using the current modeling system.

A parametric study of the effects of surface texturing on ring/liner friction indicates that there is potential for these surfaces to reduce friction by a significant amount. The method of analysis used for this study prevents detailed predictions of friction and oil flow effects from being evaluated, and also limits the size of the surface textures that can be considered. The results from this simple study, however, indicate that appropriate surface texturing may provide a substantial benefit in friction reduction, and that further study, encompassing both more detailed modeling and a larger range of parameters, is justified.

4.5. Combined optimization of lubricant and liner surface

Ring/liner friction can be reduced when lubricant viscosity is decreased in the mid-stroke region, but the resulting increase in asperity contact may result in an unacceptable level of wear. A friction reduction is also possible if appropriate surface texturing is added to the cylinder liner, but the accompanying increase in oil film thickness may cause an increase in oil consumption. Alone, each of the friction-reduction techniques studied above can reduce losses but may also have an unwanted side effect. When used together, however, the side effects may be mitigated – the decrease in oil film thickness due to reduced viscosity may be offset by the increase due to the surface texturing – while still achieving a reduction in frictional losses.

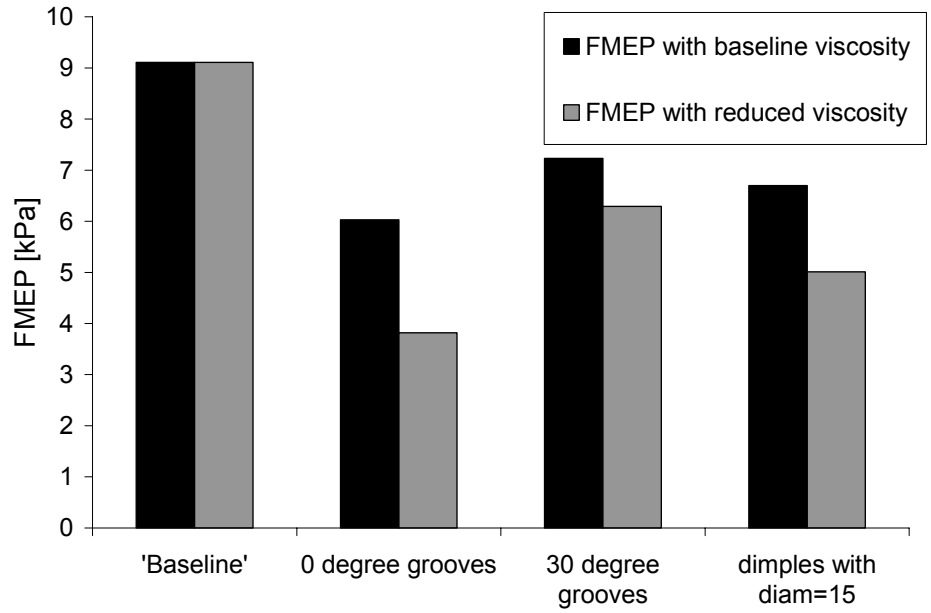

Figure 4-5: FMEP reduction due to combined lubricant and surface texturing effects, example cases

This possibility was studied using several promising surface textures. Because the surface texture study was parametric, and did not use realistic surface roughness in addition to the surface features under study, the results presented here should not be used to design an actual surface/lubricant combination. Rather, they are given as examples to illustrate the possibilities of optimizing the lubricant and surface texturing jointly, and to demonstrate the magnitudes of the possible friction-reduction benefits of doing so.

In each of the example cases, the given surface texturing was applied to the cylinder liner surface, and then the ring-pack simulation was run with varying lubricant viscosities. The viscosity at which oil film thickness and wear were closest to the original baseline case was selected as "ideal." At this viscosity, no net increase in asperity contact or oil film thickness should occur, so that changes in wear and oil consumption should be minimized.

Figure 4-5 shows the friction losses of three example surface textures, as compared to the baseline. For the baseline case the cylinder liner is untextured, and the lubricant is the baseline lubricant for the Waukesha engine (SAE 40). Surface and lubricant parameters for the example cases are given in Table 4-3. Only z, the oil "thickness" parameter from the Vogel equation (Eqn. 3.1) is varied for the lubricant, so that the viscosity temperature dependence remains the same as overall viscosity is changed.

Table 4-3: Surface and lubricant parameters for example cases

Surface texture properties		*Properties of reduced-viscosity lubricant*	
Baseline			
Type	none (smooth)	z	.09
0 degree grooves			
Type	parallel grooves	z	.025
depth, R_q	0.56 μ		
Width	19μ		
groove angle	0 deg.		
area ratio	0.24		
30 degree grooves			
Type	parallel grooves	z	.05
depth, R_q	0.56 μ		
Width	19μ		
groove angle	30 deg.		
area ratio	0.24		
dimples, diameter = 15			
Type	round dimples	z	.04
depth, R_q	0.56 μ		
Diameter	19μ		
area ratio	0.25		

As Figure 4-5 shows, adding the surface texturing alone causes friction reduction in all cases, and then additionally reducing the lubricant viscosity causes friction to decrease further. This additional decrease in friction is not as large as that due to texturing alone, but is still a sizable reduction. Also, the reduction due to reduced lubricant viscosity is approximately proportional to that due to the texturing alone. This is because the amount of viscosity decrease that is ideal – that reduces the film thickness back to the baseline value – is directly related to the increase in film thickness that is brought about by the addition of surface texturing. The friction reduction due to the surface texturing is also related to this film thickness, so that the two drops in friction – due to surface features and due to lubricant viscosity reduction – are closely related to each other.

Figure 4-6 and Figure 4-7 show the effects of the combined surface/lubricant optimization on oil film thickness and wear parameter. As was the intention of using a lubricant with reduced viscosity, in cases where the surface and lubricant were optimized together both the oil film thickness and wear parameter are very similar to the baseline case. When surface texturing is used alone, the resulting oil film thicknesses are much higher than in the baseline case, as shown in Figure 4-6. Similarly, as shown in Figure 4-7, if viscosity is reduced without any added surface texturing, a large increase in wear is predicted. Optimizing the liner surface texture and lubricant viscosity concurrently offers the opportunity to mitigate these negative side effects, while still substantially reducing ring/liner friction.

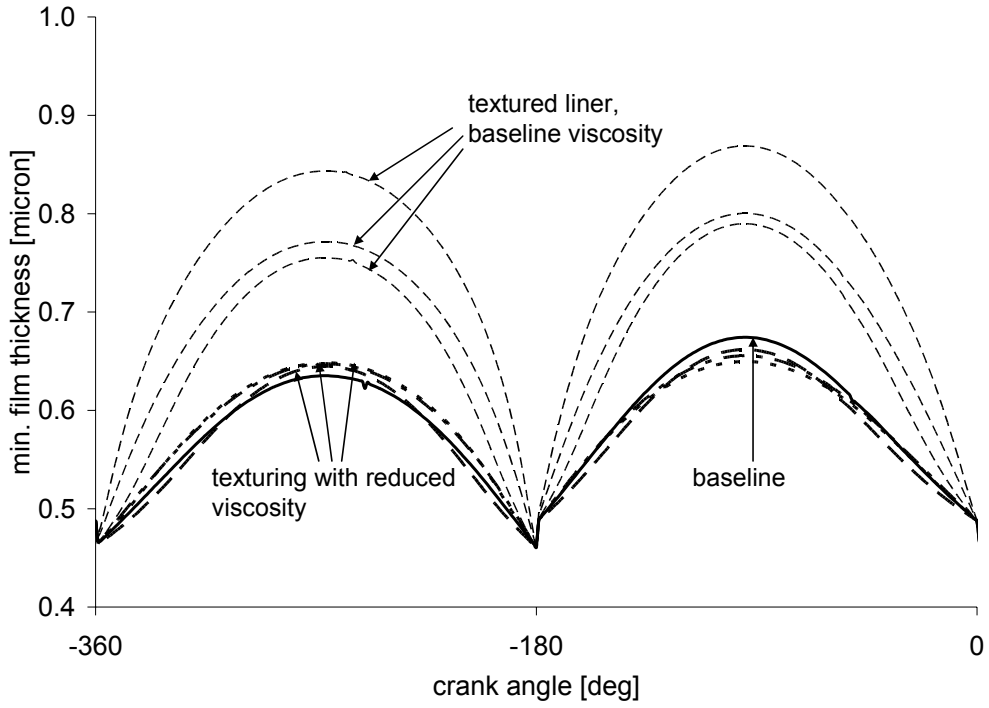

Figure 4-6: Minimum oil film thickness, for combined surface/lubricant effect example cases

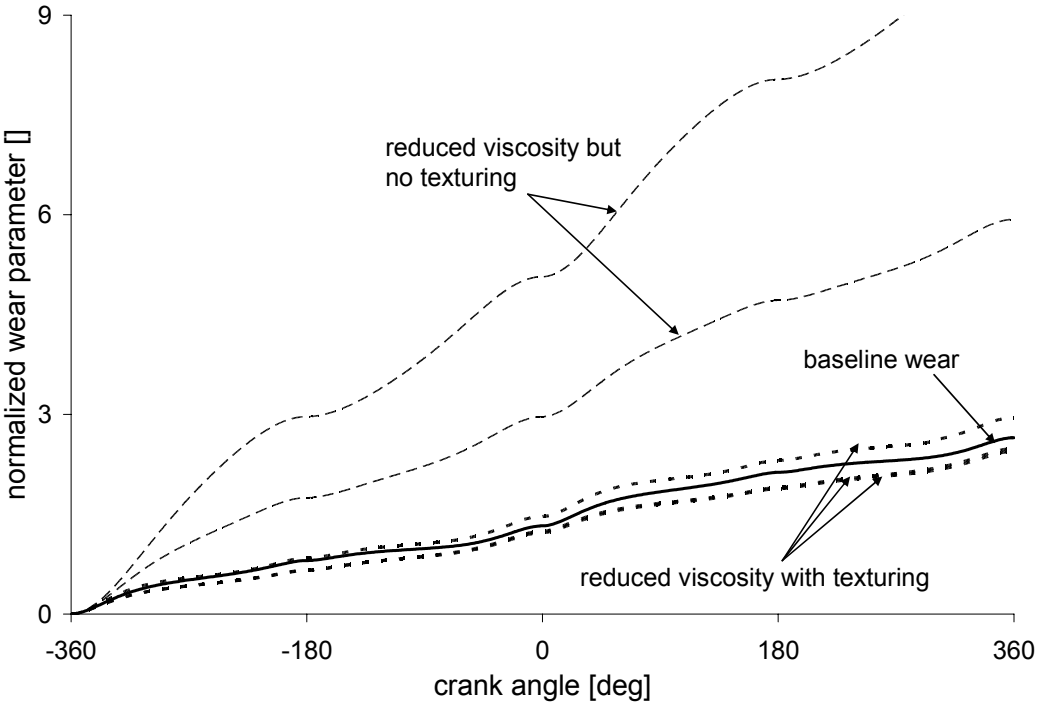

Figure 4-7: Normalized wear parameter, for combined surface/lubricant effect example cases

5. Summary of Lubricant and Surface Texture Effects on Ring-Pack Friction

The piston ring-pack is one of the largest contributors to mechanical losses in an internal combustion engine. In this study, the effects of lubricant viscosity and liner surface texturing on ring/liner friction were considered, with the intent of reducing these losses in the Waukesha VGF 18GL engine. An optimized low-friction lubricant was proposed, and a parametric study of surface texturing showed that adding appropriate surface features to the cylinder liner may also significantly reduce ring/liner friction. Also, if the lubricant and surface texturing can be optimized together, an even greater reduction in friction is possible, along with mitigation of undesired side-effects, such as oil consumption and wear, which may accompany changes made to the lubricant viscosity and surface texturing individually.

The ring-pack simulation model used for both the lubricant and surface texturing studies was based on averaged flow factor Reynolds analysis, and was developed at MIT. Inclusion of features such as ring dynamics, gas flows, and different lubrication modes makes this advanced model able to predict ring/liner friction accurately for a variety of conditions. While the lubricants studied in the first phase of this research were certainly unusual, they were not out of the realm of applicability for this model, and results of the lubricant study should be considered to be realistic. However, the textured surfaces considered in the second phase of this study may have been close to the limitations of surface roughness for which this model was intended. Also, the averaged flow-factor method takes into account less detail about fluid flows and asperity contact than is required for an in-depth study of surface texturing. Then, the results of the this study may be used to assess the effects of the various parameter considered, and evaluate the potential of texturing techniques for reducing ring/liner friction, but further, more detailed study is required to predict the effects of specific surface features with good accuracy.

The subject of the initial phase of this research was the potential of changes in the lubricant viscosity to bring about a reduction in ring/liner friction. Lubricant viscosity affects friction both directly, by having a direct affect on hydrodynamic friction, and indirectly, by influencing the oil film thickness and thus the amount of asperity contact that occurs. Increasing viscosity tends to increase oil film thickness, and thus reduce asperity contact, but causes hydrodynamic friction to increase. A viscosity that balances between the hydrodynamic and boundary lubrication modes is required for minimum friction.

Changes in ring speed and load cause the “ideal” viscosity for low friction to change during the engine cycle. The object of the lubricant study was to determine the optimum viscosity for all points in the engine cycle, and evaluate the potential for friction reduction with such an idealized lubricant. Also, the effects of viscosity change on wear were considered.

Because of changes in ring speed, boundary friction becomes large in the dead-center regions of the piston stroke, while hydrodynamic friction dominates in mid-stroke. Thus, for the reduction of ring/liner friction force, a high viscosity is desired near end-strokes and a low viscosity near mid-strokes. However, the purpose of this study was to

reduce the power lost to friction, and, because of its dependence on speed, the power lost to friction is much higher near the mid-strokes than at the end-strokes, where piston speed goes to zero. Because of this, the viscosity of the lubricant in the end-stroke regions was found to have only a small effect on ring/liner FMEP, with the major realm of influence of lubricant viscosity occurring in the mid-stroke region. For the Waukesha engine ring-pack, a friction reduction of ~7% is predicted from reduction of mid-stroke lubricant viscosity.

Although viscosity near the end-strokes has very little effect on friction losses, it does influence ring/liner wear. Slow piston speeds cause asperity contact to be high at the end-strokes, resulting in high wear rates. When viscosity is kept high in these regions asperity contact and thus wear is reduced. Advanced lubricants with appropriate shear-rate dependencies or liner cooling systems that take advantage of the temperature-dependence of the lubricant viscosity may be able to achieve this in practice. A wear parameter analysis predicts that a reduction in wear of ~25% over an engine cycle is possible.

Surface texturing, also, can be used to reduce friction between the ring and liner. Numerous studies have predicted friction reductions with the addition of grooves, dimples, or other features to sliding surfaces. In the second phase of this research, the effect of surface patterns on friction in the hydrodynamic regime was evaluated. Friction reduction was observed when the surface texturing caused an increase in flow resistance, increasing oil film thickness and thus causing a reduction in both asperity contact and hydrodynamic friction. (In the latter case, the increased film thickness causes a reduction in oil shear rate). A parametric analysis of both grooved and dimpled patterns was performed, with the two purposes of studying the effects of various geometrical parameters on this friction reduction, and evaluating the potential of textured surfaces to reduce ring/liner friction and possibly justify further research in this area.

Groove parameters studied included the groove angle, width, depth, and area ratio, while parameters for the round dimples were the dimple depth, diameter, and area ratio. For both types of texturing, friction was found to decrease strongly with the depth of the features, and for grooved surfaces friction dropped substantially as groove angle was reduced (a groove with a lower angle is more perpendicular to the direction of piston travel). Also, for both types of texture, friction decreased with increasing area ratio, although not as strongly as with depth or groove angle. Groove width and dimple diameter had only a minor effect on ring/liner friction, with the dimpled surfaces showing a slight optimum effect (the lowest FMEP was predicted for a mid-range dimple diameter).

The analytical method used in this study did not allow for accurate predictions of ring/liner friction for specific cases, but the trends and orders of magnitude of the friction results can be used to illustrate the effects of textured surfaces and their potential for friction reduction. The study has indicated that even the relatively small-scale (compared to many evaluated in the literature) surface features considered may have a substantial effect on friction power losses. A reduction in oil control ring FMEP of as much as 30%, from a smooth surface case, is predicted for the best case studied. If the results of the parametric study are applied to the Waukesha engine ring-pack, a possible friction

reduction of 15-25% is estimated through control of groove angle. While these predictions are approximate and should not be used to design actual friction-reducing surfaces, they indicate that a substantial friction reduction may be possible with the addition of appropriate textures to the cylinder liner.

In addition to studying the lubricant viscosity and liner surface texture independently, the possibility of optimizing these two parameters together was also considered. Not only can concurrent optimization of lubricant viscosity and surface texture cause a greater friction reduction than each individual parameter, the occurrence of unwanted side-effects can also be reduced. A reduction in lubricant viscosity, while reducing friction, also causes an increase in wear because of the reduced oil film thickness. Adding a surface texture to the liner may also reduce friction, but does so by causing an increase in oil film thickness which may in turn cause an increase in oil consumption. Fortunately, the effects of the two changes are opposed: reducing viscosity reduces oil film thickness, whereas adding surface texturing increases it. If the viscosity and texturing effects are considered together, the lubricant and liner surface can be designed so that oil film thickness remains constant, thus eliminating the wear and oil consumption increases, while still reducing friction.

The nature of the combined optimization of lubricant viscosity and surface texturing is essentially to use the increase in hydrodynamic pressure brought about by the texture to allow lubricant viscosity to be reduced. Then, the source of the friction reduction is purely hydrodynamic, and stems from the reduced viscosity. This study has indicated that the amount of friction reduction possible using a combined method is proportional to that possible from surface texturing alone. For the best combination of surface and lubricant studied, compared to a smooth surface with the lubricant currently used in the Waukesha engine, a reduction in FMEP of greater than 50% is predicted for the oil control ring, translating into a reduction of ~30% for the ring-pack. While friction reduction will likely be less than this when applied in real situations (particularly as many surfaces and lubricants are already well-optimized compared to the smooth surface case used as the baseline in this comparison,) this prediction indicates that there is significant potential for friction reduction via concurrent optimization of lubricant and surface properties.

The results presented above are believed to be as realistic as possible given the scope and constraints of this study. However, several approximations and simplifications have been made, and some factors not considered. Several recommendations for further study, both analytical and experimental, can be made, to both advance the state of knowledge on the topics studied here and to move towards an integrated, low-friction system for the Waukesha engine.

(B) FRICTION REDUCTION VIA PISTON DESIGN – A CUMULATIVE REPORT

6. Friction Reduction Strategies - Piston Design

The piston skirt contributes as much friction as the ring-pack to the engine mechanical losses. Like the ring-pack, its friction can be reduced if asperity contact is reduced. The piston experiences both hydrodynamic and boundary lubrication, with the dominant lubrication regime changing during the engine cycle. While the hydrodynamic frictional losses from the two sides are approximately equal and occur throughout the stroke, boundary contact is only observed on the major thrust side, during the expansion stroke. This results from the high gas pressures present after combustion, as well as the piston "slap" as it moves from the minor to the major thrust side. The boundary friction generated in this region of the stroke contributes a significant amount of total piston skirt friction.

Several piston parameters have been studied earlier in the program, including design parameters such as the skirt profile and waviness, and other factors including lubricant viscosity and skirt-liner clearance, with the goal of reducing friction. The most important parameters identified thus were oil film thickness and skirt waviness, which can both be manipulated to reduce friction by reducing skirt/liner asperity contact.

In this reporting period, emphasis has been placed in the practical design parameters which offer the greatest potential for near term implementation, viz. mechanical design of the piston itself such as piston skirt ovality, the physical dimensions of the piston skirt, and optimizing the lubricant parameters for pistons of certain geometrical and material designs. These issues have not been addressed earlier. Rather than presenting only results of these incremental developments, this report includes results of all major piston design consideration to place the effects of each parameter in the proper context. A brief review of the model formulation and approach is also included for completeness.

6.1. Typical piston designs

In general, the piston consists of an upper region, containing grooves for the piston rings, and a lower region known as the "skirt". The skirt supports the piston/liner contact pressures, and is the site of friction generation and wear. Thus, this is the main region of interest in this study. Skirt friction and wear are affected by three design characteristics, the skirt profile, the waviness, and the surface roughness. The skirt profile is of the largest scale, and describes the large-scale variation in piston radius in the axial direction. The waviness results from the piston machining process and results in circumferential surface grooves on the scale of 10μ. The roughness is on yet a smaller scale, on the order of 1μ or less, and is controlled by the skirt material and the surface finishing techniques used. All of these piston characteristics affect friction, although the amount and the manner in which they affect friction depend on several other factors, including lubricant formulation and the extent of piston wear.

Pistons are produced with many different profiles, including tapered, barrel, and others, each offering advantages and disadvantages. This study focuses on barrel-profile

pistons, such as the one shown schematically in Figure 6-1. The barrel shape of the skirt maintains a small piston diameter near the upper land, which allows for thermal expansion, while maintaining a relatively large wetted skirt area, which helps to reduce wear. The barrel shape also assists in creating a hydrodynamic oil film, and improves stability and reduces clearances by allowing for the natural secondary motion of the piston. The proportions of the barrel shape – i.e., the curvature of the bulge – have a large effect on piston/liner surface generation.

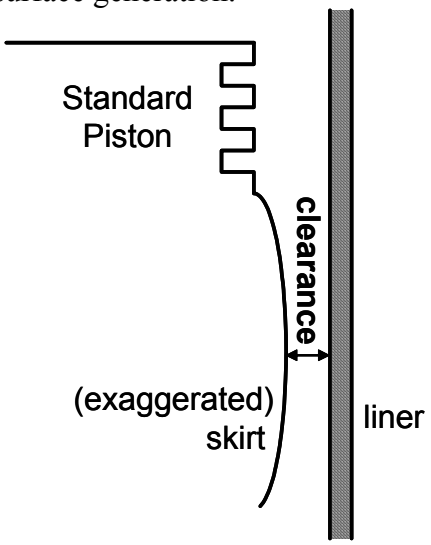

Figure 6-1: Piston with a barrel-shaped skirt

The waviness and roughness of the skirt also affect friction. Figure 6-2 shows a schematic of worn and unworn piston surfaces. For an unworn piston, the affect of the waviness dominates any roughness affects, because the waviness is on a larger scale. In this case, friction is dominated by the contact of the peaks of the waviness with the cylinder liner, causing boundary friction to occur. Contact occurs only at the high points of the machining grooves, with the height of those points determining when and how much contact occurs. As this type of contact continues, however, the peaks are worn down, as shown in the figure. In the worn case, the texture of the flat "plateaus" that has replaced the waviness peaks may become dominant. In this case, the height of flat surface roughness determines the extent of any asperity contact.

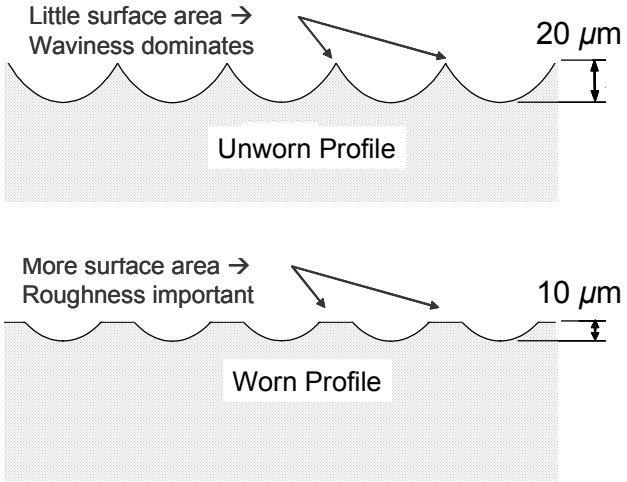

Figure 6-2: A side view of skirt waviness, worn and unworn cases.

6.2. Analytical methods

A previously developed and experimentally validated model of piston secondary motion, developed by Wong et al., was modified and used in this study [37]. The modifications to the model consisted of including the influence of temperature on lubricant viscosity and variation of oil availability to the piston during the engine cycle [38]. When the piston moves up and down in the cylinder, it experiences substantial changes in temperature, which affect the local viscosity of the oil on the piston-skirt/liner interface. While the original model did not include this effect, and assumed a constant viscosity, a Vogel equation relationship was subsequently added in order to obtain a more accurate model of oil viscosity. For simplicity, only straight-weight oils (SAE-20, SAE-30, SAE-40, and SAE-50) were included in the analysis (shear rate dependence was not considered

6.2.1. Modeling and governing equations for piston friction and lubrication

Several aspects of the piston/liner system make its analysis more complicated than the ring analysis. First, the piston is assumed to be always starved – that is, a fully-flooded condition does not exist, the piston is always only wetted over a portion of its surface. Also, the piston must be treated as a 2-dimensional system, a 1-D approximation like that used for the rings cannot be used, because of the spreading of lubricant in the tangential as well as the axial direction during wetting. In the model, the entire surface of the piston is taken into account, so that the changes in the locations of applied forces and lubricant wetting during the cycle are accounted for.

The flexibility of the piston also makes its analysis complex. In addition to tilting and displacing, as a unit within the cylinder liner, the piston skirt also deforms, in response to various applied forces. This skirt deformation is due in large part to the pressures applied by the oil film, which are in turn highly influenced by the skirt geometry. This phenomenon adds yet another iteration step to the analysis of the piston lubrication and friction.

6.2.1.1. Force and momentum balances

Simple force and momentum balances are used to model the dynamics of the piston. Vertical and lateral force balances are applied, taking into account gas pressures, piston inertia, ring forces, friction forces and thrust forces, as indicated in Figure 6-3. In the figure, the y-axis is in the vertical direction (positive up) and the x-axis is in the horizontal direction (positive to the right). Balances of forces and moments about the wrist-pin yield [37]:

$$\Sigma F_y: \quad F_g + \hat{F}_{IP} + \hat{F}_{IC} + \tilde{F}\cos\phi + \sum F_{qj} + F_f = 0 \tag{2.18}$$

$$\Sigma F_y: \quad \sum F_s \delta_s + F_{IP} + F_{IC} - \tilde{F}\sin\phi + \sum F_{rj} = 0 \tag{2.19}$$

$$\Sigma M_p: \quad -\sum F_s y_s \delta_s + M_{IP} + M_{IC} + M_{PP} + F_{IC}(a-b) - \hat{F}_{IC} C_g + F_g C_p + M_f + C_p \sum F_{qj} + \sum F_{rj} Ij = 0 \tag{2.20}$$

where the terms in the above equations are:

Table 6-1: Definition of terms in piston equilibrium equations

Parameter	Definition
F_g	Combustion gas force acting on top of the piston
$\hat{F}_{IP}$,F_{IP}	inertia force due to wrist-pin mass, x and y-directions
$\hat{F}_{IC}$,F_{IC}	inertia force due to piston mass, x and y-directions
F_q	vertical/normal force between piston and rings
F_r	horizontal/shear forces between piston and rings
F_f	total friction acting on the skirt, thrust and anti-thrust sides
F_s	side force, either F_1 or F_2 in the figure, depending on where contact occurs
δ	1 if contact occurs, 0 if it does not
$\tilde{F}$	connecting rod force
ϕ	connecting rod angle
M_{IC}	inertia moment of piston
M_{IP}	inertia moment of wrist-pin
M_{pp}	moment about wrist-pin due to wrist-pin friction
a	vertical distance from top of skirt to wrist-pin axis
b	vertical distance from top of skirt to piston center of gravity
C_g	horizontal distance between piston center of mass and wrist-pin
C_p	horizontal distance of wrist-pin from vertical piston axis (pin offset)
M_f	moment about wrist-pin due to all friction forces, thrust and anti-thrust sides
l_r	vertical distance(s) between wrist-pin axis and rings

These relationships are used to solve for the piston position and tilt as a function of time (or crank angle). Some inputs must be calculated iteratively, as they depend on the hydrodynamic lubrication of the piston, including side forces and piston/liner friction forces.

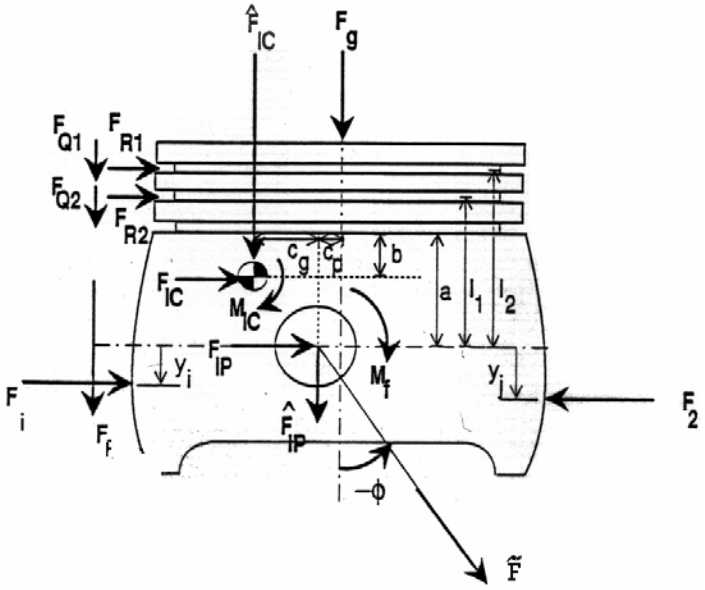

Figure 6-3: Forces and moments acting on the piston

Figure 6-4 shows the piston geometry, and definition of e_t and e_b, the eccentricities of the piston at the top and bottom of the skirt, respectively. These two terms and their time derivatives are used to define the piston tilt and displacement in the piston equations of motion:

$$\begin{bmatrix} m_{PP}(1-\frac{a}{L})+m_{Pis}(1-\frac{b}{L}) & m_{PP}\frac{a}{L}+m_{Pis}\frac{b}{L} \\ \frac{I_{Pis}}{L}+m_{Pis}(a-b)(1-\frac{b}{L}) & m_{Pis}(a-b)\frac{b}{L}-\frac{I_{Pis}}{L} \end{bmatrix} \begin{bmatrix} \ddot{e}_t \\ \ddot{e}_b \end{bmatrix} = \begin{bmatrix} F_\sigma + \sum F_s \delta_s + F_f \tan\phi \\ M_s + \sum F_s y_s \delta_s + M_f \end{bmatrix} \quad (2.21)$$

where m_{PP} is the wrist pin mass, m_{Pis} is the piston mass, L is the skirt height, F_σ and M_s, and all other terms are defined above in Table 6-1.

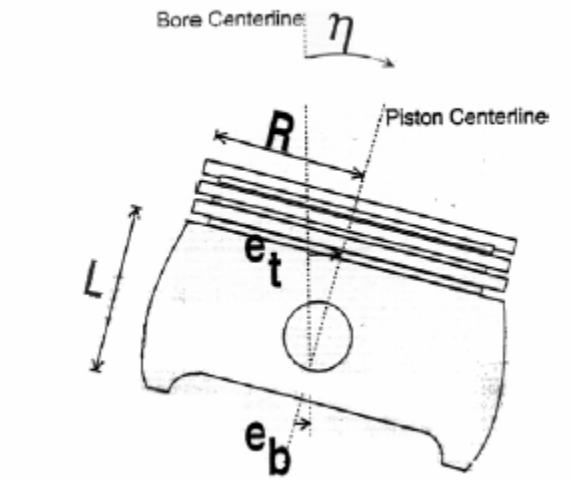

Figure 6-4: Piston geometry, showing definition of eccentricities

6.2.1.2. Reynolds equation: skirt hydrodynamic lubrication

The piston skirt experiences both hydrodynamic and boundary lubrication. In the hydrodynamic regime, the relationship between lubricant wetting and hydrodynamic pressure is defined by the two-dimensional Reynolds equation, which have been described in full in earlier annual report.

$$\frac{\partial}{\partial x}\left(\frac{h^3}{\mu}\frac{\partial p}{\partial x}\right)+\frac{\partial}{\partial z}\left(\frac{h^3}{\mu}\frac{\partial p}{\partial z}\right)=6U\frac{\partial h}{\partial x}+12\frac{\partial h}{\partial t} \quad (2.22)$$

Flow factors are used in conjunction with the Reynolds equation, to account for piston roughness and waviness. The skirt/liner separation, h, consists of four components: the factory machined (cold) skirt profile, thermal distortion, deformation due to cylinder pressure force and deformation due to pressures on the skirt. Deformation at the waviness peaks is given by:

$$\left.\begin{array}{l}\delta = \Omega - h \\ \delta = 0\end{array}\right\} \begin{array}{l}\Omega > h \\ otherwise\end{array} \tag{2.23}$$

where δ is the deformation, and Ω is the amplitude of the surface waviness.

These lubrication and deformation equations must be solved iteratively with the equations of motion to define the piston motion and friction conditions.

6.2.1.3. Boundary conditions

Several boundary conditions are required to solve the piston/lubricant/liner system. At the edges of the wetted area, the oil pressure is assumed to be equal to the ambient gas pressure (external gas pressures are assumed to be known). Then:

$$p(wetted \quad edge) = P_{amb} \tag{2.24}$$

where P_{amb} is the ambient gas pressure around the lubricant.

Also, if the skirt is symmetric, it is assumed that the pressure distribution is across a symmetry line is symmetric. For such a skirt, about thrust or anti-thrust lines:

$$\left.\frac{\partial p}{\partial x}\right|_{x=0} = 0 \tag{2.25}$$

There may be a significant amount of oil that does not contact the skirt, but must be accounted for in the analysis because of its effect on neighboring wetted areas. This oil is assumed to be at ambient pressure. Then, in the case of oil on the liner that does not contact the skirt, (is between peaks of the waviness, for example):

$$p = P_{amb} \tag{2.26}$$

The wetted area of the piston is determined by geometry and conservation of mass for the lubricant. When the piston transitions from one side of the liner to the other, a given thickness of oil is present on the liner (the thickness is specified in the model, so that the effects of oil availability can be easily assessed). The extent of the wetting is then controlled by the amount of available oil and volume it occupies when squeezed between the piston and liner. The wetting condition must be solved iteratively along with the piston dynamics and deformation.

6.2.2. Iteration and solution algorithm

The piston tilt and displacement, as well as the deformed profile of the skirt must be known in order to solve for hydrodynamic and boundary friction forces, but these

forces, in turn, must be known to calculate the piston dynamics. Using the boundary conditions described in the previous section, the pressure distribution and skirt profile are solved iteratively, using a finite-difference method in space and time, along with a relaxation scheme. The piston is assumed to be partially flooded, with wetting conditions defined by the boundary conditions given.

The numerical approach is to first determine piston-skirt side forces, using the hydrodynamic relationships, as functions of e_t, e_b and their time derivatives, and crank angle. These are then used to solve the piston dynamics equations in the time domain. The iteration is repeated until convergence is reached.

Like the ring-pack model, the piston model also takes surface roughnesses into account using averaged flow-factor techniques. The flow modeling equations used in the simulation are different than those shown above, which do not include flow factors for simplicity. Instead, averaged flow relationships are used, which account for surface texturing as explained further in [37].

6.3. Application to Waukesha engine

The project was conducted in collaboration with Waukesha Engine Dresser and Colorado State University, which operated a Waukesha VGF-18 in their laboratory. The Waukesha VGF in-line 6 engine configuration (155 mm bore x 165 mm stroke) is turbocharged, aftercooled, with modern combustion chamber design. The piston friction model was exercised with geometric and operating parameters from this engine; more details of the specifications are shown in Table 4-1 in an earlier Section 4.

7. Effects of Piston Parameters on Piston Friction

7.1. Skirt-liner clearance

As the piston travels up and down in the cylinder, it also rotates and moves transversally in a secondary motion, due to changing gas pressures and inertias. Instead of traveling along the axis of the cylinder, the piston presses against on side of the liner as it moves towards the combustion chamber, then moves to the other side as it travels down. When the piston transitions from one side to the other a "slap" occurs, when the piston hits the liner and oscillates briefly before remaining pressed against it, see Figure 7.1. The impact velocity of this slap affects the amount of noise produced by the engine as well as the piston frictional losses.

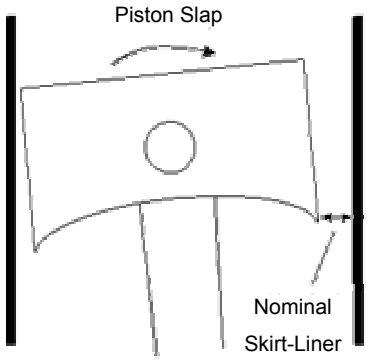

Figure 7-1: Schematic of piston and liner, showing skirt-liner clearance and piston slap

The skirt/liner clearance directly affects the impact speed of the piston slap. Figure 7-2 shows how the skirt impact velocity changes with cold clearance. A larger clearance allows the piston to accelerate over a larger distance, resulting in a faster impact speed at the slap. Large impact velocities lead to large impact forces, which lead in turn to large contact friction losses. Then, skirt/liner friction should be reduced as clearance is reduced. This was found to be the case for larger oil thicknesses, but for thinner oil films, as shown in Figure 7-3, a minimum point observed, where friction begins to increase again when clearance is decreased.

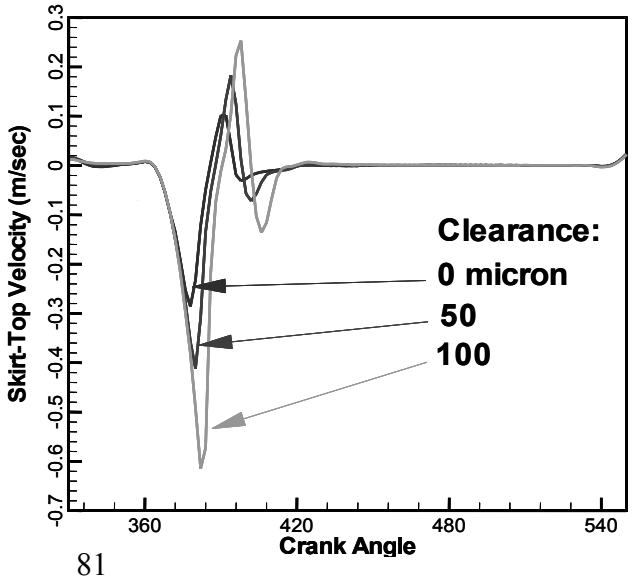

Figure 7-2: Skirt impact velocity increases as cold clearance increases

This minimum point results from asperity contact occurring at tight clearances, which increases friction, by bringing the skirt and liner surfaces closer together for low oil film thicknesses. In Figure 7-3, for large clearances the slapping velocity dominates and friction decreases as clearance decreases, while for very small clearances asperity contact becomes important and friction begins to rise while clearance is decreased. The figure also shows almost no change in hydrodynamic friction with clearance, showing that the cause for the friction change is largely due to changes in asperity contact.

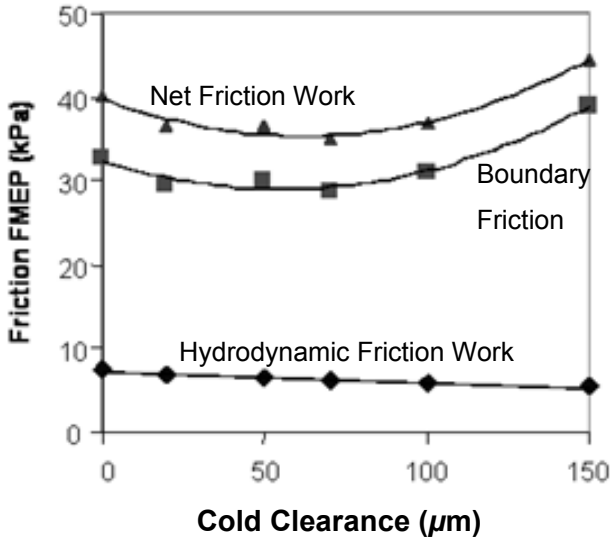

Figure 7-3: Effect of skirt/liner clearance on friction

The ideal skirt-liner clearance provides sufficient space for the oil but is not large enough to produce significant impact (Figure 7-4). For the Waukesha F18GL engine under the conditions of this study, the ideal clearance was 50 μm.

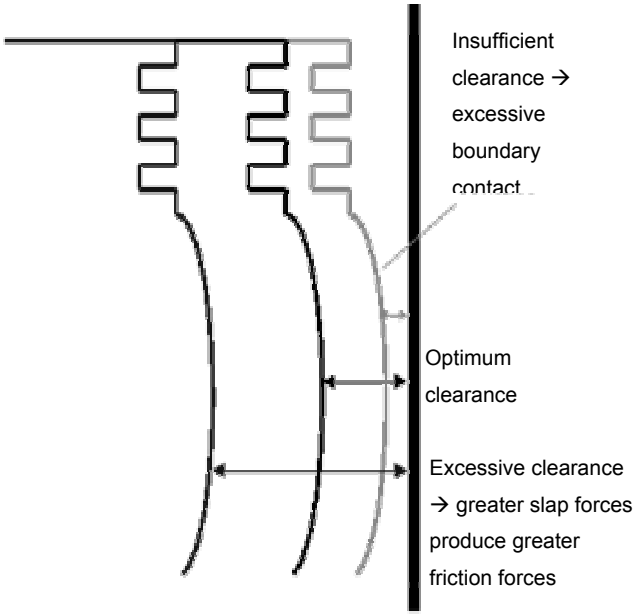

Figure 7-4: Illustration of Optimal Clearance on Friction

(Interpretation of results: insufficient clearance produces excessive contact friction, while excessive clearance produces excessive impact)

7.2. Oil supply/oil film thickness

The mechanisms of oil distribution between the piston and liner are not fully understood. For the purposes of a parametric study, a simplified model was used that allowed oil availability to be set as a model input. The current model does allow the film thickness ahead of piston skirt motion to be specified as a function of time during the cycle. It is assumed that, prior to piston impact, an oil layer of a given thickness is available on the liner. The wetting locations are determined by the boundary condition that the oil film pressure is equal to the gas pressure around the skirt at the wetted edges, as well as piston and liner geometry. This served to specify the oil supply to the skirt and the oil film thickness between skirt and liner.

Oil film thickness, which is controlled by oil supply, has a direct impact on friction. A very thin oil film enables the skirt to easily push the oil aside and contact the liner, leading to boundary friction. On the other hand, a thick oil film tends to encourage hydrodynamic lubrication by providing more contact between the film and the piston surface, thereby enabling the lateral force to be spread over a larger area. Figure 7-5 provides a schematic comparison. As the film thickness is increased to a certain point, it reduces boundary contact friction to a very small value, which minimizes net friction work loss. If film thickness is increased beyond this critical point, however, no further reductions in boundary friction are available, and hydrodynamic friction increases due to an increase in wetted area. Thus, increasing film thickness beyond the critical point can actually increase net friction.

	
Large oil film thickness	**Small oil film thickness**
Large wetted area	Small wetted area
Negligible direct surface contact	Significant direct surface contact
Primarily hydrodynamic lubrication	Primarily boundary lubrication

Figure 7-5: Schematic of large and small oil film thicknesses, showing operational characteristics of each

The oil film thickness has a much greater impact on boundary friction than hydrodynamic. Figure 7-6 shows a rapid increase in boundary friction as film thickness is decreased, due to an increase in the amount of boundary contact that occurs as the piston and liner surfaces are brought closer together. In this example, the boundary contact friction dominates, so the total friction curve follows the same trend. When the film thickness has reached about 80 μm, the boundary contact friction component is negligible, and further increases in film thickness increase hydrodynamic, and therefore net, friction loss. (The minimum point shown in the figure stems from the fitting technique used to fit the simulation data points, and probably does not have any physical basis). Only a small change in hydrodynamic friction is observed throughout the range of film thicknesses considered.

Comparing Figure 7-6 to Figure 7-3 also shows that the oil film thickness has a much larger effect on piston friction than skirt/liner clearance. The main effect of the clearance is to control friction at the "slap" period of the piston transition, while the film thickness affects skirt/liner contact throughout the cycle.

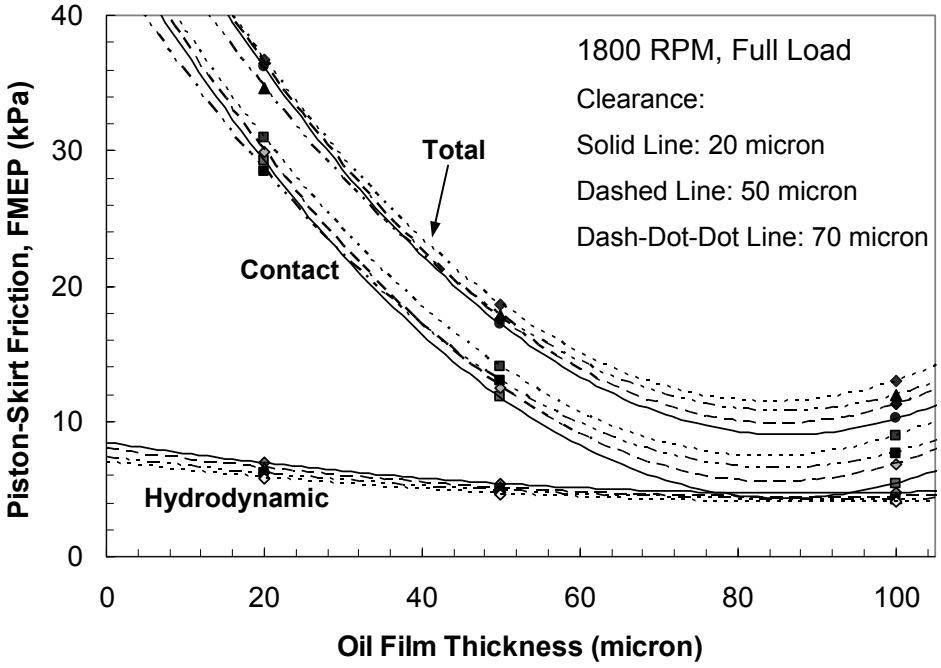

Figure 7-6: Effect of oil film thickness on skirt/liner friction
("Clearance" refers to cold skirt-to-liner clearances)

While its effect on friction is clear, the lubricant film thickness may also affect other engine parameters. For example, a thicker oil film can serve to cushion engine slap, reducing engine noise and vibration as well as friction. However, if the film is too thick, oil consumption may become a problem.

7.3. Surface finish/waviness

The piston skirt is typically machined so that it is covered by circumferential grooves, with depths on the order of 10μ, as well as smaller scale "roughness" asperities, of 1-2 orders of magnitude smaller in size. The grooves behave as oil reservoirs, supplying oil for hydrodynamic lubrication. The customary measure of groove size is waviness, which is the "amplitude" (*i.e.*, half of the peak-to-valley depth) of the groove. A schematic is shown in Figure 7-7.

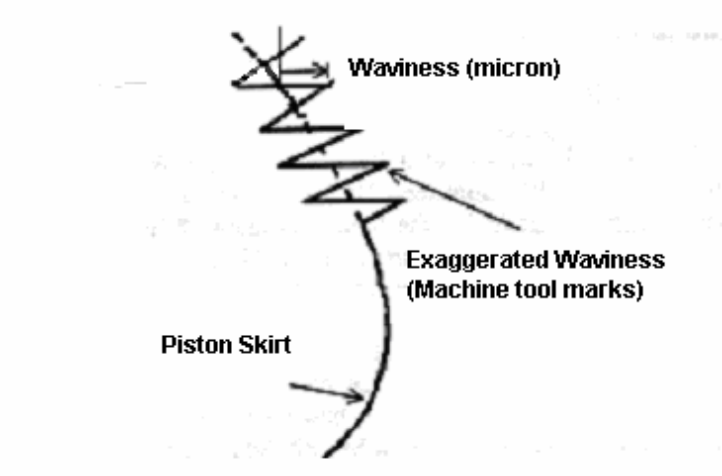

Figure 7-7: Piston skirt waviness, measured peak-to-peak values

The liner also affects oil flow and retention. In typical large natural-gas engines, liners have a honing pattern that serves much the same purpose as the waviness pattern on the piston: the grooves retain oil by surface tension and serve as an alternate supply, and they also provide flow paths for oil. Unlike the piston, in which grooves are machined circumferentially, the grooves in the liner are often oriented at an angle relative to the horizontal. The honing angle, as it is called, has a modest impact on friction. Shallow honing angles (relative to the horizontal) encourage oil to flow laterally rather than move up or down the liner, which would be undesirable.

7.3.1. Waviness vs. roughness

Surface roughness refers to the natural deviations of an actual surface from a geometrically smooth shape. Any metal shape has natural surface roughness that is related to the method of manufacture, degree of polishing, and other factors. In a ring surface, surface roughness plays an important role because it serves much the same purpose as waviness on a piston surface: the valleys serves as oil reservoirs, and the gaps between the peaks provide flow paths for oil. In a piston, however, the waviness amplitude is greater than the roughness amplitude, often by an order of magnitude. The difference between roughness and waviness in the model is illustrated in Figure 7-8. Thus, although roughness would be expected to play an important role in a piston with a nominally smooth (un-honed) surface, roughness only slightly modifies the effective amplitude of the waviness peaks in typical pistons. Therefore, roughness amplitude is expected to have a negligible effect on friction.

Tests were conducted to evaluate the effect of roughness on friction, but they showed a negligible effect, as expected. In the model, surface waviness was on the order of 10 microns, while surface roughness was on the order of only one micron, which are typical values for large natural-gas engines. The model, which assumed a sawtooth pattern for waviness, confirmed that changes in roughness had little impact on net friction.

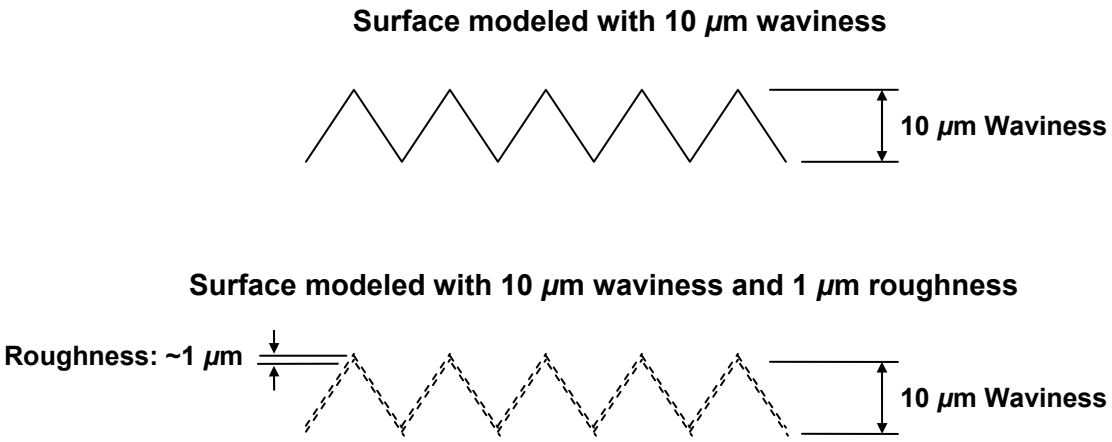

Figure 7-8: Schematic of surface waviness with and without roughness

7.3.2. Parametric study results (surface waviness)

Figure 7-9 and Figure 7-10 show that friction losses decrease as surface waviness decreases, largely due to a decrease in boundary friction. For a given availability of oil, a piston with deeper machining grooves has more volume to contain the oil – that is, the lubricant can be trapped within the machining grooves instead of staying between the piston and liner. When it is contained within the grooves, the oil is not useful as a lubricant or to support hydrodynamic pressure, and asperity contact occurs. Conversely, when the oil cannot escape into deep machining grooves and is compressed between the piston and liner, hydrodynamic pressure is generated and the piston load can be fully supported on the oil film.

The relation of friction to surface waviness suggests a dependence not only on waviness height, but on the relation of the waviness to oil availability. A smoother piston should require less oil to support hydrodynamic lubrication, while a very wavy piston should require more. Figure 7-11 indicates that this is indeed the case, and that there is a nearly linear relationship between waviness:film-thickness ratio and piston friction. Thus, in cases where very little lubricant is available to the piston a low waviness is preferred, whereas in cases where a large film thickness is possible, a smooth piston is still preferred but a wavier surface is allowable. However, in all cases, a very smooth piston is undesirable, due to factors not included in the present model.

Although skirts with low waviness values appear to produce the lowest friction, extremely smooth surfaces can lead to high friction, wear and sometimes seizure. Extremely smooth surfaces do not retain oil well, so that direct solid-solid contact, if and when it occurs, can be very poorly lubricated and quite severe. Also, the contact surface area may be larger in cases of very smooth surfaces, further contributing to friction and wear. Therefore, friction can be minimized by selecting small but nonzero waviness values, to prevent scuffing. For all other tests in this analysis, a constant waviness of 10 μm was used.

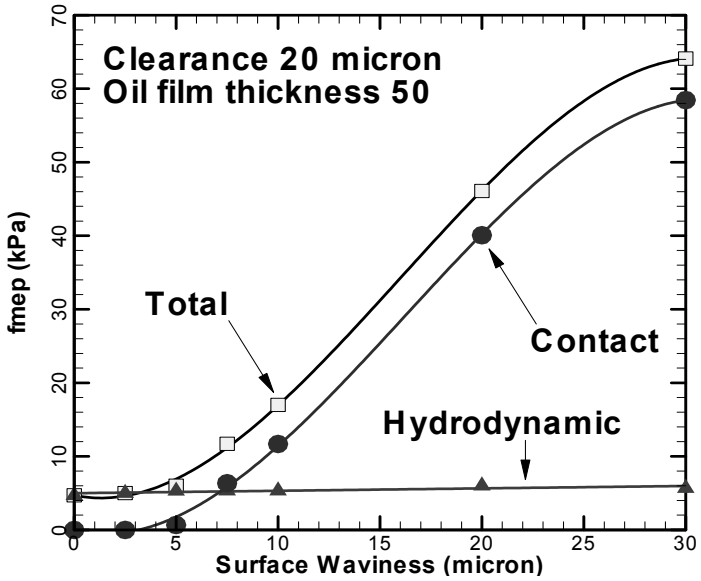

Figure 7-9: Dependence of friction on skirt waviness

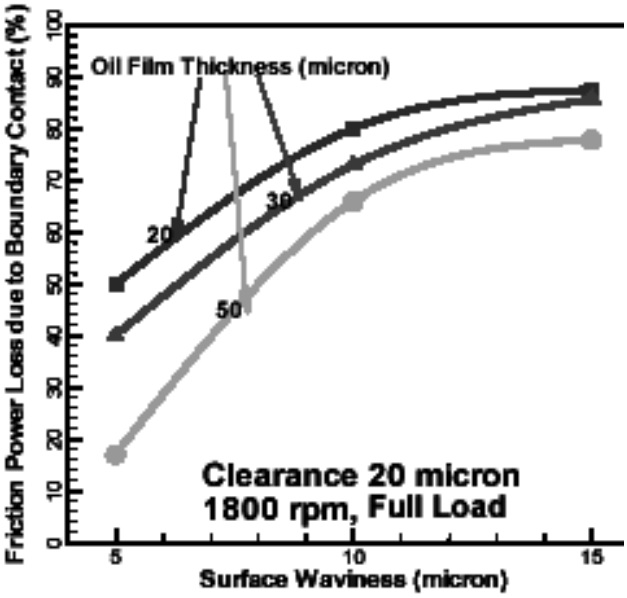

Figure 7-10: Dependence of friction power loss on skirt Waviness

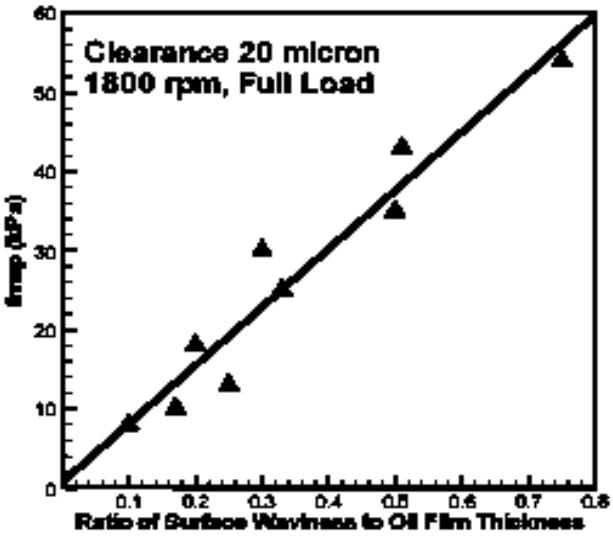

Figure 7-11: Dependence of friction loss on the ratio of waviness to film thickness

In addition to the waviness, the piston surface has a smaller scale roughness, of asperities on the scale of 1μ or less. An analysis of the effect of changing this roughness revealed almost no change in piston fmep with this variable, indicating that the effect of the roughness is dominated by the macroscopic waviness. Since the characteristic length of waviness (*i.e.*, the depth of the machined grooves) is typically an order of magnitude greater than roughness, the effect of waviness on friction loss dominates.

7.4. Piston-skirt profile/shape

A sensitivity analysis of the effects of piston curvature on skirt-friction was performed by evaluating a variety of polynomial piston-skirt axial profile shapes, shown in Figure 7-12. Each profile was defined by a simple $f(x) = x^n$ polynomial, where x was the vertical distance on the skirt (measured from the mid-point), n was the order of the polynomial, and $f(x)$ was the deviation of the profile from a perfect cylinder (which would be represented on the figure by a vertical face at 200μ). Higher-order polynomials were flatter in the midsection and dropped off dramatically at the extreme points, so that higher-order profiles were flatter overall. When cold, the maximum bulge of each profile was 200 μm, which is the same depth as the actual stock profile. For each profile, the cold skirt-to-liner clearance (measured at the point of maximum bulge to the liner) was kept constant at 20 microns.

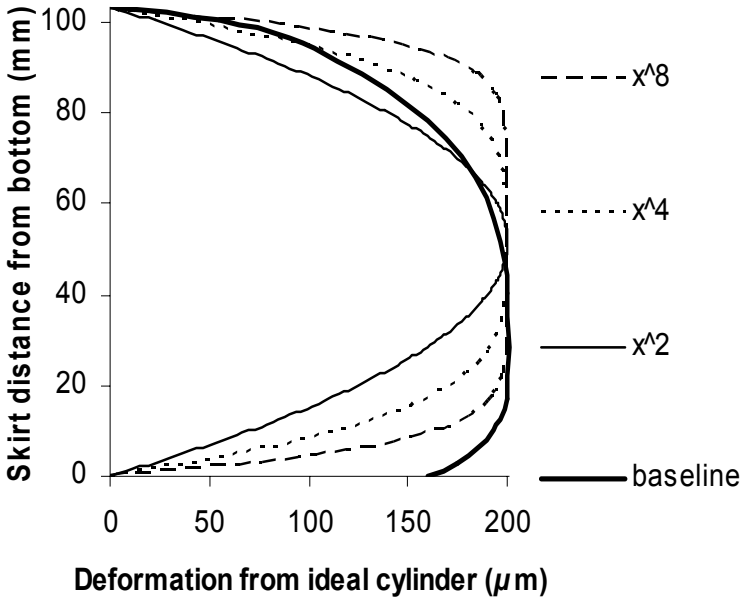

Figure 7-12: Piston profile shapes

As shown in the following figures, changing the "flatness" of the skirt changes both the hydrodynamic and boundary friction of the piston. All results shown are for the major thrust side of the piston, which is of primary interest because a large portion of total cycle friction (including almost all of the boundary friction) is generated there. Several are also shown at 50^o after TDC combustion, because hydrodynamic forces are highest at this crank angle. Also, all simulations were run using SAE 40 grade oil. There is an interaction between piston profile and oil viscosity, which is discussed in a subsequent section.

Figure 7-13 shows the effect of a changing skirt profile on the piston wetting. A flatter skirt shows both a larger wetted area and a thicker oil film. The thicker oil film indicates that separation between the piston and liner is increased, decreasing boundary contact or possibly eliminating it entirely. An increase in wetted area size and film thickness tends to lead to an increase in hydrodynamic friction losses, but this also results in a lower

average and peak oil pressures, as is shown in Figure 7-14, which could help reduce hydrodynamic friction. The increase in wetted area and oil film thickness (skirt/liner clearance) is sustained throughout the stroke, as shown in Figure 7-15.

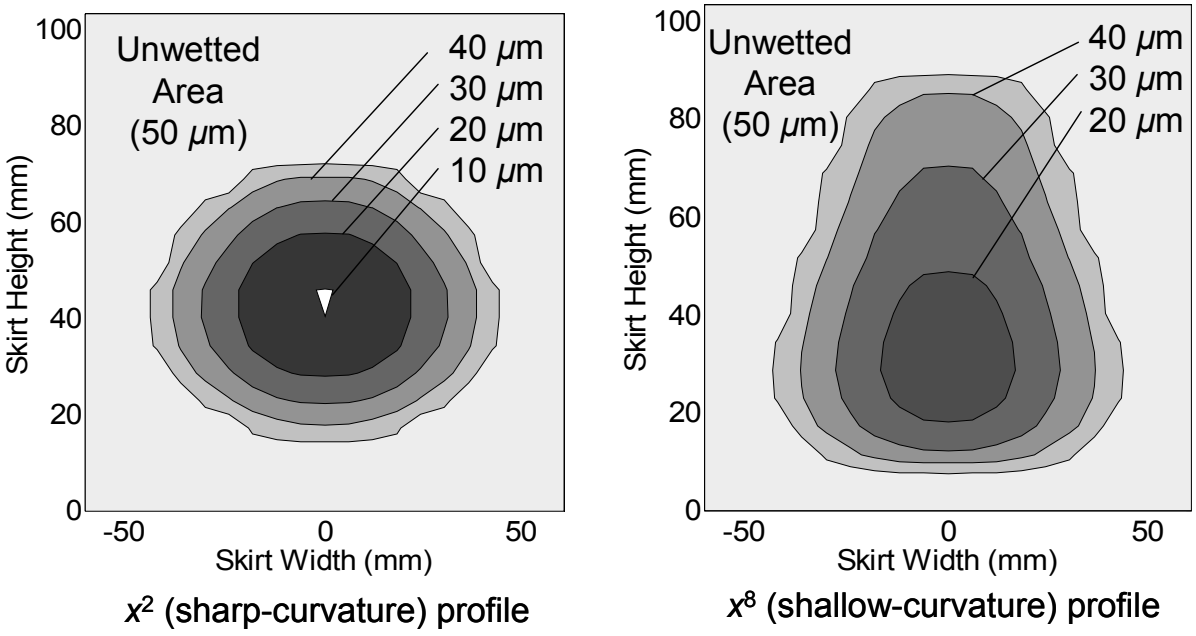

a. sharp-curvature skirt **b. shallow-curvature (flatter) skirt**

Figure 7-13: Oil film thickness in wetted areas for sharp and flat skirts, at 50° ATDC, during expansion

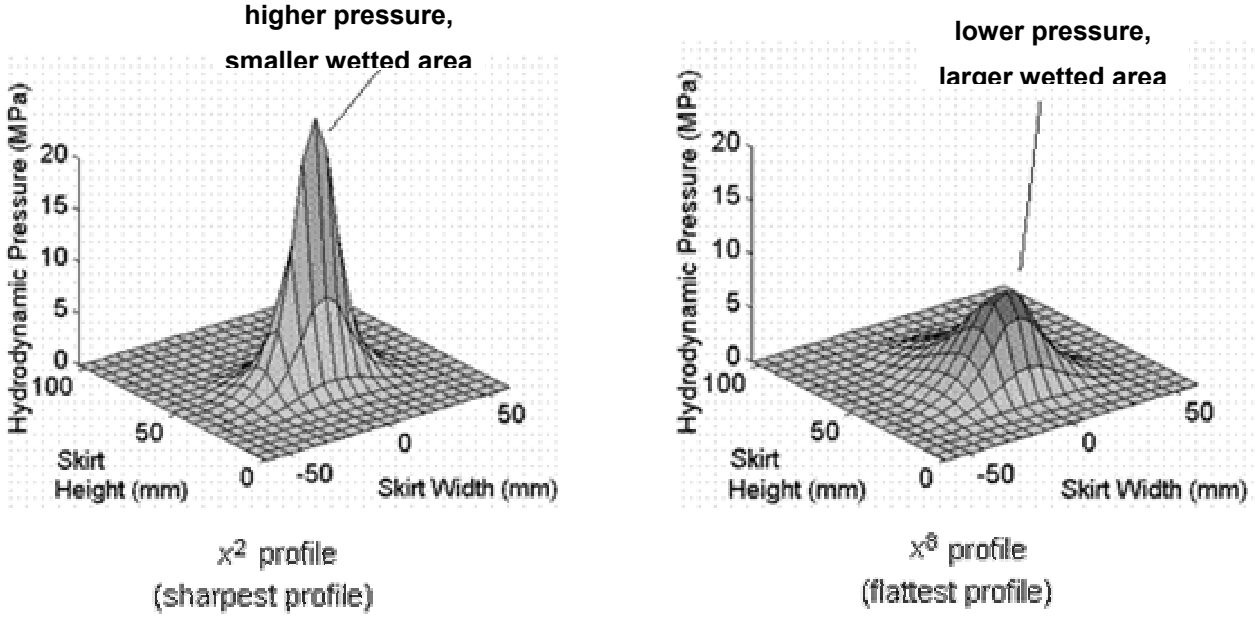

a. sharp-curvature skirt b. shallow-curvature (flatter) skirt

Figure 7-14: Pressure maps for sharp and flat skirts, at 50° ATDC, during expansion

In Figure 7-15a, the skirt-liner clearance for sharper profiles drops significantly below the waviness height, for a large portion of the cycle, meaning that substantial boundary contact is occurring and high friction forces created. For flatter profiles, skirt/liner clearance drops below the waviness height briefly, and only by a small amount, indicating that much less metal-metal contact is taking place. Figure 7-15b shows that a piston with a flatter profile experiences more wetting during the entire engine cycle, so that the change in hydrodynamic lubrication is the same throughout.

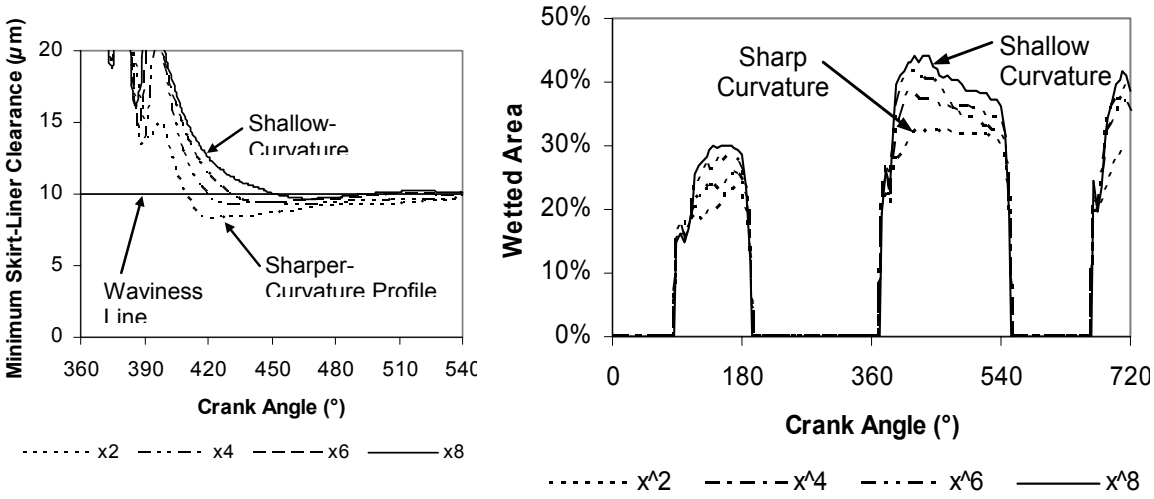

a. Details of profile effect on skirt-liner contact during 360-450° range

b. Percent wetted area for piston on thrust side

Figure 7-15: Effect of skirt-profile on skirt/liner wetting and contact

The change in skirt/liner clearance with piston profile suggests that a sharper profile experiences much more boundary friction than a flatter one. The simulation confirmed that a flatter piston profile causes a large reduction in boundary friction, along with a slight increase in hydrodynamic friction, as shown in Figure 7-16. Figure 7-16a shows that changing the piston profile has a substantial effect on the amount of boundary friction generated, with metal-metal contact almost entirely eliminated for the flattest case. In Figure 7-16b, a small increase in hydrodynamic friction is shown for flatter profiles, but the change is much smaller than the corresponding change in boundary friction. Figure 7-17 shows the cumulative cycle friction loss with profile, for two different viscosity oils. In both cases, the piston fmep decreases for flatter profiles, with boundary contact decreasing substantially along with smaller increases in hydrodynamic friction. This is the case for both oil viscosities, although the proportion of the changes in hydrodynamic and boundary friction is different for the two cases. The relationship between piston profile and lubricant viscosity is discussed further in the following section.

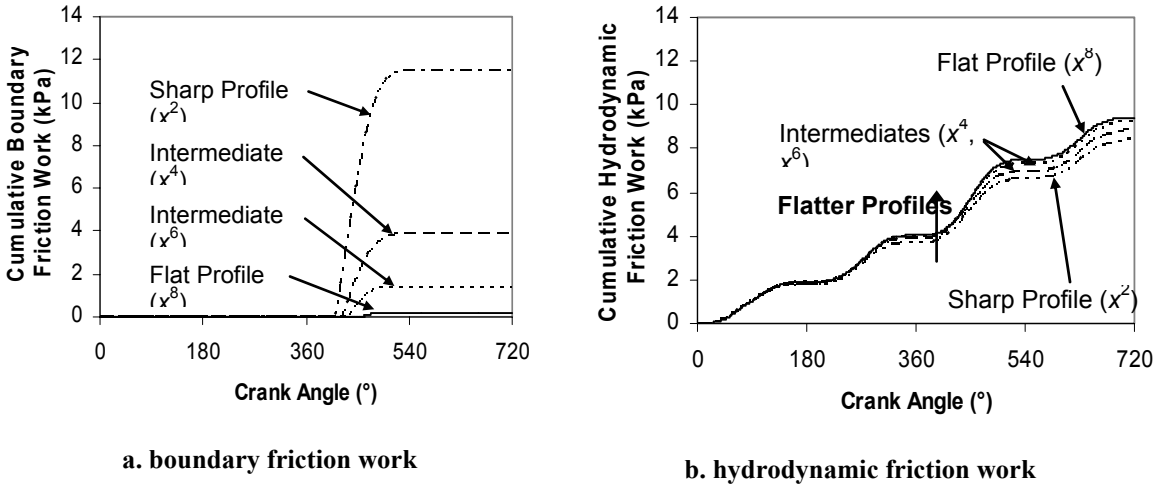

a. boundary friction work

b. hydrodynamic friction work

Figure 7-16: Comparison of cumulative friction work during the cycle, various piston skirt-profiles

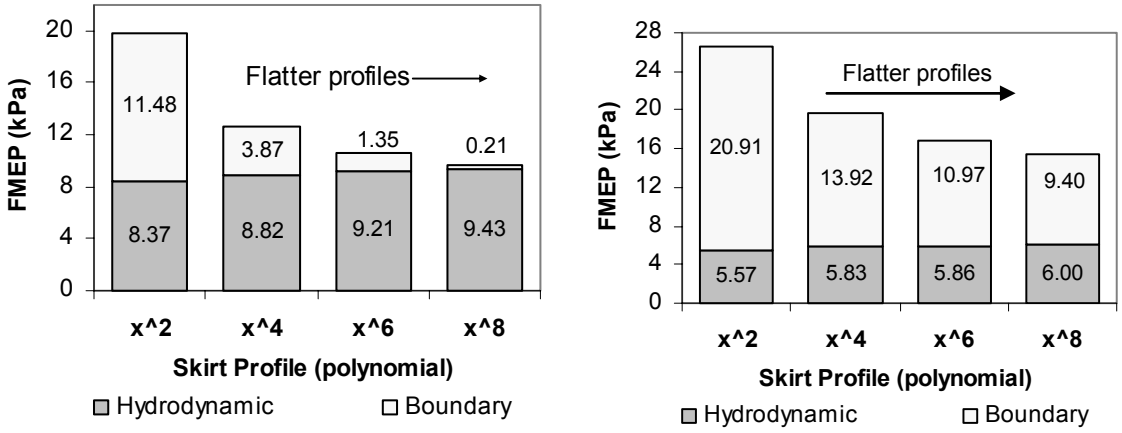

a. high viscosity (SAE-40) oil

b. low viscosity (SAE-20) oil

Figure 7-17: Effect of profile shape on hydrodynamic and boundary friction losses

7.5. Piston-skirt size

The size of the piston skirt is an important parameter in piston design. For example, a steel piston requires a dramatically different design than an aluminum piston because steel is a much denser material. Steel offers a stiffer structure that can handle much higher in-cylinder pressures, but if it is not designed carefully to reduce weight, it will require much larger connecting rods and other supporting structure, which could nullify any potential advantages. In a typical steel piston design, much of the material is removed, especially in low-stress areas like the periphery of the piston skirt. Figure 7-18 illustrates the difference in skirt size by comparing aluminum and steel pistons from MAHLE that were both designed for heavy-duty engines.

In order to gain a sense of the effect of skirt size on the friction, the baseline Waukesha F18GL piston skirt was scaled by various factors, down to 76% of the original, as shown in Figure 7-19. (Obviously, it is simplistic to change the skirt size without

modifying the profile, stiffness, or other characteristics, but this parametric study considered skirt size in isolation.) The effect of skirt size on friction can be understood by observing that smaller skirts must distribute the lateral load over a smaller area (i.e., have higher average and peak pressures), so they tend to have more boundary lubrication and less hydrodynamic lubrication. Indeed, Fig. 7-20 illustrates the dramatic increase in boundary friction as the skirt size is reduced. There is a slight decrease in hydrodynamic lubrication as the skirt gets smaller (Fig. 7-21). Figure 7-22 summarizes the results; for this specific design, it seems to be best to make this skirt as large as possible.

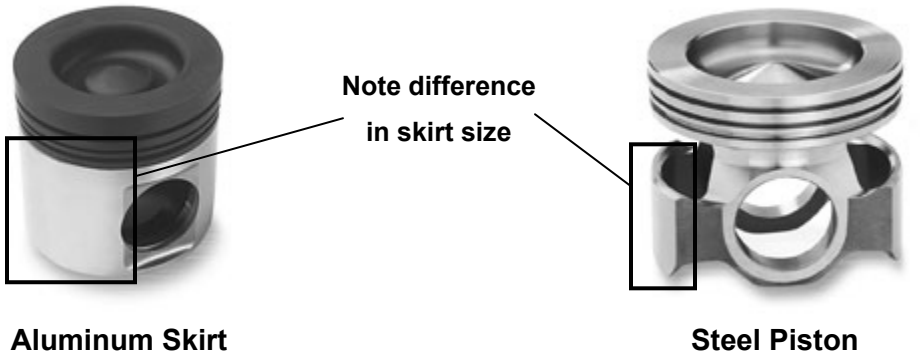

Figure 7-18: Comparison of aluminum and steel piston designs. MAHLE FERROTHERM® piston (aluminum skirt, steel crown) on left; MAHLE MONOTHERM® (all-steel) at right; both designed for heavy-duty engines

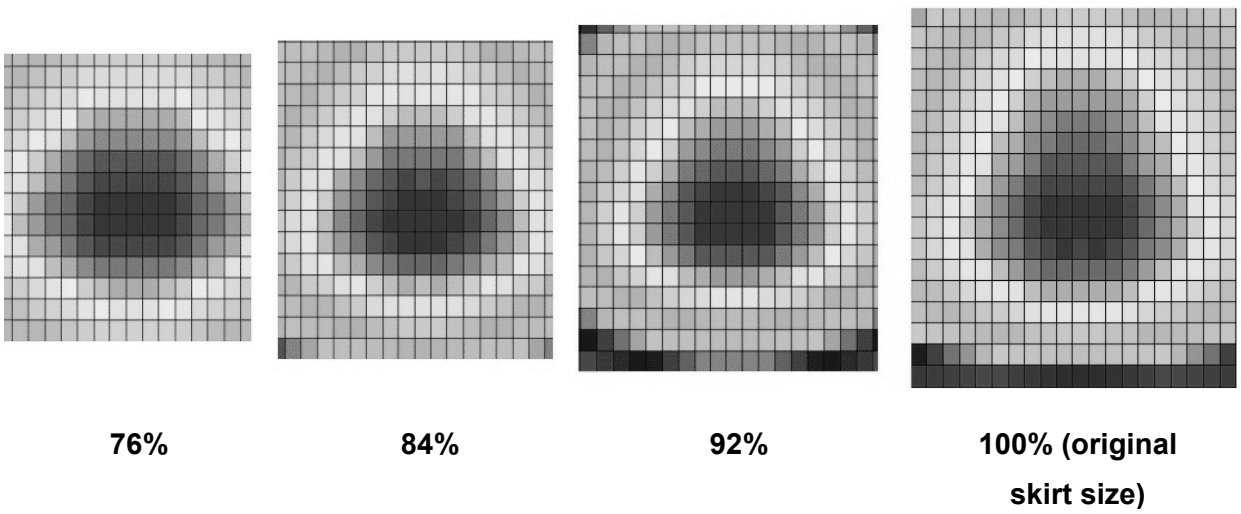

Figure 7-19: Schematic of skirts used in skirt size comparison

In actual piston designs, the tendency of smaller skirts to operate in the boundary lubrication regime can be offset by other design changes. For instance, the ovality can be adjusted to spread the load horizontally. Also, the profile can be adjusted to spread as much pressure in the center region as possible. As seen in Figure 7-14, most of the pressure is borne in the center of the skirt. Since the steel MONOTHERM® piston (shown in Figure 7-18) spreads the load horizontally across its width, it does not incur significant friction disadvantages by reducing skirt height.

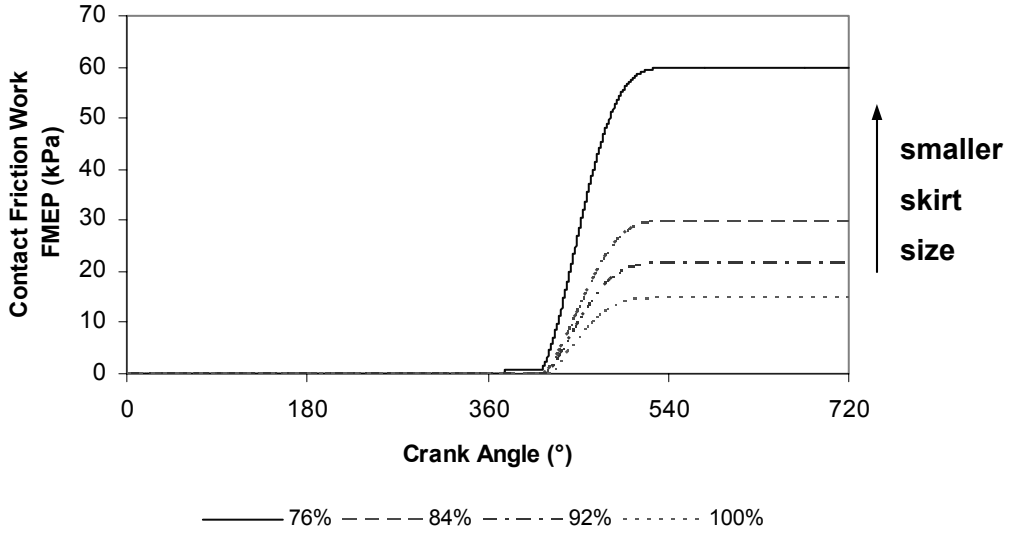

Figure 7-20: Cumulative contact friction work (thrust side, 100 μm oil film thickness, 20 μm waviness)

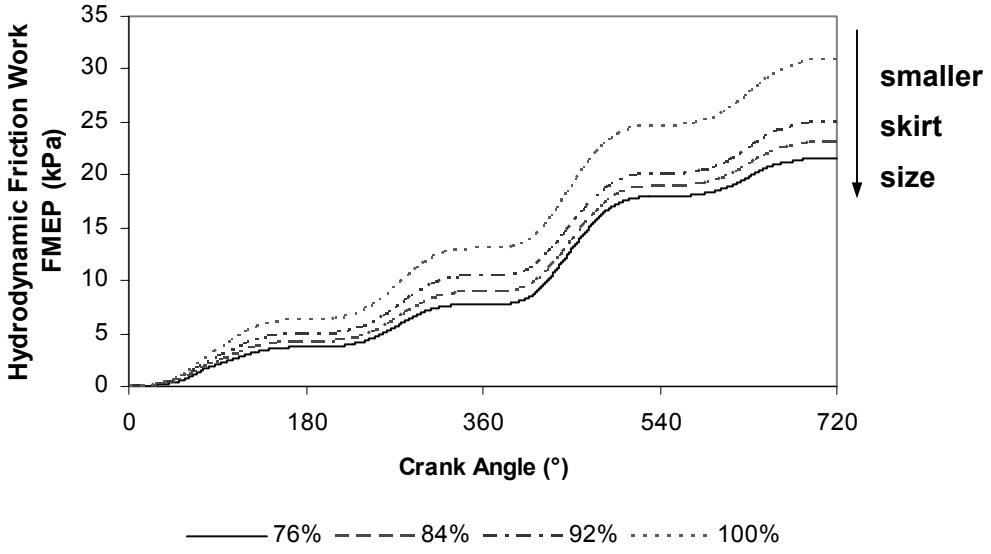

Figure 7-21: Cumulative hydrodynamic friction work (thrust side, 100 μm film thickness, 20 μm waviness)

Figure 7-22 (Right) : Skirt size vs. friction work (SAE-40 oil, thrust side, 100 μm oil film thickness, 20 μm waviness)

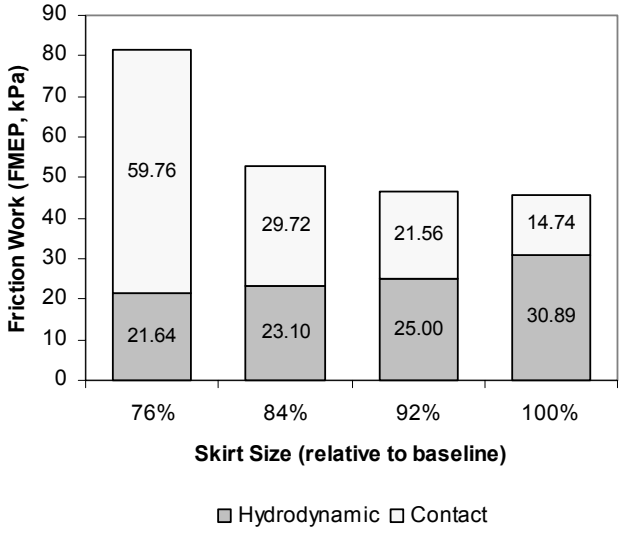

7.6. Piston ovality

The piston profile is designed not just to minimize friction, but also to minimize wear, reduce seizing, enhance guidance, etc. Piston ovality is essentially a piston profile oriented in the horizontal direction, and it fulfills several of the same purposes as the profile. As with the profile, this analysis of ovality focuses on its effect on friction. Figure 7-23 illustrates a cross-section of the piston/skirt system, emphasizing ovality.

When the engine is in operation, the piston skirt deforms in response to pressures stemming from lateral force on the connecting rod and inertial forces. Just as smooth, flattened profiles distribute pressure more evenly and thereby promote hydrodynamic friction, pistons with less ovality have the potential to reduce friction by conforming more closely to the liner. However, the same caveat regarding the profile applies to ovality: the system must be evaluated *after* the piston has been deformed by operational temperature and lateral pressure. The piston model used for this study included both thermal and pressure deformation effects.

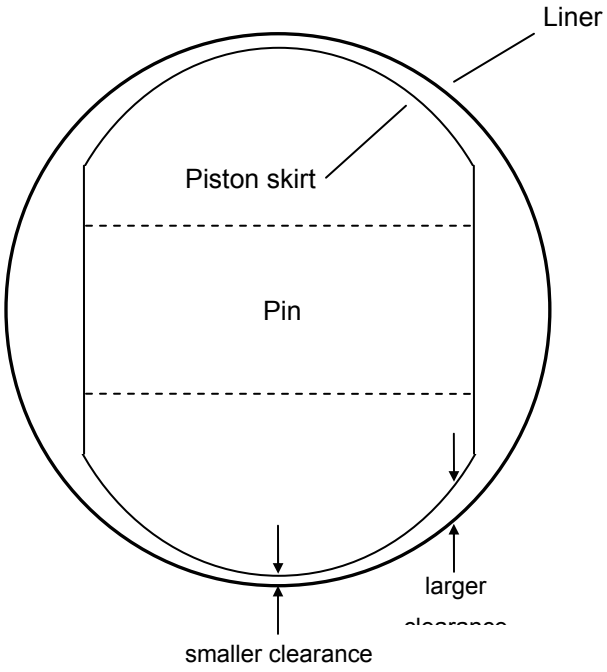

Figure 7-23: Diagram of piston skirt in the liner, showing ovality

Ovality is analogous to profile shape because both modify the effective clearance between the piston and liner. The objective of both is to facilitate a relatively flat oil film with gradual gradients in order distribute the lateral force over as large an area as possible. This promotes hydrodynamic lubrication and reduces wear. The ovality is to be adjusted so that it closely matches the shape of the liner, particularly at points in the cycle when the lateral force is high. (A comprehensive model of the engine would include deformation of each component in the power cylinder, including the liner, connecting rod, and pin, but such a model is extremely complex and requires intensive computation for even simple comparisons. The model exercised in this study included only deformation of the piston. However, the principle of piston-liner conformity applies in both types of models.)

Since reducing the ovality (i.e., making the piston more round) enables it to better conform to the liner surface, it is predicted that reducing ovality will also reduce friction. However, it is important to not completely eliminate ovality (i.e., make a perfectly circular piston). The lateral pressure is highest along the thrust and anti-thrust lines, so these areas will deform the most. A perfectly round piston will thus deform preferentially along the thrust and anti-thrust lines, leading to "negative ovality," or a concave shape that shifts pressure away from the thrust/anti-thrust lines. This could cause instabilities and produce undesirable high-pressure patches.

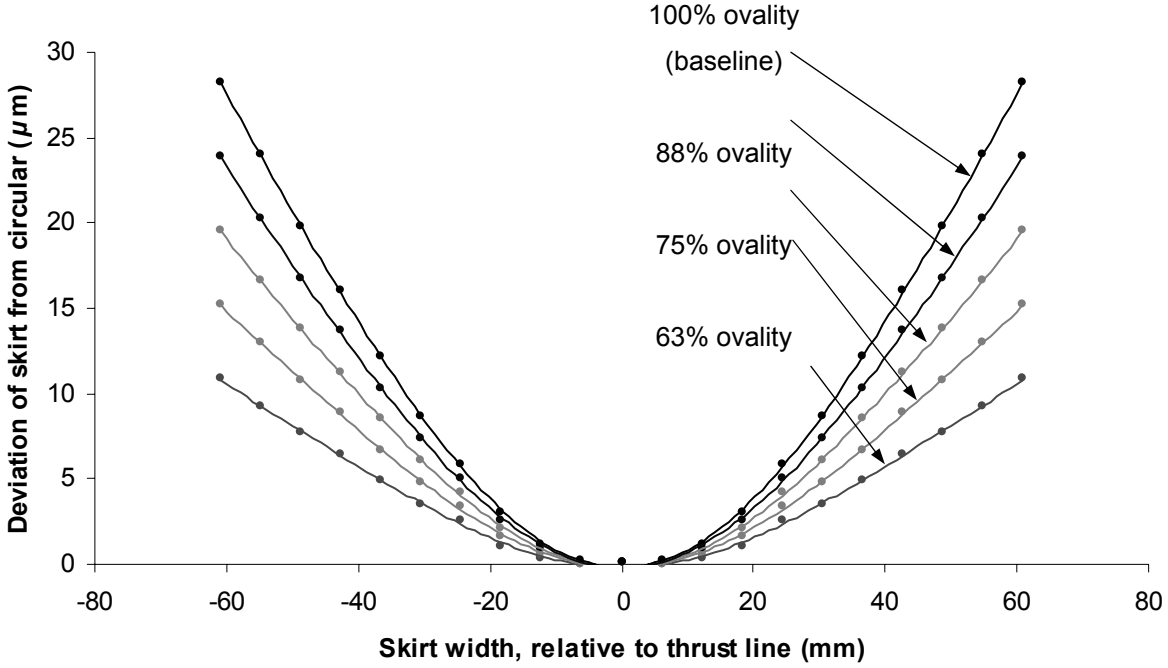

Figure 7-24: Cross-sectional view of piston, showing ovality. The baseline (100%) ovality was reduced to produce a more circular shape that conforms more closely to the liner surface (the *x*-axis in the figure).

In order to study the effect of ovality on friction, the baseline ovality was reduced by various proportions, as shown in Figure 7-24. Reducing ovality is equivalent to making the piston more circular, thereby causing it to conform more closely to the liner. Pistons with several relative ovality values were tested, and their effects on friction are shown in Figures 7-25 to 7-27. The model results confirm the prediction that reducing ovality dramatically reduces contact friction (it is eliminated entirely for 63% and 50% ovality pistons), thereby reducing net friction as well.

Since ovality can be adjusted independently of the piston profile, the two parameters can be jointly optimized to achieve ideal results. The profile is difficult to optimize because the piston rotates during the stroke—especially near the top-dead center—effectively changing the profile. The ovality does not change as much, however, since the piston does not rotate significantly about the thrust/anti-thrust axis. Therefore, in principle, the ovality can be optimized more precisely than the profile. Ideally, the two can be jointly optimized to minimize boundary contact friction while also achieving other objectives, such as smooth guidance throughout the stroke. Joint optimization requires specific, detailed information about the system in question.

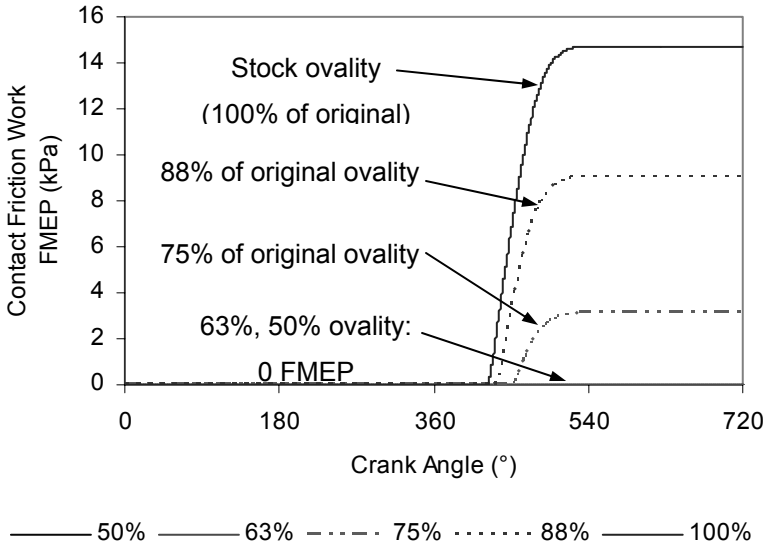

Figure 7-25: Cumulative contact friction work vs. ovality (thrust side, 100 μm oil film thickness, 20 μm waviness). Profiles that are more circular (i.e., have lower ovality) have lower contact friction work loss.

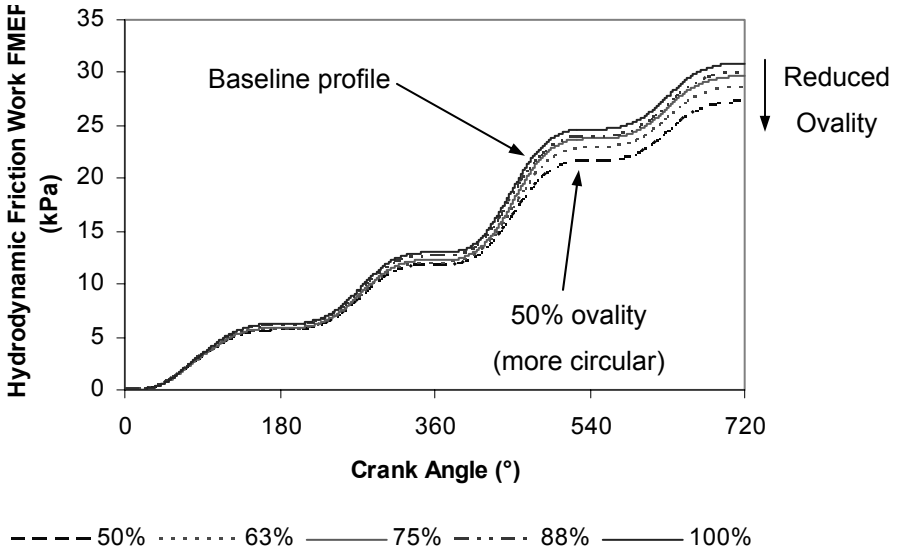

Figure 7-26: Cumulative hydrodynamic friction work vs. ovality (thrust side, 100 μm film thickness, 20 μm waviness). Reducing ovality slightly decreases hydrodynamic friction loss.

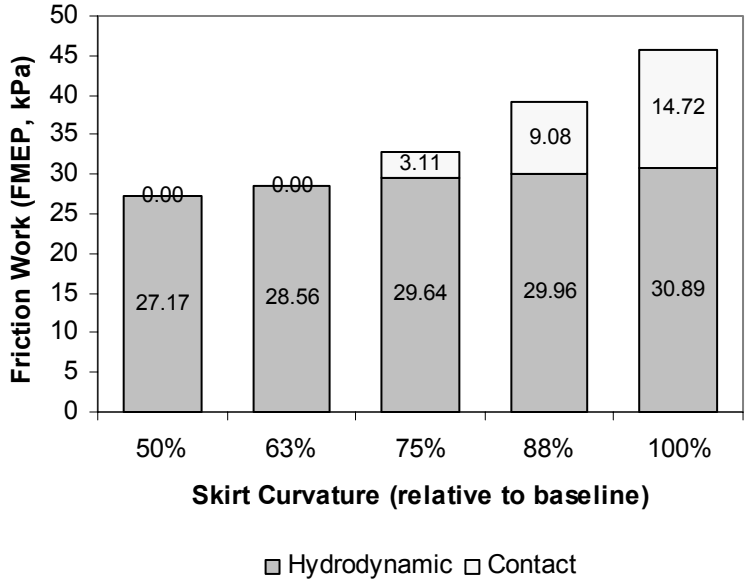

Figure 7-27: Ovality vs. net friction work (SAE-40 oil, thrust side, 100 μm oil film thickness, 20 μm waviness)

8. Effects of Lubricant Viscosity on Piston Friction

Reducing viscosity is an effective method to reduce friction, but reducing it beyond a critical point can promote both higher friction and substantially greater wear. Although high-viscosity oil produces greater friction work by increasing shear stresses, the greater shear stresses enable it to support a greater load (at a given sliding speed). The ability of viscous oils to sustain loads is essential for piston support, since this property helps avoid direct contact between the components. If the viscosity is reduced below the level required for hydrodynamic support, the piston surface will contact the liner surface and incur boundary contact friction. Typically, a design goal is to reduce boundary friction as much as possible, both because boundary friction involves significantly higher friction loss than hydrodynamic friction and because it promotes wear.

8.1. Engine oil temperatures and dependence of viscosity on temperature and shear rate (Vogel and Cross equations)

Hydrodynamic friction between the piston and liner is highly dependent on lubricant viscosity, and the viscosity is heavily dependent on temperature. As temperature increases, viscosity decreases dramatically. A robust model will treat viscosity as a function of temperature (instead of assuming a constant value) in order to predict friction accurately.

The temperature dependence of viscosity is specified by the Vogel equation (Eq. 8.1), where T is temperature (in °C), and the other variables are properties of the particular oil used. The θ_1 and θ_2 terms have units of °C, and k has units of cSt. Note that the Vogel equation is applicable only to single-grade oils, in which viscosity does not depend on shear rate. Since most large natural-gas engines use straight-weight oil (partially due to cost constraints), the Vogel equation is an accurate correlation between temperature and viscosity for these applications.

$\nu_0 = k \exp\left(\frac{\theta_1}{\theta_2 + T}\right)$	Eq. 8.1

The previous piston model assumed that viscosity was constant throughout the cycle, but this is not a very accurate approximation, since viscosity varies by a factor of 2 between top dead center and bottom dead center (Figure 8-1). Therefore, the model was modified such that viscosity was calculated from temperature and oil properties according to the Vogel equation, Eq. 8.1. At each crank angle increment, the current viscosity of the oil was determined, and Fig. 8-2 illustrates how the viscosity varied throughout the cycle.

Note the approximately sinusoidal nature of the viscosity as the piston moves up and down on the liner: the viscosity decreases toward the top of the stroke. The highest lateral pressure on the piston skirt occurs when the connecting rod force is highest, which happens when cylinder pressure is maximum. The pressure is maximum near TDC just after firing. The TDC position corresponds to the valleys on the curves in Figure 8-2, when viscosity is low. Since viscosity is low and lateral pressure is high at TDC, this area

is most vulnerable to boundary friction and its concomitant wear. In the field, the top of the liners exhibits the most wear, which is consistent with this prediction.

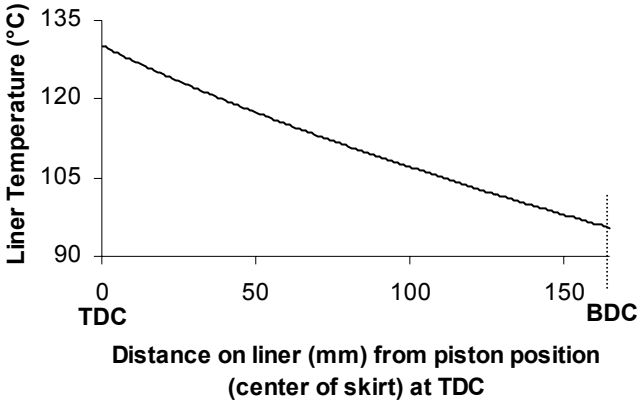

Figure 8-1: Liner temperature vs. position

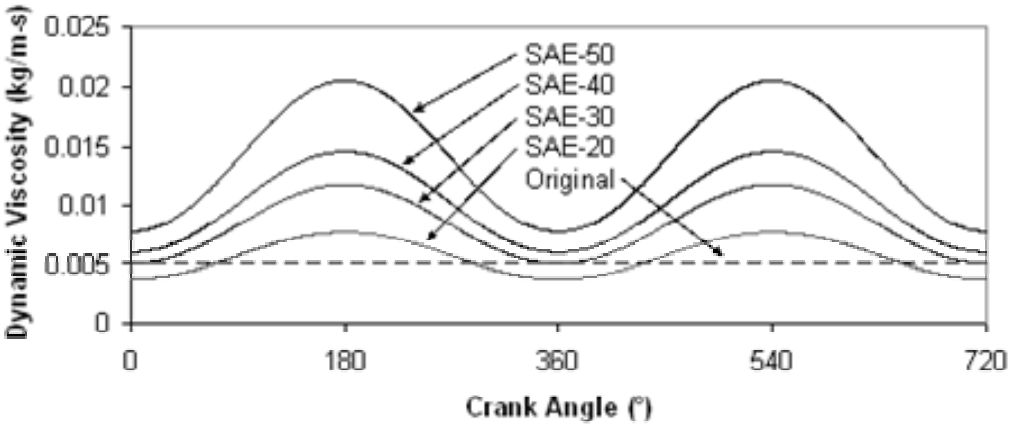

Figure 8-2: Viscosity vs. crank angle for straight-weight oils (original, constant viscosity shown for reference)

All lubricants display a strong dependence of viscosity on temperature. However, the viscosity of multi-grade oils also depends on shear rate—i.e., the ratio of sliding speed to film thickness. Multi-grade oils are formulated so that the viscosity is high when shear rate is low; hence, when piston speed is low near TDC and BDC, the shear rate is also low, and oil is more viscous. This increases hydrodynamic support. However, during mid-stroke when the piston is moving faster, it is already in the hydrodynamic regime, and the high shear rate causes the multi-grade oil to reduce its viscosity, decreasing friction work.

The viscosity characteristics of multi-grade oils are modeled by the Cross Equation (Eq. 8.2) , where γ is the absolute value of the shear rate (units of s^{-1}) and β is the critical shear rate (s^{-1}); β depends on temperature also. The μ_0 term is the low-shear oil viscosity and μ_∞ is the high-shear viscosity, m is a correlation constant controlling the width of the transition region, and μ is the viscosity at shear rate γ (i.e., it is the viscosity to be calculated). Note that for single-grade oils, $\mu_\infty = \mu_0$.

$$\mu = \mu_0 \frac{1 + \frac{\mu_\infty}{\mu_0}\left(\frac{\gamma}{\beta}\right)^m}{1 + \left(\frac{\gamma}{\beta}\right)^m}$$	Eq. 8.2

The oil properties (specified by β, μ_0, & μ_∞) can be optimized to minimize friction. Hypothetically, the oil characteristics could be adjusted such that at high temperatures and low speeds (which are characteristic at TDC), the viscosity increases substantially. However, at high speeds during mid-stroke movement, the viscosity decreases to reduce hydrodynamic friction loss. Finally, at BDC where both speeds and temperatures are low, the viscosity would be increased again. Scenarios similar to this one have been explored for the ring pack, and while they cannot be readily implemented in practice, they provide valuable guidance for optimizing multi-grade oils for low-friction operation.

8.2. Dependence of piston-liner separation (clearance) on oil viscosity

Minimum clearance, or separation, between the piston and liner is a crucial lubrication parameter because it directly affects wear and boundary friction. If the minimum clearance is large, then the oil film is relatively thick, and the piston is supported hydrodynamically. However, if the minimum clearance is small for significant portions of the cycle, then boundary friction will likely be large as well. Oil viscosity has a direct impact on minimum clearance. As viscosity increases, both the shear stress and the supported load increase as well. Since the supported load is constant for a given engine, the shear stress can be reduced to maintain the same oil film thickness. Since shear stress is inversely proportional to separation distance (as an approximation), one would expect an increase in viscosity to lead to a corresponding increase in minimum separation.

Figures 8-3 and 8-4 depict the model predictions of skirt-liner separation for the entire cycle. To generate the plots, the minimum clearance value for the skirt at each crank angle was determined. A 10 μm waviness value was assumed in this scenario, so when oil film thickness dropped to about 10 μm, boundary contact began. Fig. 8-4 shows a close-up view of the minimum clearance around the 360° crank angle, which is top dead center at the beginning of the expansion stroke, and it clearly shows that an increase in viscosity promotes greater separation between skirt and liner. As stated earlier, this is the point in the cycle when most of the wear is generated, so the greater separation provided by more viscous lubricants can produce substantial reductions in wear. According to Figure 8-4, low-viscosity oils such as SAE-20 do not provide adequate hydrodynamic pressure to support the piston, and the deficiency must be balanced by increased boundary contact friction, which leads to increased wear.

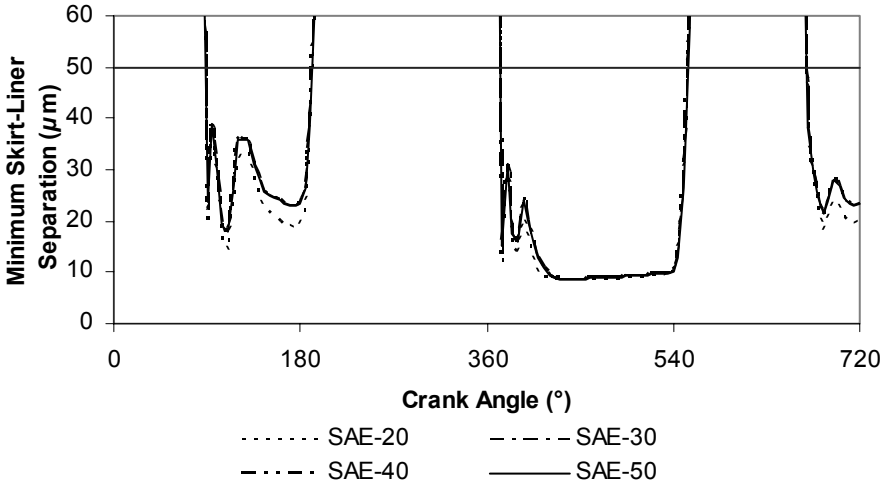

Figure 8-3: Minimum piston-liner separation vs. oil viscosity (thrust side, 50 μm oil film thickness, 10 μm waviness)

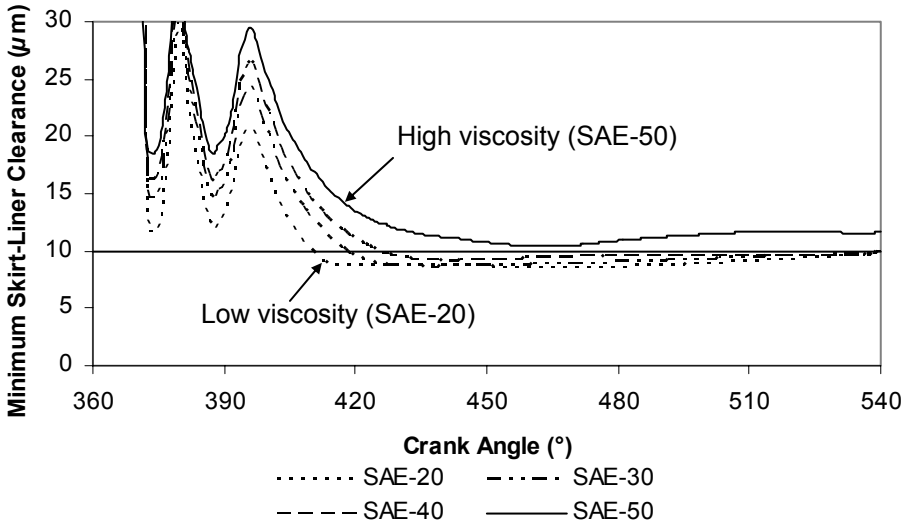

Figure 8-4: Close-up view of minimum separation vs. viscosity (thrust side, 50 μm oil film, 10 μm waviness)

A direct result of the greater separation that results from a more viscous lubricant is that the wetted area decreases. Since the piston "floats" higher in the oil film to produce greater separation, the wetted area decreases proportionally (in this model, a constant oil film thickness is assumed). Figure 8-5 illustrates this trend for the thrust side of the piston skirt; highly-viscous oils like SAE-50 have significantly less wetted area and significantly greater minimum skirt-liner clearance than low-viscosity oils like SAE-20. Decreasing wetted area (assuming all else held constant) has the additional advantage of decreasing hydrodynamic friction. The off-center areas of the contact patch sustain only moderate pressure but they incur significant hydrodynamic drag. Thus, by decreasing the wetted area, viscous oils reduce hydrodynamic friction relative to what it would be with identical wetted areas. However, the reduction in hydrodynamic friction due to decreased wetted area is more than offset by the increase in friction due to increased shear stress, so increasing viscosity always increases hydrodynamic friction.

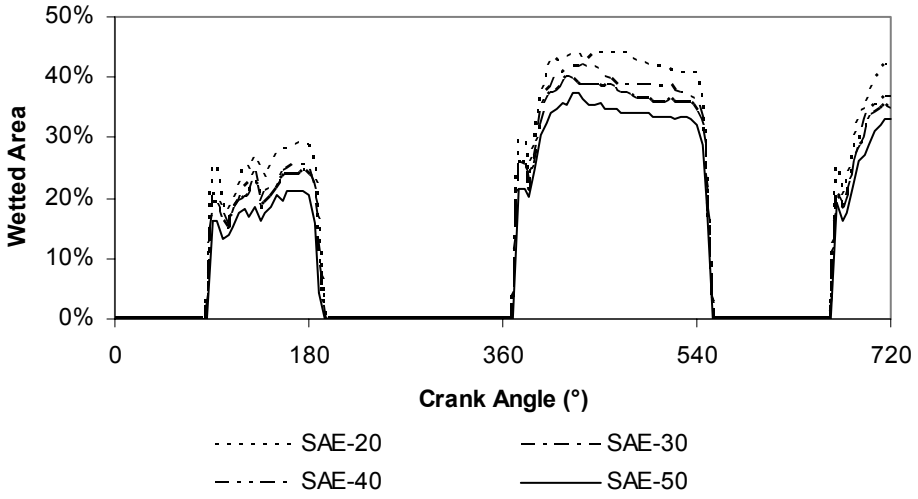

Figure 8-5: Percent wetted area vs. oil viscosity (thrust side, 50 μm oil film thickness, 10 μm waviness)

8.3. Effects of oil viscosity on piston-skirt friction

In general, more viscous oils tend to increase hydrodynamic friction, because of the increase in shear stress associated with higher viscosity, but decrease boundary contact, because the thicker oil films supported by highly viscous oils provide greater separation for two surfaces. This is the case for the piston. As oil grade is increased (where the grade is closely correlated to viscosity), the skirt/liner clearance increases, as shown in Figure 8-4. For the most viscous oil, SAE-50, boundary contact is completely eliminated, as indicated by the maintenance of a skirt/liner clearance greater than 10μ, the height of the skirt waviness.

As oil viscosity is increased, piston hydrodynamic friction increases, while boundary friction decreases. The effect of changing viscosity on the overall friction depends on the running conditions of the piston – if boundary contact contributes substantially to total piston friction, then increasing lubricant viscosity is likely to reduce overall friction. Conversely, if very little boundary contact is taking place, decreasing lubricant viscosity is more likely to lower total losses – even if asperity contact then increases, it will be outbalanced by the decrease in hydrodynamic friction. The value of the "ideal" oil viscosity, at which friction losses are minimized, is dependent on several factors, including the piston profile.

Figure 8-6 and Figure 8-7 show the dependence of piston friction on viscosity, for two different piston profiles. For a sharply curved profile, increasing viscosity causes a decrease in friction for all of the oil grades assessed. This is because the sharp profile of the piston causes substantial boundary contact to occur for all viscosities (as described in the preceding section). For the flatter profile, however, a minimum friction is found for SAE-40 oil, where hydrodynamic and boundary friction balance to provide the lowest overall friction.

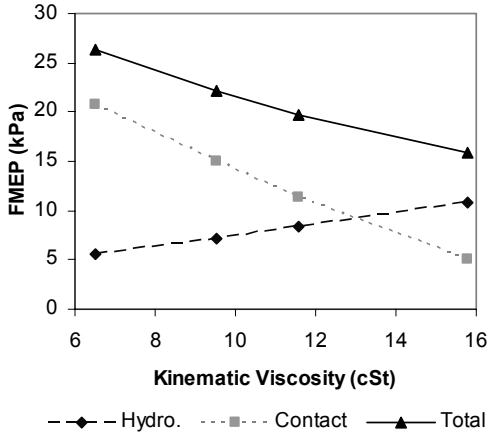

a. Friction change with oil viscosity

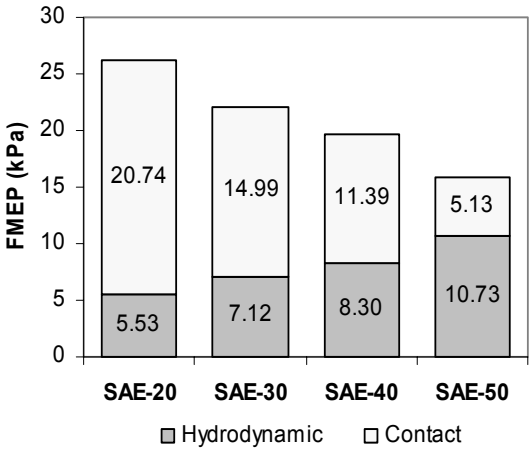

b. Friction change with oil weight

Figure 8-6: Friction change with oil viscosity, sharp curvature profile

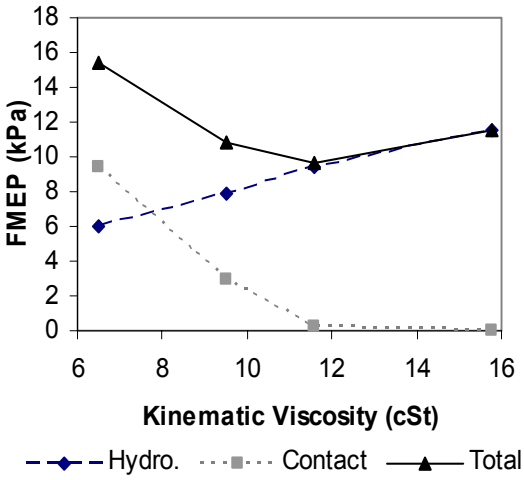

a. Friction change with oil viscosity

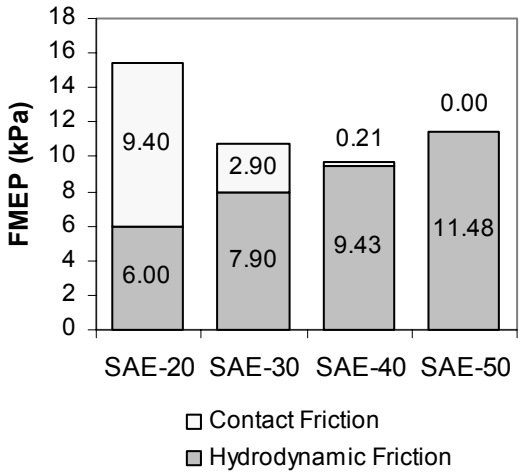

b. Friction change with oil weight

Figure 8-7: Friction change with oil viscosity, shallow curvature profile

9. Summary of Parametric Effects and Strategies on Piston-Friction Reduction

9.1. Parametric effects of piston friction

Each of the parameters studied above has the potential to affect friction, but they offer varying benefits. Figure 9-1 provides a rough comparison of each effect, assuming everything else remains constant. Obviously, the improvements are not additive; for example, if the waviness is excessive, profile curvature will no longer have much of an effect on friction. In order to reduce friction, the piston should be designed to provide a relatively even skirt-liner clearance in order to enhance hydrodynamic lubrication and avoid boundary lubrication. This can be achieved by using a relatively flat profile, adjusting piston ovality to match the liner shape, and reducing waviness peaks so they do not contact each other. Moreover, selecting the lubricant such that the viscosity is high enough to provide adequate hydrodynamic support, but not so high that is induces excessive drag, is also crucial to controlling friction. A key observation from this study is that the piston-liner system is highly-integrated, and changing one variable affects many other parameters.

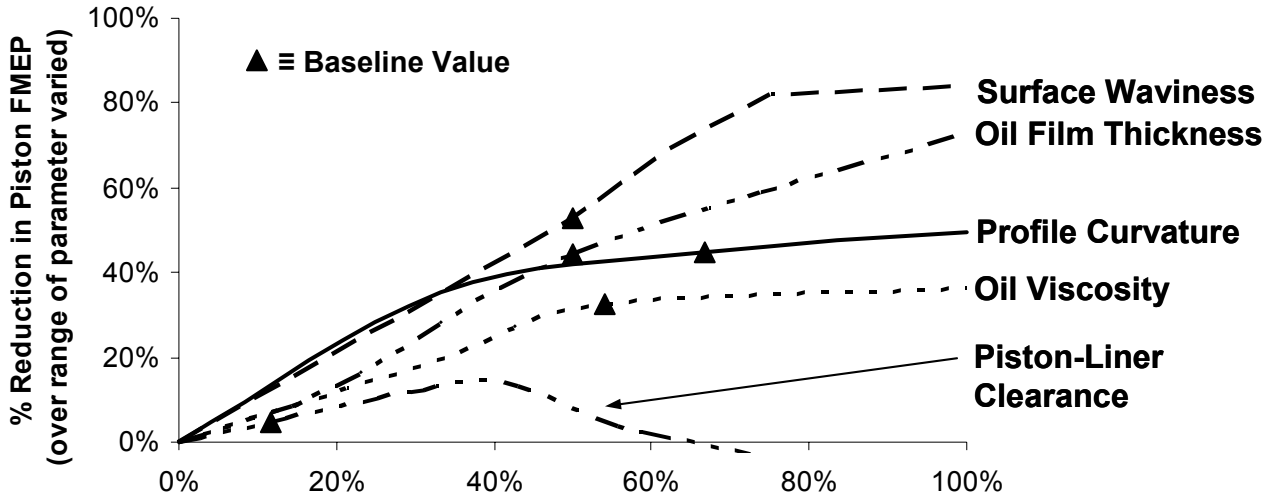

End of Range (0%)	% Change in Parameter	End of Range (100%)
20 μm	Surface Waviness	0.1 μm
0 μm	Oil Film Thickness	100 μm
x^2	Profile Curvature	Flattest (x^8)
0 μm	Piston-Liner Clearance	150 μm
8.1 cSt	Oil Viscosity (100° C)	20.4 cSt

Figure 9-1: Comparison of effects of various piston design parameters on friction; baseline values reflect parameters selected for the default engine

9.2. Piston friction reduction strategies

Piston friction arises from a complex combination of design characteristics, material and surface features, oil properties, and engine operating conditions. For the running conditions in the Waukesha engine, the most substantial reduction in friction arises from reducing boundary contact on the thrust side, which is the source of a large portion of the cycle total. The two most important design parameters identified thus far are oil film thickness and piston surface waviness. Increasing the oil film from 20 to 50 microns can reduce friction by 50%, primarily by providing more separation between the piston and liner, reducing contact friction. Similarly, reducing piston waviness from 10 to 5 microns can also reduce friction loss by 50%, by increasing piston/liner clearance at a given oil supply, as shown in Figure 7-6. While the result of changing both of these parameters clearly will not be 100% reduction in piston friction, substantial friction reduction should be possible.

Other parameters under consideration are the skirt-to-liner clearance, piston profile shape, and lubricant viscosity, all of which may entail friction reductions of 15-30%. Skirt-to-liner clearance can be optimized to reduce friction, either from piston slap, for large clearances, or metal-metal contact, for small clearances. Piston profile shape can also be optimized, primarily by flattening the profile to reduce boundary contact. Lubricant viscosity has a dual effect on piston friction: increasing viscosity decreases boundary friction, but also increases hydrodynamic friction. The viscosity can be optimized to minimize the total, taking into account the piston profile and other factors that contribute to the hydrodynamic/boundary balance.

Many other parameters contribute to piston friction which have not yet been considered. The most important of these is the skirt stiffness. Preliminary investigation indicates that a more flexible skirt can reduce friction, by increasing wetted area and decreasing contact friction. This possibility will be studied further. Also, analysis of the piston and liner surface textures will be carried out, to assess the possibilities for further friction reduction.

9.3. Summary of piston friction study

The parameters of the piston-liner system of a reciprocating engine are complex and highly interdependent, but numerical models have enabled significant progress to be made toward understanding them. In this project, which focused on reducing friction, the effects predicted by the model comport with physical intuition. Reducing viscosity reduces hydrodynamic friction while also reducing hydrodynamic pressure, but excessive reduction in viscosity makes the system vulnerable to boundary contact, which increases net friction. Thus, the strategy is to design the power cylinder system to operate primarily in the hydrodynamic lubrication regime while utilizing the lowest-viscosity oil practical.

The model confirmed that increasing oil film thickness (by increasing oil supply) tends to increase hydrodynamic support, which can supplant high-friction boundary contact. Thus, increasing oil film thickness can reduce friction losses. However, excessive oil supply can increase hydrodynamic drag needlessly and lead to heightened oil consumption, which can have serious negative consequences for aftertreatment and exhaust. Therefore, methods other than simply increasing oil film thickness are preferred.

Changes to the design of the piston can promote hydrodynamic lubrication without increasing the supply or viscosity of the oil. The piston and liner geometry can be modified to maintain a smooth, even distribution of film thickness and hydrodynamic pressure. By avoiding pressure concentrations and the sharp film thickness gradients that cause them, the piston skirt is less likely to push the oil film aside and enter the boundary lubrication mode. The model confirmed that a relatively flat piston profile provides the best hydrodynamic support over the majority of the cycle because it conforms most closely to the liner. Likewise, a profile that contains minimal ovality (i.e., is nearly as circular as the liner) maintains an even distribution of film thickness and pressure, thereby maximizing hydrodynamic support and minimizing friction loss.

Some pistons are constructed of steel, which is significantly denser than the aluminum that is typically used. In order to reduce weight, much of the material is removed, including some around the piston skirt. Changing skirt size is expected to have a major impact on the distribution between hydrodynamic and boundary lubrication. The model predicted that smaller skirt sizes are at greater risk for boundary lubrication, with its concomitant increase in friction, since they concentrate the same lateral force over a smaller area. Therefore, if a smaller skirt surface is necessary, the other variables, such as piston profile and ovality, must be approached with great care to ensure adequate hydrodynamic support.

Finally, surface modifications can be selected to minimize friction. Although circumferential grooves (waviness) retain oil by surface tension and provide useful flow paths for oil, they can dramatically increase friction if their amplitude is excessive. The model predicts that if the amplitude is significantly greater than the average clearance between piston and liner, then the peaks of the grooves will penetrate through the oil film and scrape against each other, leading to boundary contact and its concomitant friction and wear. Therefore, waviness amplitude should be no larger than what is needed to provide adequate oil pathways and retain sufficient oil by surface tension. Moreover, the model indicated that the naturally-occurring asperities on the piston surface do not significantly affect friction, provided that they are substantially smaller than the machined grooves.

The contributions of each parameter to friction reduction are not additive, since each parameter affects the others. The most effective strategy is to combine a variety of techniques to achieve an overall decrease in friction while avoiding significant disadvantages. For example, the piston profile and piston ovality must be considered together because they both affect the separation between the skirt and liner. The waviness amplitude, skirt size, and cold skirt-liner clearance must be evaluated together with viscosity, since a low-viscosity lubricant tends to promote boundary lubrication and consequent high friction. By applying the computer model to a specific power cylinder arrangement, an optimized combination of design changes can be selected to minimize net friction loss and improve reliability.

(B) EXPERIMENTAL

10. Experimental Validation of Low-Friction Ring Designs

During this reporting period, the testing of low-friction piston ring designs have been completed. The experiments were carried out in a facility at the Engines and Energy Conversion Laboratory at Colorado State University. This report presents a comprehensive report of the rings tested and the experimental results. A technical conference paper has been prepared and was presented at the Spring 2006 ASME-ICED Conference (ASME-ICED 2006-1327). In the experiments, an instrumented Waukesha VGF 18GL engine was used to measure friction losses with the different proposed ring designs. A summary of the low-friction ring designs was given in previous reports but is included here for reference in the following sections.

10.1 Summary of Low-Friction Designs

New designs for each of the three engine rings have been proposed. While the designs for the top and oil control rings directly reduce ring/liner friction, the proposed second ring design does not directly affect friction, but is intended to offset adverse effects from the altered oil control ring. Because most of the ring-pack friction comes from the top and oil control rings, these rings were the main focus of the friction-reduction strategies.

10.1.1 Top Ring

As discussed in the analysis sections, most of the friction between the top ring and liner is generated near TDC of combustion, where high cylinder gas pressures push the ring into the liner with high force. To reduce friction during this period, a skewed barrel top ring is proposed. A schematic of the skewed barrel ring is shown in Figure 10-1.

In the figure, P_1 is the in-cylinder gas pressure, while P_2 is the gas pressure on the second land, which is much lower than P_1 near TDC combustion. The skewed barrel increases the area exposed to the high gas pressure on the front side (facing the liner) of the ring. This gas pressure results in a force pushing the ring away from the liner, which partially balances the high gas pressure on the back of the ring, reducing the net ring/liner force. Reducing the ring/liner force causes a reduction in friction as well as wear in this region.

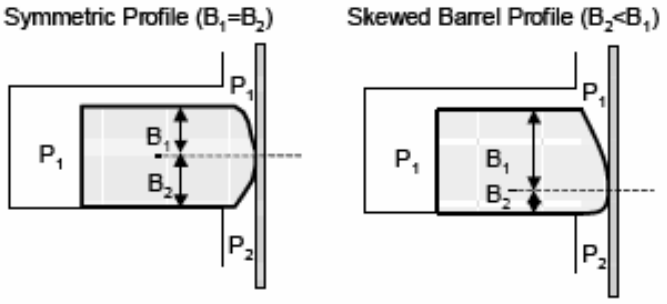

Figure 10-1: Low-friction top-ring design

Figure 10-2 shows the expected reductions in top ring friction as barrel skewness is increased. The x-axis shows "normalized B_2", which is a measure of the height of the ring below the centerline – a smaller B_2 indicates a greater amount of skewness. OS1 and OS2 are two oil supply conditions that have been studied in the ring analysis, and have relatively little effect on top ring friction. As the figure shows, top ring friction decreases approximately linearly with barrel skewness, with possible top ring friction reductions of 30-40% for very skewed barrels. This translates to a total ring-pack friction reduction of ~20%, as shown in Figure 10-3.

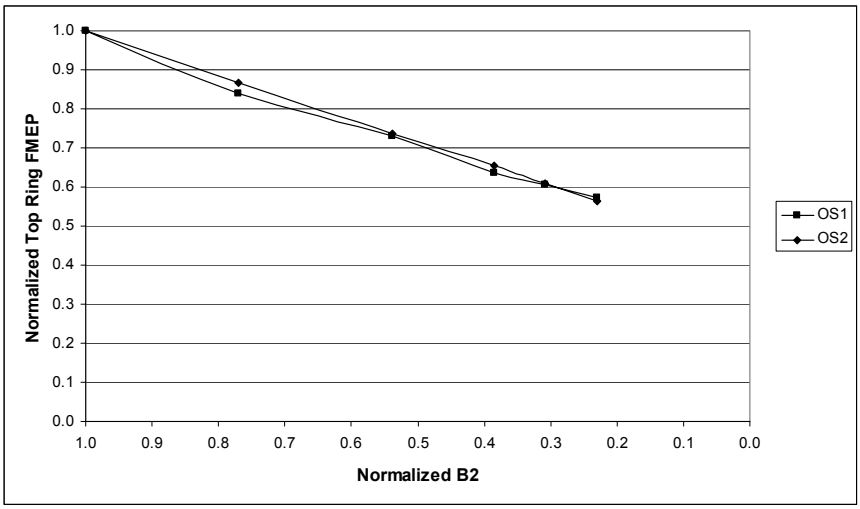

Figure 10-2: Effect of barrel skewness on top ring frictional losses

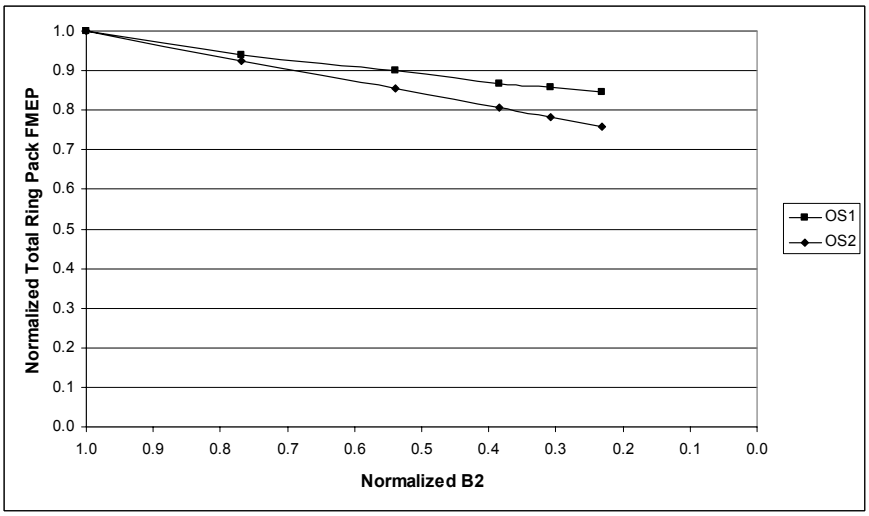

Figure 10-3: Effect of barrel skewness on total ring-pack frictional losses

10.1.2 Oil-Control Ring

The main source of frictional losses between the OCR and liner is the high tension in the ring, which is required to ensure the good ring/liner conformability that is required for oil flow control. The high tension causing a high ring/liner force, which leads to high friction. A reduced tension oil control ring is proposed, to reduce the

ring/liner normal force, and thus reduce friction as well. Figure 10-4 and Figure 10-5 show the effect of reducing oil control ring tension. There is a linear decrease of OCR friction as the ring's tension is reduced, with an OCR friction reduction of ~40% possible when the ring tension is reduced by half. This translates to an overall ring-pack friction reduction of ~25%. When the top and oil control ring designs are combined, a ring-pack friction reduction of up to 45% is predicted.

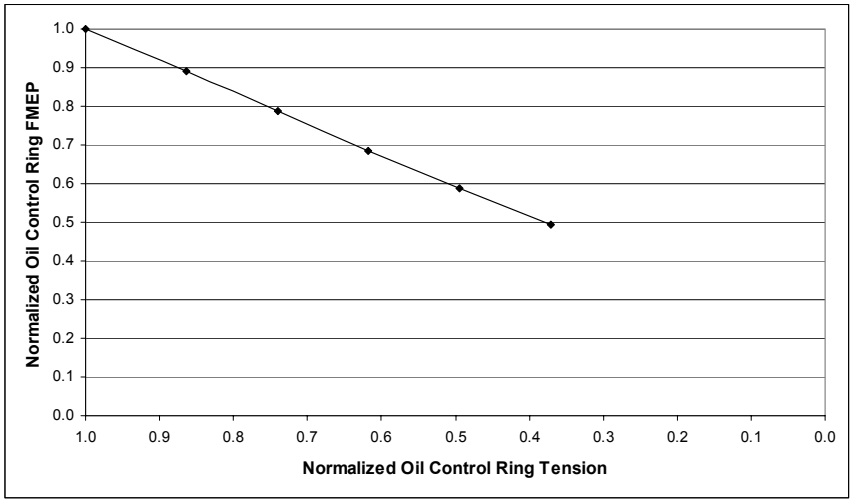

Figure 10-4: Effect of oil control ring tension on OCR frictional losses

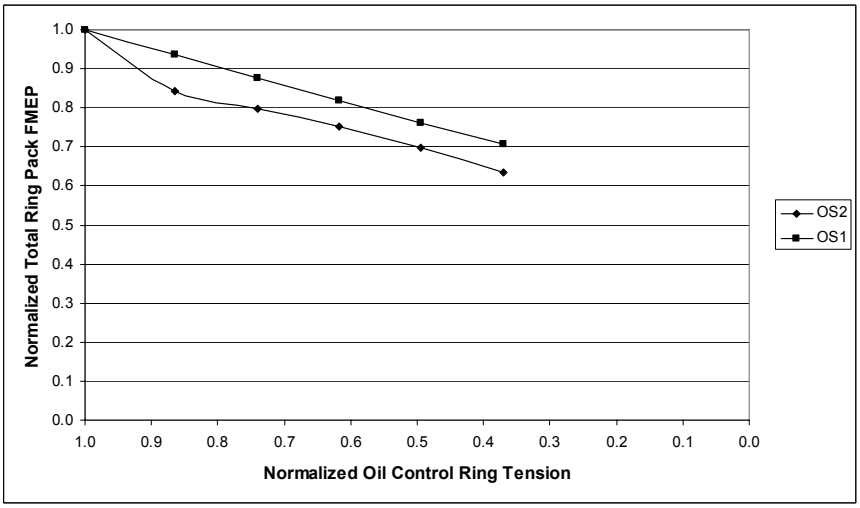

Figure 10-5: Effect of oil control ring tension on total ring-pack frictional losses

10.1.3 Second Ring: Reducing Oil Consumption

Reducing the oil control ring tension can greatly reduce frictional losses, as shown, but this comes at the expense of an increase in oil consumption. The low tension ring is less able to conform to the cylinder liner, and is thus less able to control the film thickness that is allowed past the ring and into the combustion chamber. A negative twist second ring is proposed to offset this increase in oil consumption.

The benefit expected from the negative twist second ring lies in the ring dynamics, and in particular in the balance between the ring inertia and applied gas pressures near TDC of combustion. Near TDC, the inertia of the ring pulls it upwards – towards the top of the groove – because the piston acceleration is downwards (either the piston is slowing down approaching the TDC position, or it is increasing in speed in the downward direction, after TDC). Gas pressures, conversely, push the ring down, towards the bottom of the groove, because it is higher above the ring than below. The balance between these forces determines where the ring sits in the groove, and whether it is stable. When the ring position is stable there is no effect on oil consumption. When the position is unstable, "ring flutter" can occur, in which the ring moves up and down in the groove for a portion of the stroke, allowing high-pressure gases to blow behind the ring. These high pressure gases can blow oil accumulated behind and below the second ring back down to the crank case, thus reducing oil consumption.

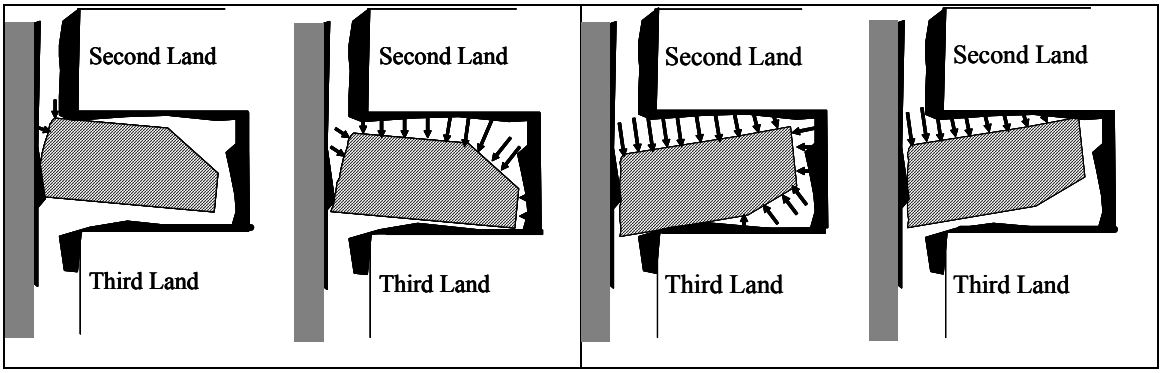

a) Positive Twist – stable.

b) Negative Twist - unstable, encourages 2nd ring flutter.

Figure 10-6: Second-ring designs to reduce oil consumption

Figure 10-6 shows both positive twist and negative twist scraper rings, with the arrows showing net gas pressure. The positive twist case is stable – when the ring is at the top of the groove, the area exposed to the gas pressures is low, so the force pushing down is small. Inertia dominates the force balance and the ring remains at the top of the groove. When the ring is at the bottom, the area exposed to gas pressures is large, and the ring remains pressed to the groove bottom because of high gas forces.

The negative twist case is unstable. When the ring is at the top of the groove, a large area is exposed to the high gas pressure, so the force pushing the ring down is relatively high. If it is great enough to overcome the ring inertia, the ring will be pushed down to the groove bottom. When the ring is at the bottom of the groove, the high-pressure gas exerts a force not only on the top but also on the bottom of the ring, so that the net downward force is reduced. This may allow the ring inertia to bring it back up to the top of the groove, where the cycle begins again.

The ring movement caused by the negative twist allows gas to flow behind the second ring near TDC combustion, blowing accumulated oil back towards the crank case. It is hoped that this oil consumption reduction mechanism will offset any increases that occur when oil control ring tension is reduced.

10.2 Friction Measurements

10.2.1 Experimental approach

Several approaches have been used for measuring frictional losses in internal combustion engine, including custom-built 'floating liner' engines [51]-[53] and engines with instrumented connecting rods [54]. The approach used in this project was selected because it could be performed in an unmodified, full-scale engine at full load.

In this study, friction was measured on a Waukesha VGF F18 in-line 6 cylinder power generation engine. This engine is rated at 400bhp (298kW) at 1800 rpm and was equipped with extensive instrumentation. Measurements were made at 1800 rpm and 70, 80, 90, and 100% of full load. FMEP was calculated by calculating the net (indicated) mean effective pressure (NMEP) from pressure traces and subtracting the brake mean effective pressure (BMEP) from it, as shown in Eq. 10.1. This method is simple to perform, as long as NMEP and BMEP can be measured accurately. Although the FMEP was a measurement of the mechanical efficiency of the engine as a whole, changes in FMEP were attributable to the changes in piston rings, as everything else was held constant.

$$FMEP = NMEP - BMEP \qquad \text{(Eq. 10.1)}$$

Cylinder pressure measurements were made with Kistler 6067C water cooled pressure transducers (generously donated by the Kistler Corp. for this project). These transducers were selected for the high level of accuracy needed in computing mean effective pressures. The pressure sensors output a charge signal that was converted to a 0 to 5V signal using Kistler 5010B charge amplifiers. These signals were then scaled and recorded by a Hi-Techniques Win600 high-speed data acquisition (DAQ) system. The Hi-Techniques system recorded the pressure signals in all six cylinders as well as three inter-ring pressure sensors in cylinder 5 (Fig. 10-7 and 10-8). Kistler 6052A transducers were selected for installation on the liner due to their compact size. The inter-ring pressure traces were used to verify the model predictions for the land pressures around TDC and bottom dead center (BDC). Figure 10-7 illustrates a typical pressure trace set recorded by the four pressure transducers in cylinder 5. The Hi-Techniques system was used to record raw pressure measurements as well as calculated values such as IMEP and burn durations.

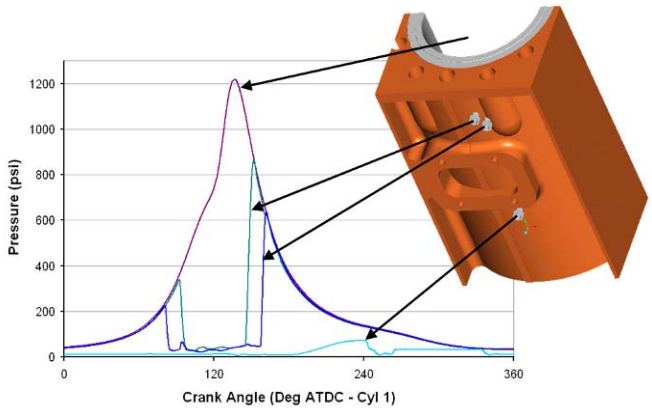

Figure 10-7 - Cylinder 5 Pressure Transducer Measurements

The location of the cylinder liner pressure transducers installed on cylinder 5 is shown in Fig. 10-8.

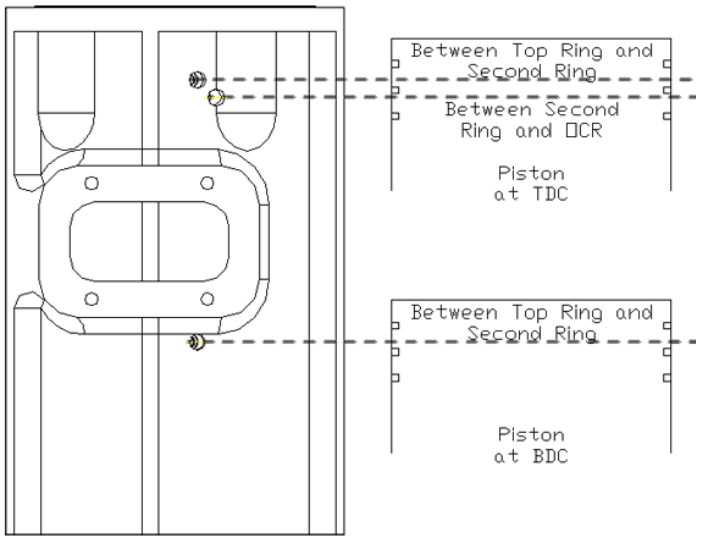

Figure 10-8 - Cylinder 5 Pressure Transducer Locations

A BEI brand optical encoder was used to synchronize the pressure measurements to the crankshaft position. Initially, an increment of 0.25 crank angle degrees (CAD) was used. However, it was found that this did not provide sufficient resolution to distinguish the expected friction reduction. An offset of a single encoder pulse (0.25 CAD) resulted in a change of more than 1.5 psi (10.3kPa) in IMEP (or FMEP). This issue was alleviated by using an encoder with a 0.1 CAD resolution. A one pulse offset with the new encoder (0.1 CAD) resulted in a 0.7psi (4.8kPa) change in IMEP. In order to prevent potential encoder coupler flexure problems and other synchronization errors, an independent optical pick up was placed on the flywheel as seen in Fig. 10-9. This signal was used as a consistent reference to locate the crankshaft rotational position. Use of the 0.1 CAD resolution encoder resulted in a drawback because the Hi-Techniques system could only sample 500 cycles at that resolution, which was ½ of the desired number of samples. This issue was resolved by collecting two consecutive data samples of 500 cycles each at each desired operating point.

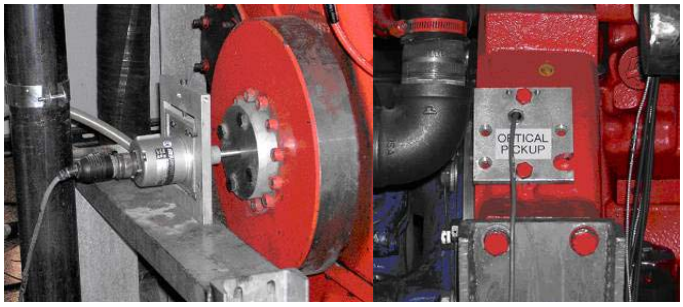

Figure 10-9 - Optical Encoder and Optical Pickup

The NMEP values were calculated from the raw pressure output files of the Hi-Technique using Eq. 10.2 through Eq. 10.4 [55]. The independent optical signal was used as the reference to validate the location of TDC for the encoder.

$$NMEP = -\frac{\frac{2\cdot\pi}{360}\int_{-360}^{360} P\cdot dV}{V_d} \quad \textbf{(Eq. 10.2)}$$

P, dV and V_d represent the instantaneous pressure, rate of change of the volume, and the displacement volume respectively. Equation 10.3 was used to determine the displacement volume.

$$V_d = \frac{\pi\cdot B^2}{4}L \qquad \textbf{(Eq. 10.3)}$$

B and L represent the cylinder bore and the stroke length respectively. The final equation needed to determine the NMEP is Eq. 10.4.

$$dV = \frac{\pi\cdot B^2}{4}\left\{a\cdot\sin(\theta)\left[1+\frac{a\cdot\cos(\theta)}{\sqrt{L^2-a^2\cdot\sin^2(\theta)}}\right]\right\}d\theta \qquad \textbf{(Eq. 10.4)}$$

In the equations above, *a* is the crank radius and θ is the angular crank position relative to TDC.

The engine was loaded using Midwest Dynamometer model 322 eddy current dynamometer (Fig. 10-10) and a Dyn-Loc IV Digital Dynamometer controller. The controller used a load cell as feedback in its closed-loop control. The speed was monitored using a magnetic pick up attached to the shaft of the dynamometer. Calibration on the load cell was performed before every day of testing. It should be noted that the load cell used to measure torque was calibrated to an accuracy of +/-7.4 ft-lb (10 Nm). BMEP was calculated from Eq. 10.5.

$$BMEP = \frac{4\pi\tau}{V_d} \qquad \textbf{(Eq. 10.5)}$$

τ is the brake torque measured by the load cell at the dynamometer.

The oil consumption of the engine was measured with an AVL 403S automatic oil consumption meter, shown in Fig. 10-11. This instrument was selected due to its high accuracy and simplicity. The meter had a refill accuracy of ±l gram and a level measurement accuracy of ±2μm. A constant-volume method was used.

Figure 10-10 – Eddy Current Dynamometer

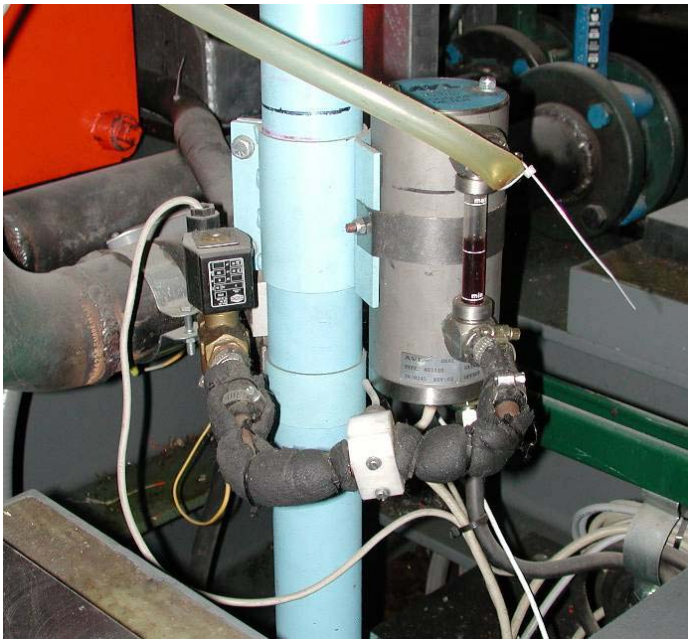

Figure 10-11 - AVL Automatic Oil Consumption Meter

This method involves adding a known quantity of oil and measuring the time required for the oil level to return to its original level. This was then repeated automatically. A minimum testing time of 3 hours was used to allow the oil consumption measurement to equilibrate. After each test, the total consumed oil and total time were used to calculate the rate of oil consumption. Figure 10-12 was a typical output of the oil consumption meter. After a few hours of measurement, the oil consumption rate was found to stabilize.

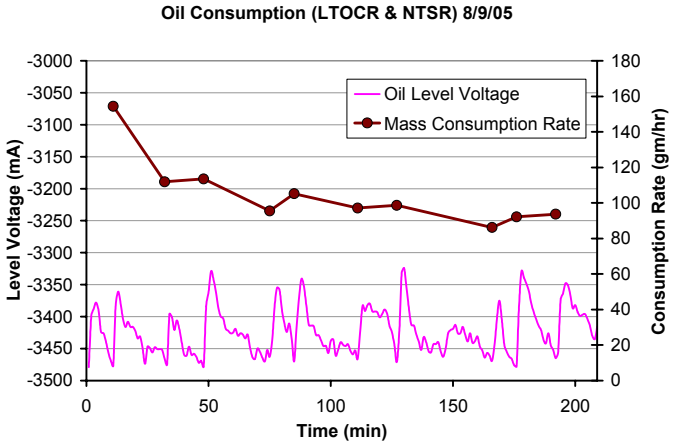

Figure 10-12 - Output from the Oil Consumption Meter (LTOCR & NTSR @ 1800rpm and 400bhp (298kW))

The ring blow-by was also of interest in this experiment. A J-Tech Associates VF563B in-line flow meter specifically designed for blow-by flow measurement was used, as shown in Fig. 10-13. Its accuracy was ±2% of full scale, which was 16 ACFM for this meter. This meter used the principle of vortex shedding to measure the flow rate of the blow-by gases. A small strut inside the flow tube created Karman vortices, and the frequency of the vortices was measured by an ultrasonic beam.

Figure 10-13 - Blow-by Flow Meter

The engine was also equipped with other instrumentation required to maintain the engine at the desired operating conditions. A National Instruments™ DAQ system was used to control and record all parameters of interest on the engine including temperatures, flow rates, pressures, emissions, speed, and load.

10.2.2 Engine test procedure

Early in the testing it was found that variations in combustion stability could affect the FMEP measurements with this technique. In essence, day-to-day variation in natural gas composition from the pipeline were affecting the combustion stability at high load and biasing the NMEP measurements. In order to alleviate this condition, a closed loop air-fuel ratio controller was installed, and the engine was operated at a relatively "rich" condition.

An air-fuel ratio sweep was performed to identify the best operating air-fuel ratio for these tests. This desired operating air-fuel ratio was selected at a point where the Coefficient of Variation (COV) of IMEP all of the cylinders were not affected by fuel composition changes. The COV of IMEP of cylinder 6 and the engine average is plotted against exhaust O_2 level in Fig. 10-14. Cylinder 6 is displayed because it has a tendency to become unstable at lower exhaust O_2 levels than the other cylinders. All subsequent tests were performed at 6% O_2.

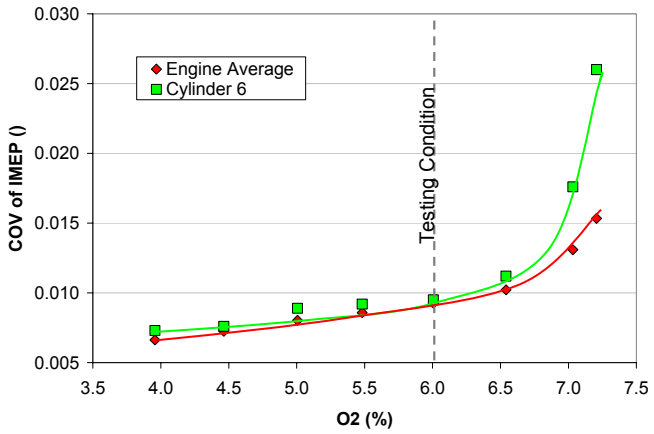

Figure 10-14 - COV of IMEP of Cylinder 6 and the Cylinder Average

Each day of testing, the engine was brought to the desired operating conditions and allowed to stabilize. Thermal stability was achieved when the cooling water achieved 180°F (82.2°C) and the oil temperature achieved 175°F (79.4°C). After these temperatures were reached, they were maintained at that level by a closed-loop control system. After the engine stabilized, all important operating conditions, such as exhaust O_2, were verified. The DAQ logging system was also started. This recorded temperatures, pressures, flows, and load. The conditions were recorded at 1Hz for a minimum of 5 minutes and averaged. The Hi-Techniques also recorded pressure traces while the DAQ system was running. Five hundred cycles of cylinder pressure were saved twice in order to obtain the desired 1000 cycles of data. The high number of cycles was desired in order to minimize the effects of cycle-to-cycle variations that naturally occur in the engine. After all of the data was collected, the values were averaged and all calculations were made, including FMEP.

It should be noted that small changes in Brake Thermal Efficiency (BTE) due to the changes in friction could not be measured with the existing facilities. The fuel composition was measured at the beginning of each test day with a gas chromatograph

(GC). This information was used to calculate the fuel's energy content (Lower Heating Value, LHV) and molecular weight. The molecular weight was used in conjunction with the measured volumetric flow rate to calculate the fuel mass flow rate. However, measurement errors in the fuel composition and volumetric flow rate were found to be greater than the changes in BTE due to the reductions in engine friction.

During oil consumption measurements, the engine operating conditions, especially temperature, were held constant. The oil consumption meter was started and allowed to run for a minimum of 3 hours. During the oil consumption measurement, the data logging procedure described above was performed several times.

Due to the small expected changes in FMEP relative to the numerous random variations possible in the measurements, several tests were performed at each operating condition and then averaged. The average FMEP value at each operating condition and the 95% confidence interval were calculated. In order to verify that the engine baseline friction did not 'drift' over time, repeated baseline engine builds were tested.

10.2.2.1 Piston ring change procedure

An important element in the procedure for testing different rings was the process of changing them. This process usually took between 2 and 3 full days to complete. The first step was to remove all of the wires, tubing and instrumentation that "gets in the way" or connects to parts that must to be removed (Fig. 10-15).

Figure 10-25 - Assembled Test Engine

All of the coolant systems were drained and sections of the exhaust and intake were removed. The valve covers, rocker arms, and push rods were then removed, followed by the fuel regulator and oil cooler. Jacket water connections were also disconnected. The

head bolts were removed and the heads lifted off of the engine. The pistons were removed using the access openings in the side of the engine to remove the connecting rod cap screws. Finally, the pistons were removed from the engine from the top (Fig. 10-16).

Figure 10-16 - Piston Removal

Figure 10-17 - Disassembled Test Engine

The disassembled engine can be seen in Fig. 10-17. The rings were then changed one piston at a time, and the engine was then re-assembled in the reverse order. During this process, engine parts were cleaned and examined, and gaskets and seals were replaced as needed. The need to disassemble and rebuild the engine for every configuration of the rings tested had the potential to introduce additional variability in the

measurements. Although it is unreasonable to expect that the engine condition was absolutely identical after every rebuild, extreme care was taken during this procedure. In addition, in order to ensure consistency in the ring exchange procedure, a single person was tasked with changing the rings every time.

The rings tests were performed in the following order:

1. LTOCR and NTSR 1
2. Baseline 1
3. LTOCR
4. Baseline 2
5. SBTR
6. LTOCR and NTSR 2
7. Baseline 3
8. Low-friction Configuration (LTOCR, NTSR, SBTR)

A summary of the various actions taken to improve the sensitivity of the FMEP measurements includes:

- Using an encoder with a smaller increment, 0.1 CAD instead of the 0.25 CAD encoder used initially.
- Using an independent optical pickup on the flywheel to verify the location of TDC.
- Increasing the number of measurements at each operating condition.
- Operating the engine at lower exhaust O_2 levels in order to decrease the effects of fuel composition on combustion stability.
- Implementing a closed loop controller to maintain exhaust O_2 levels.
- Changing rings in a way that minimized variation during the engine rebuilds, and randomize the ring test order.

10.3 Results and Discussion

The main goal of this study was to determine the effect of the piston ring design on FMEP. A plot summarizing the different test sets is shown in Fig. 10-19. Each ring configuration data set was averaged and plotted along with the 95% confidence interval (CI) as the error bars. The CI was calculated from Eq. 10.6 [56].

$$CI = z_{\alpha/2}\frac{\sigma}{\sqrt{n}} \qquad \text{(Eq. 10.6)}$$

Where n is the number of samples in the set, $z_{\alpha/2}$ is the value obtained from the standard normal distribution, and σ is the standard deviation of data set. For a 95% confidence, $z_{\alpha/2}$ is 1.96.

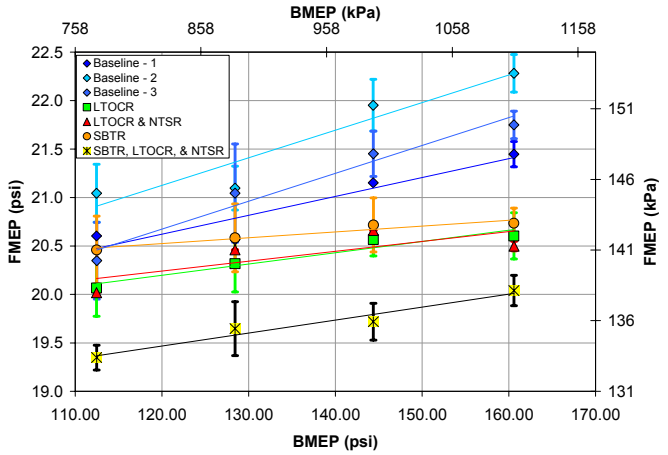

Figure 10-18 - FMEP vs. BMEP@ 1800rpm (separate baseline results)

The baseline ring pack was tested three times (with different 'builds') in order to verify that the baseline engine friction was not changing over time. This also allowed us to investigate whether the engine tear-down and rebuild process had a significant effect on the FMEP measurements. The three baseline engine tests are shown in Fig. 10-18. A slight FMEP difference can be seen between the three baseline tests. However, the friction reduction trends discussed here are still valid. The data presented in Fig. 10-19 and all other subsequent plots includes all baseline tests to compute the average and statistics.

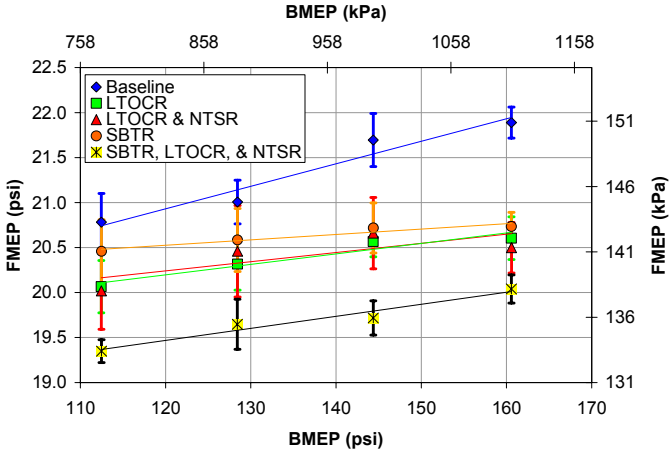

Figure 10-19 - FMEP vs. BMEP @ 1800rpm (combined baseline results)

The FMEP results of the various rings were compared with the baseline configuration to determine the reduction in FMEP. The friction reductions measured tend to be conservatively predicted using the MIT model (Fig. 10-20). The error bars on the model predictions show the bounding oil supply conditions used by the model. The error bars on the experimental differences in Fig. 10-20 were calculated using Eq. 10.7 [56].

$$Error = z_{\alpha/2}\sqrt{\frac{\sigma_1^2}{n_1}+\frac{\sigma_2^2}{n_2}} \qquad \textbf{(Eq. 10.7)}$$

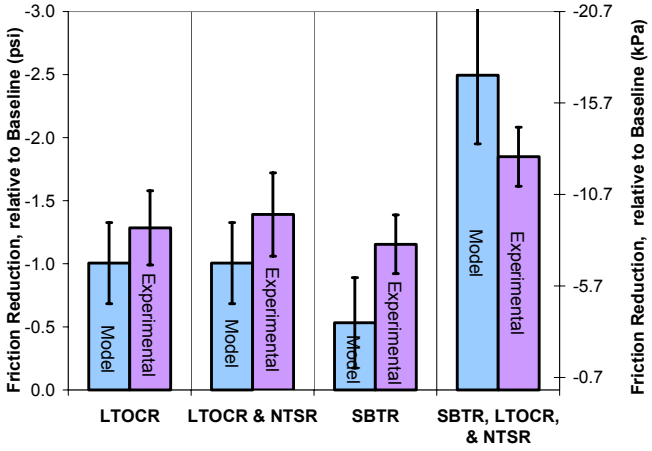

Figure 10-20 - Experimental and Modeled FMEP Results @ 1800rpm and 400bhp (298kW)

The mechanical efficiency (η_{mech}) was also calculated using Eq. 10.8

$$\eta_{mech} = \frac{BMEP}{NMEP} \qquad \text{(Eq. 10.8)}$$

These mechanical efficiency results are shown in Fig. 10-21 and Fig. 10-22.

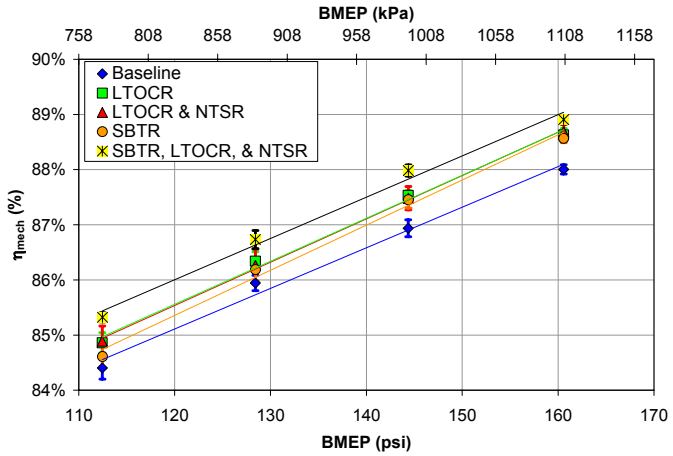

Figure 10-21 - η_{mech} vs. BMEP @ 1800rpm

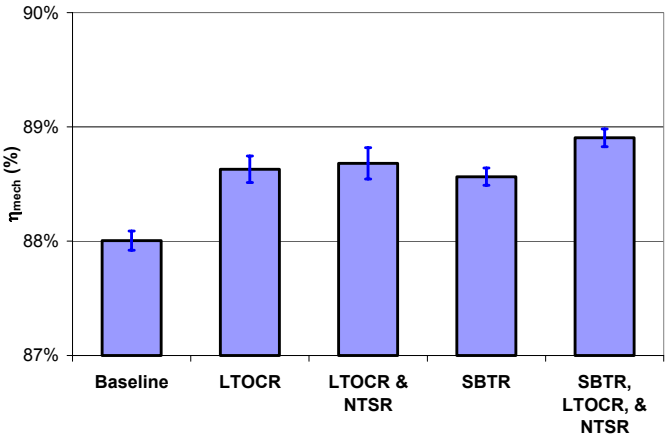

Figure 10-22 - η_{mech} vs. BMEP @ 1800rpm and 400bhp (298kW)

The measured oil consumption of the engine is shown in Figure 10-23. Oil consumption measurements are notoriously variable over time, and due to the relatively short tests times used to measure oil consumption in this study (~3 hours), the measurements are thought to only be an indication of the general trend of the consumption rate. In general, the oil consumption tended to increase when the LTOCR were used and then returned to the somewhat lower value with the NTSR. The SBTR appeared to have a relatively small effect the oil consumption**.**

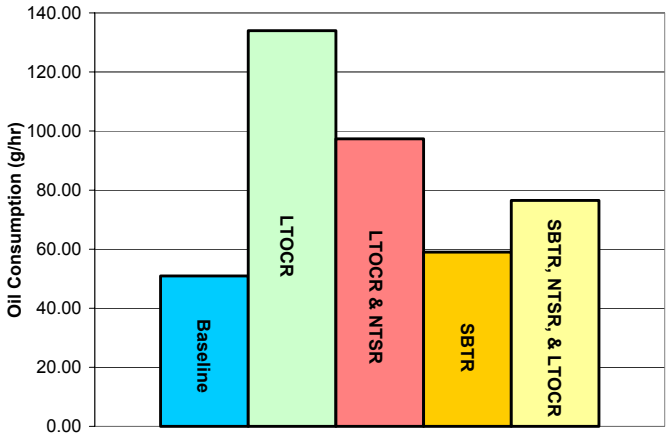

Figure 10-23 - Measured Oil Consumption @ 1800rpm and 400bhp (298kW)

The average blow-by measurements and 95% confidence intervals are shown in Figure 10-24. As shown, all ring configurations display a slightly increasing blow–by rate with increasing engine load. However, blow-by differences between all configurations are relatively small. The NTSR seemed to have a slightly higher blow-by

than the others, which was expected from the ring pack design characteristics and numerical predictions. However, the change does not appear to be very significant and is not cause for concern.

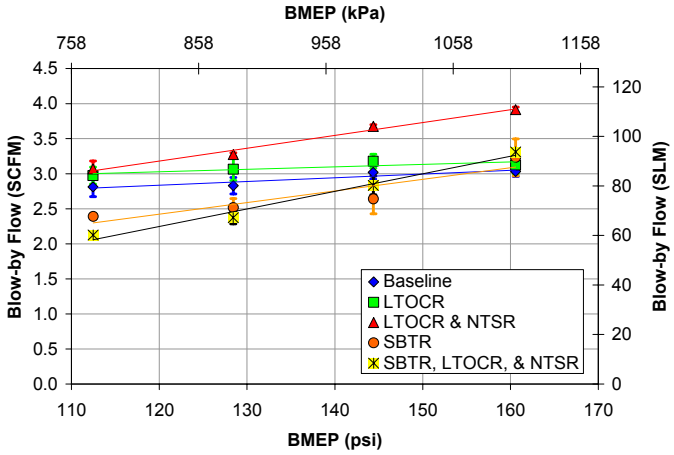

Figure 10-24 - Blow-by Flow vs. BMEP @ 1800rpm

The blow-by flow was also compared to the values predicted by the model in Fig. 10-25.

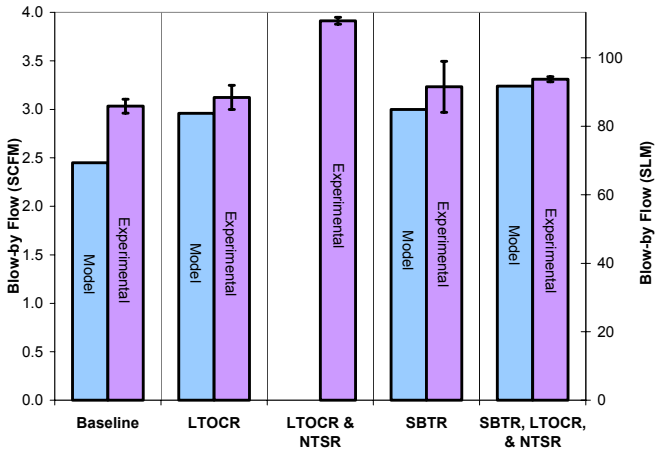

Figure 10-25 - Experimental and Modeled Blow-by Flow Results @ 1800rpm and 400bhp (298kW)

10.4 Summary and conclusions of experimental validation

A ring pack model developed at MIT was used to design a low-friction ring pack configuration for a Waukesha VGF 18 liter engine. The low-friction ring pack features a skewed barrel top ring, a negative twist second ring, and a low-tension oil control ring. The MIT model predicted that the low-tension oil control ring has a potential to decrease ring pack friction by 20-30% and the skewed barrel top ring has the potential to reduce ring pack friction by 15-25%. Use of the negative twist second ring can help offset the adverse effects of the LTOCR on the rate of oil consumption.

In order to measure the small reductions in FMEP on an unmodified full-scale engine, it was necessary to improve the instrumentation used on the engine and the methodology used for measurements. The experimental results from this study showed that the SBTR and LTOCR rings can indeed reduce FMEP, and that the NTSR can help control the oil consumption rate. The results of combining all three ring designs showed a total engine FEMP reduction of 7-10% from the baseline configuration without significantly increasing oil consumption or blow-by flow. The measured FMEP reductions were in good correspondence with the model predictions**.**

III SUMMARY AND CONCLUSIONS

The power cylinder is the main contributor to friction power losses in modern internal combustion engines. In this study, a combined analytical and experimental investigation on reducing friction in all power cylinder components was conducted, with particular emphasis on analysis on lubricant, surface finish, and piston design parameters in this reporting period. Results show that there is potential for friction reduction in all of the areas investigated. Experiments on recommended low-friction ring-pack designs have been completed, and testing of low-friction lubricant is in progress.

The focus of this study was on gas-fired reciprocating engines operating in high load, low speed conditions, with specific focus on the Waukesha VGF 18GL engine, which was used as the baseline engine in all studies. Previous annual reports indicated that a friction reduction of ~35% was possible with optimized ring designs. In this reporting period, demonstration of low-friction ring-pack designs in the Waukesha engine confirmed total engine FEMP (friction mean effective pressure) reduction of 7-10% from the baseline configuration without significantly increasing oil consumption or blow-by flow. This represents a substantial (30-40%) reduction of the ring-pack friction alone. The measured FMEP reductions were in good agreement with the model predictions. Further improvements via piston, lubricant, and surface designs offer additional opportunities.

In addition to component mechanical design, two other areas were also investigated; the effects of lubricant viscosity and liner surface texturing on ring/liner friction were considered. An optimized low-friction lubricant was proposed and testing is being done on the Waukesha engine.

Effects of lubricant viscosity were studied as follows: (a) by changing the overall viscosity uniformly over the entire engine cycle, and (b) by preferentially changing, theoretically, the viscosity variations during the engine cycle, such as a higher viscosity near the end strokes and a lower viscosity near the mid-stroke. The rationale is that boundary lubrication is dominant near the end strokes which would benefit from a higher oil viscosity and higher oil film thickness, while near the mid-stroke of the engine cycle, hydrodynamic friction is dominant, which can be reduced by a lower viscosity. These variations could be achieved by lubricant formulation using viscosity dependency on shear rate, or by the temperature dependence of lubricant viscosity, or by proper thermal management of the engine. Results show that the strongest effect on friction reduction was by lowering the overall viscosity level of the lubricant everywhere in the engine cycle. While lowering viscosity near the mid-stroke region preferentially would also reduce friction in the same way, in that region, as lowering the viscosity everywhere, the effect on overall friction reduction by increasing oil viscosity near the end strokes was not as large as anticipated. The reason is that while boundary friction is reduced with higher oil viscosity near the end-strokes, hydrodynamic friction is also increased near the end strokes. The tradeoff obviously depends on the balance of asperity contact reduction versus hydrodynamic friction increase in the region near the end-strokes of piston travel.

Analysis of friction modifiers showed that asperity contact friction decreases in proportion to the reduction in friction coefficient. Hydrodynamic friction is not adversely

affected. Thus friction modifiers are effective in friction reduction, but their practical implementation could be complex as they could affect engine deposits and/or other lubricant formulation issues. Further analysis and testing in this area are needed.

A parametric study of surface texturing showed that adding appropriate surface features to the cylinder liner may also significantly reduce ring/liner friction. Also, if the lubricant and surface texturing can be optimized together, an even greater reduction in friction is possible, along with mitigation of undesired side-effects, such as oil consumption and wear, which may accompany changes made to the lubricant viscosity and surface texturing individually.

Friction reduction was observed when the surface texturing caused an increase in flow resistance, increasing oil film thickness and thus causing a reduction in both asperity contact and hydrodynamic friction. A parametric analysis of both grooved and dimpled patterns was performed. Other surface parameters were also studied and reported last year and thus will not be repeated here.

This year, surface groove parameters studied included the groove angle, width, depth, and area ratio, while parameters for the round dimples were the dimple depth, diameter, and area ratio. For both types of texturing, friction was found to decrease strongly with the depth of the features, and for grooved surfaces friction dropped substantially as groove angle was made more perpendicular to the direction of piston travel. Also, for both types of texture, friction decreased with increasing area ratio, although not as strongly as with depth or groove angle. Applied to the Waukesha engine ring-pack, a possible friction reduction of 15-25% is estimated through control of groove angle. Groove width and dimple diameter had only a minor effect on ring/liner friction, with the dimpled surfaces showing a slight optimum effect. The lowest FMEP was predicted for a mid-range dimple diameter.

For the best combination of surface and lubricant studied, compared to a smooth surface with the lubricant currently used in the Waukesha engine, a reduction in FMEP of greater than 50% is predicted for the oil control ring, translating into a reduction of ~30% for the ring-pack. This prediction indicates that there is significant potential for friction reduction via concurrent optimization of lubricant and surface properties.

Friction reductions of up to 50% are predicted for optimized piston design, resulting from reducing waviness alone. Pistons with large waviness experience asperity contact at larger film thicknesses, leading to high boundary friction losses. Reducing waviness reduces boundary contact, and thus friction. Other piston parameters were studied and also show the potential to contribute to a reduced friction design, including piston/liner clearance, ovality and skirt profile. Lubricant effects were also considered. The challenge that remains is a series of component design and validation experiments, which could take as much time and effort as the ring-pack and lubricant experiments.

The design strategies developed in this study have promising potential for application in all modern internal combustion engines as they represent simple, low-cost methods to extract significant fuel savings and to reduce harmful environmental damage, without compromising engine performance.

IV CONTINUING PLANS

Results have shown that there is a synergistic benefit of using low-friction lubricant concurrently with implementing low-friction low-wear material/surface designs. Hence current analyses will focus on the application of low-friction lubricants for various surface designs. The current analysis will be continued and expanded, concurrent with in-engine testing and verification. Experiments that are on-going but have not been contained in this report include the low-friction lubricant tests. A cooperative partnership has begun and will continue with a large lubricant manufacturer to design and provide lubricants for future testing. Preliminary results are very promising. Actual material testing would best be implemented after the initial low-friction lubricant tests.

Studies strongly indicate that piston friction is comparable to ring-pack friction and deserves as detailed a study and testing as low-friction ring-packs. Low-friction piston design will be recommended. However, procurement and implementation of piston design validation experiments would follow the lubricant and material demonstrations in an engine in that sequence. However, expanded studies of piston friction reduction beyond the current period may be appropriate and would be recommended.

The current program has possible spinoffs in other applications such as in the transportation industry including automotive, marine, or in diesel power generation applications. Discussions with various government agencies and University-Industry workshops will be continued to ensure that the full potential for friction reduction in these areas will be fully explored and further areas for study identified. The progress made in this ARES program has far greater implications for applications than in one focused industry.

Potential deployment of low-friction engine components or lubricants in the near term is not only possible, but quite probable, if future continued funding permits.

V ACKNOWLEDGEMENT

This project is sponsored by the United States Department of Energy, Office of Distributed Energy, Advanced Reciprocating Engine Systems (ARES), as part of the Advanced University Reciprocating Engines Program (AUREP) under DOE Cooperative Agreement Number DE-FC26-02NT41339. We appreciate the participation of Colorado State University, Dr. Bryan Willson, Ted Bestor, Dr. Rudy Stanglmaier, Kirk Evans, Kris Quillen, and others, in performing the experiment and validation of the results. They are our important university partner in this project. The authors would also like to thank our industrial partner, Waukesha Engine Dresser, Inc., for their support and insight in this study. The authors would like to specifically acknowledge the technical contributions of Ed Reinbold, Rick Donahue, Andy May and Jim Zurlo of Waukesha, who have worked closely with the MIT team and provided useful input and suggestions throughout the duration of the project. We thank the DOE ARES project monitors, Tom George, Rob Martinez, William Cary Smith, and our technical project monitor Raj Sekar, and in particular the DOE manager and sponsor, Ronald Fiskum for their encouragement and support. Feedback from other industry participants such as Caterpillar and Cummins was very helpful. Prior work and the methodology used in the analyses were supported by related research in the MIT Industrial Consortium on Lubrication in I.C. Engines.

VI REFERENCES

1. "Lubricant Additves – Chemistry and Applications" Edited by L. R. Rudnick, Marcel Dekker, Inc, 2003, ISBN: 0-8247-0857-1
2. Hegemier, T., Stewart, M., "Some Effects of Liner Finish on Diesel Engine Operating Characteristics," SAE paper 930716, 1996.
3. Jeng, Y., "Impact of Plateaued Surface on Tribological Performance," Tribology Transactions, vol . 29, pp. 354-361, 1996.
4. Jocsak, Jeffrey "The Effects of Surface Finish on Piston Ring-Pack Performance in Advanced Reciprocating Engine Systems," Master's Thesis, Massachusetts Institute of Technology, Cambridge, MA, June 2005
5. Water, F., Fundamentals of Manufacturing for Engineers, UCL Press, London, 1996.
6. Rohde, S.M., "A Mixed Friction Model for Dynamically Loaded Contacts with Application to Piston Ring Lubrication," Proc. of the 7th Leeds-Lyon Symposium on Tribology, Westbury House, pp. 19-50, 1980.
7. Liu, J.J., et. al., "Current and Future Approaches for Laser Texturing of Thin Film Media," IEEE Transactions on Magnetics, vol. 36, pp. 125-132, 2000.
8. Etsion, I., "State of the Art in Laser Surface Texturing," ASME Journal of Tribology, vol. 127, pp. 248-253, 2005.
9. see: "The Future of the Surface: Optimum Tribosystems Through Functionally Optimized Surfaces," www.Gehring.de/enpdf/LaserHoning.pdf
10. Tian, T., "Modeling the Performance of the Piston Ring Pack in Internal Combustion Engines", PhD Thesis, Department of Mechanical Engineering, Massachusetts Institute of Technology, June 1997
11. Greenwood, J.A., Tripp, J., "The Contact of Two Nominally Flat Surfaces," Proc. Inst. Mech. Engrs., vol. 185, pp. 625-633, 1971.
12. Hu, Y., et. al., "Numerical Simulation of Piston Ring in Mixed Lubrication – A Non-Axisymmetrical Analysis," ASME Journal of Tribology, 1993.
13. Elderton, P.E. and Johnson, L.J., Systems of Frequency Curves, London: Cambridge University Press, 1969.
14. Chung, Y., Schock, H.J. and Brombolich, L.J., "Fire Ring Wear Analysis for a Piston Engine," SAE Paper # 930797, 1997.
15. Patir, N. and Cheng, H.S., "Application of Average Flow Model to Lubrication Between Rough Sliding Surfaces," ASME Journal of Lubrication Technology, vol. 101, pp. 220- 230, 1979.
16. Tian, T., et.al., "A Piston Ring-Pack Film Thickness and Friction Model for Multigrade Oils and Rough Surfaces," SAE paper 962032, 1996.
17. Arghir, et. al., "Theoretical Analysis of the Incompressible Laminar Flow in a Macro-Roughness Cell," ASME Journal of Tribology, vol. 125, pp. 309-318, 2003.
18. Hamilton, D.B., Walowit, J.A. and Allen, C.M., "A Theory of Lubrication by Microasperities", ASME J. Basic Eng., vol. 88, pp. 177-185, 1966.
19. Anno, J.N., Walowit, J.A. and Allen, C.M., "Microasperity Lubrication", ASME Journal of Lubrication Technology, vol. 90, pp. 351-355, 1968.
20. Anno, J.N., Walowit, J.A., and Allen, C.M., "Load Support and leakage from Microasperity- Lubricated Face Seals", ASME Journal of Lubrication Technology, vol. 91, pp. 726-731, 1969.
21. Tian, H., Saka, N., Suh, N., "Boundary Lubrication Studies on Undulated Titanium Surfaces", Tribology Transactions, vol. 32, pp. 289-296, 1989.

22. Tonder, K., "Inlet Roughness Tribodevices: Dynamic Coefficients and Leakage", Tribology International, vol. 34, pp. 847-852, 2001.
23. Suh, N., Tribophysics, Englewood Cliffs, NJ: Prentice-Hall, Inc., 1986.
24. Petterson, U. and Jacobson, S., "Influence of Surface Texture on Boundary Lubricated Sliding Contacts", Tribology International, vol. 36, pp. 857-864, 2003.
25. Blatter, A., et. al., "Lubricated Sliding Performance of Laser-Patterned Sapphire," Wear, vol. 232, pp. 226-230, 1999.
26. Kovalchenko, A., Ajayi, O., Erdemir, A., Fenske, G., Etsion, I., "The Effect of Laser Surface Texturing on Transitions in Lubrication Regimes During Unidirectional Sliding Contact", Tribology International, vol. 38, pp. 219-225, 2005.
27. Sadeghi, F., et. al., "Advanced Natural Gas Reciprocating Engine: Parasitic Loss Control Through Surface Modification," presented at ARES/ARICE Low Engine Friction Alliance Workshop, Cambridge, MA, Dec. 1, 2005.
28. Etsion, I., et. al., "Analytical and Experimental Investigation of Laser-Textured Mechanical Seal Faces," Tribology Transactions, vol. 42, pp. 511-516, 1999.
29. Ronen, A., Etsion, I., Kligerman, Y., "Friction-Reducing Surface-Texturing in Reciprocating Automotive Components," Tribology Transactions, vol. 44, pp. 359-366, 2001.
30. Ryk, G., Kligerman, Y., Etsion, I., "Experimental Investigation of Laser Surface Texturing for Reciprocating Automotive Components," Tribology Transactions, vol. 45, pp. 444-449, 2002.
31. Siripuram, R. and Stephens, L., "Effect of Deterministic Asperity Geometry on Hydrodynamic Lubrication", ASME Journal of Tribology, vol. 126, pp. 527-534, 2004.
32. Hsu, S., "Integrated Surface Modification Technology Development," presented Sept. 15, 2005.
33. Michail, S.K. and Barber, G.C., "The Effects of Roughness on Piston Ring Lubrication Part I: Model Development," Tribology Transactions, vol. 38, pp. 19-26, 1995.
34. Kotwal, C. and Bhushan, B., "Contact Analysis of Non-Gaussian Surfaces for Minimum Static and Kinetic Friction and Wear," Tribology Transactions vol. 39, pp. 890-898, 1996.
35. Pinkus, O., Theory of Hydrodynamic Lubrication, New York:, McGraw-Hill Book Co., 1961.
36. Ronen, A., Etsion, I., and Kligerman, Y., "Friction-Reducing Surface-Texturing in Reciprocating Automotive Components," Tribology Transactions vol. 44, pp. 359-366, 2001.
37. Wong, V., Tian, T., Lang, H., Ryan, J., Sekiya, Y., Kobayashi, Y. and Aoyama, S., "A Numerical Model of Piston Secondary Motion and Piston Slap in Partially Flooded Elastohydrodynamic Skirt Lubrication", International Congress and Exhibition, Detroit, MI, Paper 940696, (1994).
38. 1. Mufti, R. and Priest, M., "Experimental Evaluation of Piston-Assembly Friction Under Motored and Fired Conditions in a Gasoline Engine," ASME Journal of Tribology, Vol. 127, 2005, pp. 826-836.
39. Wakuda, M., et al. "Effect of surface texturing on friction reduction between ceramic and steel materials under lubricated sliding contact," Wear vol. 254, pp. 356-363, 2003.

40. Kweh, et. al., “Micro-Elastohydrodynamic Lubrication of an Elliptical Contact with Transverse and Three-Dimensional Sinusoidal Roughness,” ASME Journal of Tribology, vol. 111, pp. 577-584, 1989.
41. Richardson, D.E., ASME Paper 99-ICE-196, 1999 ASME-ICED Spring Conference.
42. Wong, V. W., Tian, T., Smedley, G., Jocsak, J., ”Low-Engine-Friction Technology for Advanced Natural-Gas Reciprocating Engines”, Annual Technical Progress Report, June 1, 2003 – Jume 30, 2004, DoE Cooperative Agreement No. DE-FC26-02NT41339
43. Rabute, R., Tian, T., “Challenges Involved in Piston Top Ring Design for Modern SI Engines”, Transactions of the ASME, Journal of Engineering for Gas Turbines and Power, 123, April 2001, pp. 448-458
44. Tian, T., Wong, V. W., “Modeling the Lubrication, Dynamics, and Effects of Piston Dynamic Tilt of Twin-Land Oil Control Rings in Internal Combustion Engines”, Transaction of ASME, Journal of Engineering for Gas Turbines and Power, 122, January 2000, pp.119-129
45. Moughon, L., Wong, V. W., “Effects of Lubricant and Piston Design on Reciprocating Engine Friction”, ASME-ICED Fall Technical Conference, ASME Paper ICEF2005-1343
46. Etsion, I., Kligerman, Y., Shinkarenko, A., ”Improving Tribological Performance on Piston Rings by Partial Surface Texturing”, Transaction of the ASME, Journal of Tribology, 123, July 2005, pp 632-638
47. Sadeghi, F., Bolander, N. W., Gerber, G. R., ”Piston Ring Friction Reduction Through Surface Modification”, ASME-ICED Fall Technical Conference, ASME Paper ICEF2005-1346
48. Jocsak, J., Li, Y., Tian, T., Wong, V. W., “Analyzing the Effects of Three-Dimensional Cylinder Liner Surface Texture on Ring-Pack Performance with a Focus on Honing Groove Cross-Hatch Angle”, ASME-ICED Fall Technical Conference, ASME Paper ICEF2005-1333
49. Tian, T., “Dynamic Behaviors of Piston Rings and their Practical Impact. Part 1: Ring Flutter and Ring Collapse and their Effects on Gas Flow and Oil Transport”, ImechE 2002, pp. 209-227
50. Tian, T., “Dynamic Behaviors of Piston Rings and their Practical Impact. Part 2: Oil Transport, Friction and Wear of Ring/Liner Interface and the Effects of Piston and Ring Dynamics”, ImechE 2002, pp. 229-247
51. Takiguchi, M., Machida, K., Furuhama, S., “Piston Friction Forces of a Small High Speed Gasoline Engine”, Transaction of the ASME, Journal of Tribology, 110, January 1988, pp. 112-118
52. Yoshida, H., Kazunori, K., Sagawa, J., “Effects of Surface Treatments on Piston Ring Friction Force and Wear”, S.A.E. transactions, 99, 1990, pp. 1236-1245
53. Hamatake, T., Kitahara, T., Wakuri, Y., Soejima, M., “Friction Characteristics of Piston Rings in a Reciprocating Engine”, Lubrication Sci., 6-1, Oct 1993, pp.21-40
54. Kim, M., Kiehne, T., Matthews, R. D., “Friction Force Measurements Using the Instantaneous IMEP Method and Comparison with RINGPAK Simulations”, ASME-ICED Fall Technical Conference, ASME Paper ICEF2005-1300
55. Heywood, J.B., “Internal Combustion Engine Fundamentals”, McGraw-Hill Inc., © 1988
56. Devore, Jay L., “Probability and Statistics for Engineering and The Sciences”, Fifth Edition, Duxbury Thomson Learning, © 2000